Oriented Antibodies as Versatile Detection Element in Biosensors

Thesis committee

Promotor
Prof. dr. H. Zuilhof
Professor of Organic Chemistry
Wageningen University

Co-promotor
Dr. J. Beekwilder
Scientist
Plant Research International, Wageningen

Other members
Prof. dr. R. G. H. Immink, Wageningen University
Dr. R. M. Anthony, KIT Biomedical Research, Amsterdam
Dr. T. Bachmann, University of Edinburgh, UK
Prof. dr. A.H. Velders, Wageningen University

This research was conducted under the auspices of the Graduate School VLAG (Advanced studies in Food Technology, Agrobiotechnology, Nutrition and Health Sciences).

Oriented Antibodies as Versatile Detection Element in Biosensors

Anke Kristin Trilling

Thesis

submitted in fulfillment of the requirements for the degree of doctor

at Wageningen University

by the authority of the Rector Magnificus

Prof. Dr. M. J. Kropff

in the presence of the

Thesis Committee appointed by the Academic Board

to be defended in public

on Friday 7 June 2013

at 4 p.m. in the Aula.

Anke Kristin Trilling
Oriented Antibodies as Versatile Detection Element in Biosensors.

PhD thesis, Wageningen University, Wageningen, The Netherlands, 2013.
With references and summaries in English, Dutch and German.

ISBN: 987-94-6173-568-3

To my family.

TABLE OF CONTENTS

CHAPTER 1

General Introduction

ABSTRACT

The aim of this thesis is to explore orientation of detection elements on biosensor surfaces. To this end, different aspects of a biosensor set-up, such as surface chemistry, coupling chemistry and biological detection elements are discussed. Further on, the basics of surface plasmon resonance, an often used optical biosensor, are described.

1.1 BIOSENSORS

The desire to provide real-time monitoring of target analytes is the driving force in the biosensor research sector. One of the best-known examples is the development of the glucose biosensor for diabetes patients. The development of this biosensor started with the pioneering work by Clark and Lyons in 1962.[1] Glucose oxidase, an enzyme catalyzing the oxidation of glucose, coupled to an amperometric oxygen electrode was used as detection element for glucose determination. In 1967, Updike and Hicks[2] entrapped glucose oxidase in a polyacrylamide gel on an electrode to generate one of the first ´enzyme electrodes`. This innovation served as fundament for the probably most successful product generated for biomedical microanalysis: the glucose biosensor. This biosensor is able to determine the approximate concentration of glucose in blood and is used for diabetes management, mainly because of its simple handling for users: ´prick-apply-read`. A small volume of blood from a finger prick is placed on a disposable test strip that the electrochemical analyzer reads and uses to calculate the blood glucose level. To provide this function, biosensor devices such as the glucose biosensor consist of two main parts: A biological detection element and a transducer. The biological detection element provides specificity by binding to an analyte of interest. In the glucose biosensor, the biological detection element is an enzyme (glucose oxidase) which reacts with a target analyte (glucose) in the blood. This binding event causes changes in optical, mass, thermal or electrical properties proportional to the amount of target analyte. These changes are converted into a measurable electrical signal by a physicochemical detector component, the transducer. In a glucose biosensor, the reaction between glucose oxidase and glucose produces an electric current and this current is translated to a number by the transducer for an easy read-out by the user.

In addition to the health care sector, biosensing-devices find their application in the detection of infectious diseases, food contamination or the detection of biological threat agents in the environment. Development in these fields aims for low cost, easy handling, reliability and miniaturization. Given the diversity of technologies available today it is beyond the scope of this overview to cover all the changes happening in the biosensor field. In this introduction I will treat the following aspects:

a) advances in nanotechnology leading to more sensitive detection methods,
b) progress in surface chemistry,
c) improved coupling chemistry and
d) development of engineered biological detection elements.

Progress in these fields will steer the sensitive and specific detection of target analytes in the future.

1.2 NANOTECHNOLOGY

Nanotechnology refers to the techniques and methods for studying, designing, and constructing things at the nanometer scale.[3] By definition nanotechnology uses materials or devices that have structural features on the nanometer scale (from 1 to 100 nanometers).[3] One nanometer (nm) is one billionth, or 10^{-9}, of a meter. By comparison, chemical bonds between two atoms are in the order of 0.1 to 0.2 nm in length, the DNA double-helix has a diameter of about 2 nm and the bacterium *Escherichia coli*, present in the humans digestive system, is 2000 nm in length.

Nanomaterial is especially interesting because nanoparticles possess different properties compared to the bulk material. Whereas gold is known to be relative inert, gold nanoparticles can act as a catalyst that can oxidize carbon monoxide.[4] A gold nanoparticle (90 nm in size) will appear blue-green instead of being shiny as the bulk material. This change results from the fact that nanoparticles absorb colors on the red and yellow end of the color spectrum instead of reflecting the light like the bulk material does.[4] In the same way, ensembles of nanoparticles can possess collective characteristics that are different to those of individual nanoparticles.[5] To explore and use these properties in new devices is the key challenge in nanotechnology. Two main approaches are used in the nanotechnology world: the ´bottom-up` and the ´top-down` approach (Fig. 1).

In the ´bottom-up` approach, molecular components assemble themselves via molecular recognition, without guidance from an outside source to the final structure. Self-organization of nanoparticles can result in a variety of structures such as chains,[6] vesicles[7] or crystals.[8] The arrangement is directed through non-covalent interactions (e.g. hydrogen bonding, metal coordination, hydrophobic forces, van der Waals forces, π-π interactions and/or electrostatic interactions)[9] as well as electromagnetic

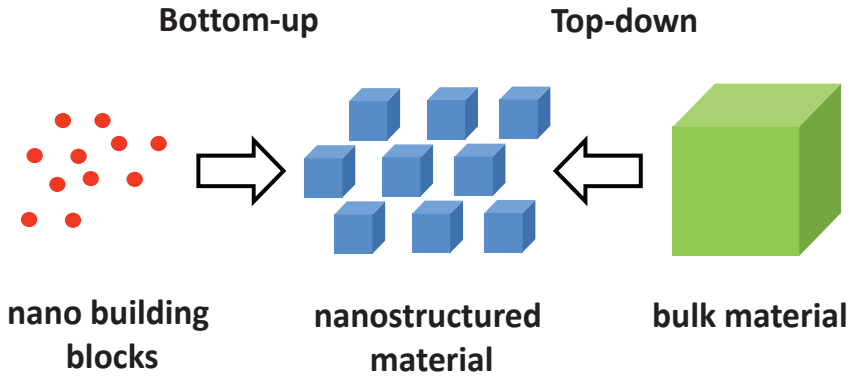

Figure 1. The ´bottom-up` and ´top-down` nanostructure assembly approaches.

interactions. In nanobiotechnology, biological molecules such as carbohydrates and lipids can be used as building blocks for the construction of highly ordered structures as it can be observed in nature.[10] The challenge is to control the assembly of biomolecules into bioactive nanostructures.[11]

In the ´top-down` approach, larger objects are used to construct nanodevices without atomic-level control. A process called photolithography is often used to carve a desired pattern in the material. Silicon wafers are often used in the construction of complex devices and microelectronic circuits. One simple example of the device fabrication process includes the formation of an SiO_2 layer and its selective removal using photolithography. The top surface of the wafer is first coated with a light sensitive material called photoresist. With a light source shining through the mask, only selected parts of the photoresist on the silicon wafer will be exposed to the light. When a negative resist is used, only the light exposed areas become polymerized and more difficult to dissolve in solvents. The wafer is then dipped in a developer that removes only non-polymerized photoresist at places where it was not exposed to light. Areas of the silicon wafer that are not covered with photoresist can then be used to etch away material. Today, the challenge to produce features that are much smaller than the wavelength of visible light, which is in the 400-700 nm range, dominate the field.

With the advances in nanotechnology also the field of biosensors experienced a revolution, especially in the area of surface characteristics. As sensors mainly operate through the variation of a surface parameter, increasing the interaction area will lead to an increased sensitivity.[12] Xie et al.[13] used multi-walled carbon nanotubes in a novel glucose sensor to significantly improve its sensitivity for glucose detection. The carbon nanotubes were functionalized with platinum nanoparticles and used to immobilize the enzyme. This improved, amongst other parameters, the loading of the enzyme and resulted in a higher electroactive surface area. Knowledge about interactions between biomolecules and inorganic materials plays a crucial role in the field of biosensors and needs to be explored further.

Today, scientist work towards the development of high-throughput biosensors, bringing together the field of nanotechnology with current detection platforms. With the advances achieved in the field of microfluidics, the analysis of small sample volumes (10^{-9}–10^{-18} L) as well as automated sample preparation is possible.[14] Further developments include simultaneous multitarget (´multiplex`) bio-detection assays, to screen for more than only one target analyte at a time. Barcoding technologies using nanoparticles are under development to enable large numbers of analytes to be measured in a single sample.[15] In this application, particles - each with a unique striping pattern (e.g. a specific DNA sequence) - are coated with a unique detection element, which binds specifically to a particular target analyte. A conclusion can be drawn by a read-out of the striping patterns. In a similar way, semiconductor nanocrystals, or quantum dots (QDs) have been investigated for such purposes.[16] QDs are

highly fluorescent, nanometer-size (1-20 nm) clusters of a few hundred to thousands atoms. A glucose biosensor based on QDs was developed to accurately determine the concentration of glucose.[17] The color of the quantum dot is determined by the size of the particle and can be tuned. Each color batch can be functionalized with different detection elements providing a quick and simple read-out. Such systems may yield next generation point of care (POC) testing solutions providing results in a very short period of time at or near the location of the patient and over a whole spectrum of diseases.

1.3 Surface Chemistry

Since the relative surface area exposed to the environment increases rapidly as device structures become smaller and smaller, a high surface to volume ratio is achieved with nanomaterial such as nanoparticles or nanotubes (Fig. 2). This fact implies that surface properties start to play a considerable role when the volume decreases. Surface chemistry can be used to modify the surface characteristics, e.g. by the use of organic monolayers.

Organic monolayers are thin molecular films of precisely one organic molecule thickness attached in a dense packing on the substrate. The attachment can be weak or strong, and can rely on either physical adsorption (e.g. electrostatic interactions) or chemical adsorptions (formation of chemical bonds).[18] The work of monolayers on gold,[19] glass[20] and oxidized aluminium[21] served as landmark in the field of organic monolayers and nowadays organic monolayers can be prepared on numerous surfaces. The exceptionally thin organic monolayers (2-5 nm) can provide the inorganic surface with added functionality via the adaptable tailoring of monolayer properties. Therefore, organic monolayers find application in many fields such as surface hydrophobicity, surface passivation, chemical and biological sensing, and molecular electronics.[22] These monolayers keep the bulk features of the material (electrical, optical, magnetic, mechanical and structural), while their surface properties (wetting, passivation, bio-resistance, biochemical affinity) can be tuned through

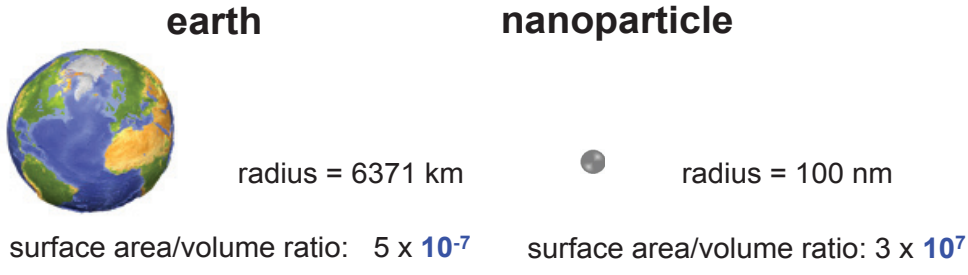

Figure 2. Depiction of relative surface area of earth compared to a nanoparticle.

a nanometer-sized grafting.[18]

Alkanethiol monolayers on gold belong to the most studied systems due to the high affinity of the thiol group towards gold.[23] Alkanethiols in solution self-assemble on the gold substrate to well defined self-assembled monolayers (SAMs). Because of the semi-covalent nature of the Au-S bond, diffusion of already adsorbed alkane-chains along the substrate is possible. As a result, monolayers on gold are nearly defect free.[22a, 23] However, the special property of the Au-S bond is also the limitation of these monolayers since these films have only a limited chemical and thermal stability. In addition is gold not compatible with silicon complementary metal–oxide–semiconductor (CMOS) due to its high diffusion rate and the deep electronic traps it forms in silicon.[24] This damages the carrier (electron and hole) properties of silicon-based semiconductor materials. Therefore, the industry is looking for new material to replace gold.

Copper was evaluated as electrical interconnection material on a semiconductor chip due to its high electrical conductivity and relatively high melting point.[25] The drawback of copper is on the contrary, that it readily oxidizes in the presence of air and corrodes in aqueous solution. However, in principle these weaknesses might be overcome with densely packed organic monolayers on copper. SAMs on copper were first studied by Laibinis and Whitesides.[26] They showed that copper is more reactive to alkanethiols than gold and that alkanethiols form dense monolayers with quasi-crystalline packing.[26] It was also shown that self-assembled monolayers can act as barrier film that hamper oxidation of a copper surface.[27] Therefore, with regard to the biosensing interface, SAMs on oxide-free copper can be advantageous to achieve control at the molecular level and were investigated in this thesis.

Next to passivation and tuning of surface properties, SAMs can be used for biofunctionalization. Coupling of biomolecules is achieved through the intermediate layer between the surface and the detection element. In addition, biosensing can be tuned to be more selective by choosing a suitable coupling chemistry to immobilize the detection elements on the surface.

1.4 Coupling Chemistry

The function of a biosensor depends on the biochemical specificity of the detection element. The successful integration of the biological detection element with the transducer is the most critical component for the realization of any biosensor. Biomolecules such as enzymes,[28] antibodies[23] and microorganisms[30] have been used as biological sensing elements. Here, only proteins will be discussed as a representative group of biomolecules to stay within the scope of this introduction.

A protein consists of a folded polymer, a sequence formed from the 20 possible amino acids. Since amino acids have hydrophilic and hydrophobic groups, these polymers tend to fold in aqueous solution to form an ordered three-dimensional sha-

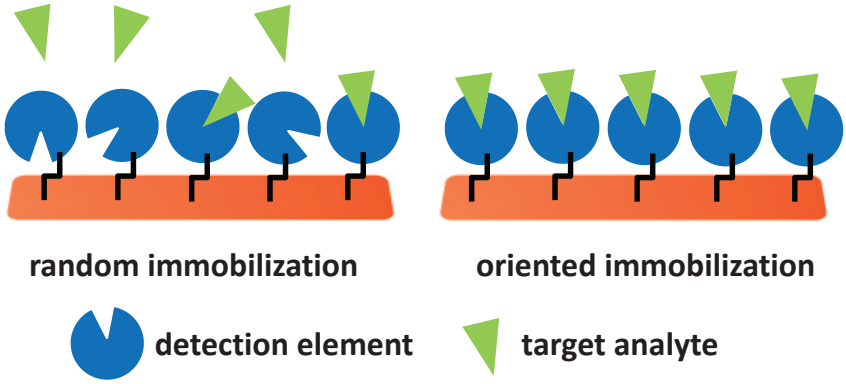

Figure 3. Depiction of random and oriented immobilized detection elements on a surface.

pe. This shape is characterized by a low-energy configuration with the hydrophilic groups outside and the hydrophobic groups inside and driven by a number of non-covalent interactions of the polymer such as hydrogen bonding, ionic interactions, van der Waals forces, and hydrophobic packing. Since the three-dimensional shape is responsible for the activity of the protein, any immobilization method needs to be compatible with the conformation of the detection element. To improve efficiency and robustness of biosensors, the orientation of the surface immobilized detection elements is a critical factor to consider as well as the nature of its bond to the surface.

Immobilization strategies can be divided in random and oriented approaches (Fig. 3). Random immobilization is often achieved using surface exposed amino acid residues such as amine, carboxyl or sulfhydryl groups. In contrast uses oriented immobilization unique chemical functionalities (e.g. carbohydrate groups of the protein) or specific amino acid motives (e.g. His_6 tag on the protein) to direct the immobilized protein in a specific position. Oriented detection elements will show an optimized availability for the target analyte and therefore improve biosensor performance (Fig. 3). Immobilization can result in covalent or non-covalent protein attachment, however, in terms of stability and regeneration potential is covalent immobilization advantageous. A more detailed description about available immobilization strategies can be found in chapter 3 of this thesis.

1.5 Engineered Biological Detection Elements

Biosensor specificity relies strongly on the specificity of the immobilized detection element. In the field of proteins, antibodies represent a class of glycoproteins which were used as detection element in this thesis. Conventional antibodies (Immunoglobulin Gs, IgGs) consist of two light and two heavy chains (Fig. 4). The

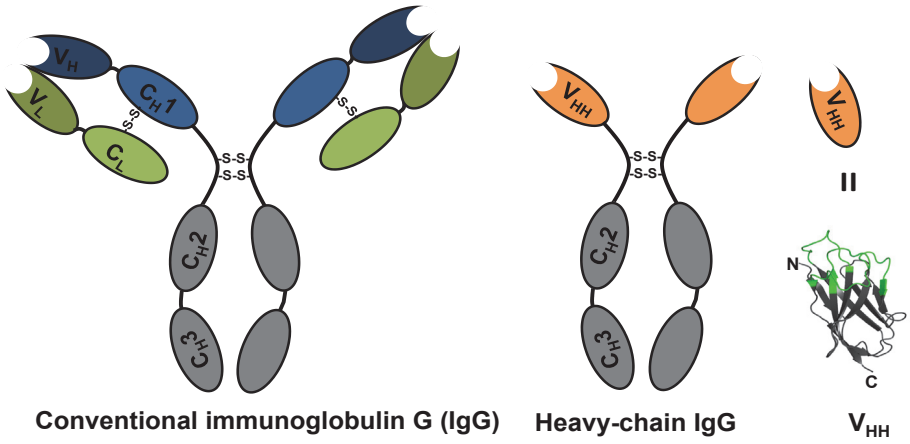

Figure 4. Schematic depiction of antibodies. Left: Immunoglobulin G (IgG) consists of 2 heavy chains (gray/blue) and 2 light chains (green). Antigens bind to the variable regions V_L and V_H. Right: Heavy-chain IgG contains only 2 heavy chains. Antigens bind only to one variable domain (V_{HH}). The V_{HH} domain has a mass of only 15 kDa. The ribbon diagram of V_{HH} shows the target analyte binding site in green.

chains are divided into constant (C) and variable (V) regions. The variable domain is responsible for the specific interaction with the antigen. Apart from conventional IgGs, heavy-chain IgGs can be found in dromedary, llama, alpaca and camel.[31] These antibodies lack the light chain and have only one single domain that binds to the antigen (Fig. 4). The heavy-chain antibodies can be minimized to the variable domain, known as V_{HH}, which was employed in this thesis as detection element in biosensors. These V_{HH}s have the same high binding ability towards the antigen as the whole heavy-chain IgG, but are much smaller in size, and can easily be produced in microbes such as *Escherichia coli* or yeast. In this thesis, V_{HH}s specific for tuberculosis or foot-and-mouth disease virus (FMDV) were employed as detection element in biosensors. V_{HH} are already very small in size and stable, but can be further ´tuned` using protein engineering approaches.

Protein engineering describes the process of designing proteins with advantageous properties using different techniques of molecular biology. In this manner, detection elements that have a smaller size, a longer shelf-life or a higher affinity towards the target analyte can be obtained.

One method used for protein engineering is site-directed mutagenesis. This technique can be used to introduce desired changes in the protein structure if detailed structural knowledge of protein folding and interaction are available. Replacement, deletion and addition of single amino acids or short amino acid sequences can be performed to modify proteins. The group of Orner[32] used a computational method to identify stability interferences in self-assembled proteins. By site-directed muta-

tion of two asparagine residues with hydrophobic amino acides, *Escherichia coli* bacterioferritin (EcBfr) proteins folded into α-helical monomers and assembled into more stable cages. However, to predict the effects of various mutations remains a challenge.

If information about protein folding and interaction is missing, methods mimicking natural evolution can be applied to improve protein properties. Random mutagenesis via error-prone polymerase chain reaction can be applied to a protein followed by a selection strategy to pick out protein variants with new characteristics. Further rounds of mutation and selection will follow to select proteins with desired properties. This method was recently successfully applied to select for more temperature stable bacteriolytic enzymes.[33] In another approach, a technique known as DNA shuffling,[34] mixes and matches pieces of protein variants with improved properties in order to produce better results. The drawback of the two latter methods is that they require high-throughput, which is not feasible for all applications.

Eventually, even unnatural amino acids can be incorporated into proteins by protein engineering thanks to new methods that allow the inclusion of novel amino acids in the genetic code.[35] Introduction of unique functional handles in proteins can therefore be used to achieve site-specific protein modification or coupling on a biosensor surface (chapter 6). Combined with recombinant protein expression in hosts such as bacteria, yeast or plants, numerous detection elements are available today. With the use of protein engineering techniques, protein properties can be adjusted to the needs of the biosensors. However, ´tuning` of protein properties is limited by the rules of biological interactions and time-consuming.

1.6 Surface Plasmon Resonance as Model Biosensor

Different read-out types of biosensors evolved during the last decades. The ´transducer`, which transforms the physical quantity into a measurable electrical signal, can recognize a mass change, a thermal change, an altered surface charge or a change in optical properties. In the latter one, the signal measured by the transducer is light. The sensor detects changes in the refractive index which correlates to changes in concentration, mass or number of analyte.

The BIAcore 3000 instrument used as model biosensor in this thesis integrates surface plasmon resonance (SPR) technology with a microfluidic system to monitor molecular interactions. SPR is an optical phenomenon based on total internal reflection of plane polarized light at the interface between a metal film and a liquid phase.[36] Total internal reflection of light can occur when light from the material of high refractive index arrives at an interface with a material of lower refractive index, e.g. at a metal-liquid interface. Only if the light arrives above a certain critical angle of incidence at the interface, no light is refracted across this interface and total internal reflection occurs. During this phenomenon, an electromagnetic field component,

known as evanescent wave, penetrates a short distance into the liquid phase.[36] At a certain angle of incidence all light is adsorbed and no longer reflected, this angle is known as angle of minimum reflected intensity.[36] Computer interpolation routines can calculate this angle to a high degree of accuracy. The interaction between target analyte and immobilized detection element at the surface will cause a change in the refractive index which will lead to a change of the angle. The measured signal is a direct measure of the angle of minimum reflected intensity. The unit of SPR response (Resonance Unit, RU) is an arbitrary unit where 1 RU corresponds to an angle shift of 0.0001°.

SPR-sensing methods allow to observe binding on-line, meaning that a dynamic image of the binding events at the surface is obtained. Moreover, the analysis is label-free, meaning that no secondary detection elements (such as enzymes, secondary antibodies or particles) are needed. The signal of SPR is proportional to the molecular mass of the bound analyte: small molecules like peptides are more difficult to detect than large particles such as viruses. In the CM5 dextran sensor chips, used in this thesis, the gold surface is modified with a carboxymethylated dextran layer. This dextran hydrogel layer forms a hydrophilic, flexible environment for th e immobilized biomolecules with a layer-thickness of about 100 nm.

1.7 Outline of this Thesis

The work presented in this thesis combines surface chemistry and protein functionalization with the aim to generate a platform for oriented immobilization of antibodies in biosensors. Chapter 2 investigates the formation of organic monolayers on oxide-free copper. Detailed studies were performed to characterize the monolayers and proof its quality. Apart from being the first oxide-free monolayers on copper reported thus far, further functionalization was successfully investigated.

Chapter 3 gives an overview about approaches used to orient antibodies on surfaces. It also summarizes methods used to characterize the orientation of immobilized antibodies in a more direct manner.

In chapter 4 a set of detection elements for tuberculosis bacteria is described. These are variable domains of llama heavy-chain antibodies, known as V_{HH} proteins. A number of V_{HH}s, selected by phage display, were expressed by *Escherichia coli* bacteria and characterized for binding towards *Mycobacterium tuberculosis* bacteria. Specificity of V_{HH}s was investigated and the antigen was identified.

In chapter 5 the impact of orientation on the analyte binding capacity was studied by SPR as model biosensor. Established techniques (NH_2 coupling, biotyinylation) were used to immobilize V_{HH}s, and a comparison between oriented and random immobilized V_{HH}s was made. The effect of molecular weight, epitope number and affinity of the target analyte was investigated.

In chapter 6, a novel coupling chemistry was used to immobilize V_{HH}s, and in

this case the same chemistry could be used for oriented and random immobilization. V_{HH}s were engineered and functionalized with a non-natural amino acid to bear either one or five azide groups. Azide groups served as unique chemical handles on the V_{HH}s and were used to click proteins onto a cyclooctyne-modified surface in an oriented and random approach. Spectacular effects on biosensor sensitivity were observed when V_{HH}s were immobilized in an oriented manner.

Finally, in chapter 7, the main results of this thesis are summarized and remaining problems as well as ideas for future research are discussed.

1.8 References

1 LC Jr Clark, C Lyons *Annals of the New York Academy of Sciences.* 1962, 102, 29-45.

2 a) SJ Updike, GP Hicks *Nature.* 1967, 214, 986-988.
b) SJ Updike, GP Hicks *Science.* 1967, 158, 270-272.

3 T Vo-Dinh *Methods in Molecular Biology.* 2005, 300, 1-13.

4 Nanotechnology For Dummies, 2nd Edition *Publisher: Wiley / For Dummies.* ISBN: 978-0-470-89191-9

5 Z Nie, A Petukhova, E Kumacheva *Nature Nanotechnology.* 2010, 5, 15-25.

6 a) GA DeVries, M Brunnbauer, Y Hu, AM Jackson, B Long, BT Neltner, O Uzun, BH Wunsch, F Stellacci *Science.* 2007, 315, 358–361.
b) Z Nie, D Fava, E Kumacheva, S Zou, GC Walker, M Rubinstein *Nature Materials.* 2007, 6, 609–614.

7 a) S Park, JH Lim, SW Chung, CA Mirkin *Science.* 2004, 303, 348–351.
b) MS Nikolic, C Olsson, A Salcher, A Kornowski, A Rank, R Schubert, A Frömsdorf, H Weller, S Förster *Angewandte Chemie - International Edition.* 2009, 48, 2752–2754.

8 a) SY Park, AKR Lytton-Jean, B Lee, S Weigand, GC Schatz, CA Mirkin *Nature.* 2008, 451, 553–556.
b) CR Iacovella, SC Glotzer *Nano Letters.* 2009, 9, 1206–1211.

9 WF Smith *Nature Nanotechnology.* 2007, 2, 77-78.

10 Y Min, M Akbulut, K Kristiansen, Y Golan, J Israelachvili *Nature Materials.* 2008, 7, 527-538.

11 A Tinazli, J Piehler, M Beuttler, R Guckenberger, R Tampé *Nature Nanotechnology.* 2007, 2, 220-225.

12 VK Khanna *Sensor Review.* 2008, 28, 39-45.

13 J Xie, S Wang, L Aryasomayajula, VK Varadan *Nanotechnology.* 2007, 18, 1-9.

14 S Choi, M Gory, LYM Sin, PK Wong, J Chae *Microfluidics and Nanofluidics.* 2011, 10, 231–247.

15 a) CS Thaxton, R Elghanian, AD Thomas, SI Stoeva, J-S Lee, ND Smith, AJ Schaeffer, H Klocker, W Horninger, G Bartsch, CA Mirkin *PNAS.* 2009, 106, 18437–18442.
b) D Zhang, MC Huarng, EC Alocilja *Biosensors & Bioelectronics.* 2010, 26, 1736-1742.
c) JM Nam, S-J Park, CA Mirkin *Journal of the American Chemical Society.* 2002, 124, 3820-3821.

16 Y Zhang, T-H Wang *Theranostics.* 2012, 2, 631-654.

17 X Li, Y Zhou, Z Zheng, X Yue, Z Dai, S Liu, Z Tang *Langmuir.* 2009, 2, 6580-6586.

18 Environmental Sciences, 'Environmental Biosensors' *Publisher: InTech.*

ISBN 978-953-307-486-3, Chapter 8, Silicon and Silicon-Related Surfaces for Biosensor Applications.

19 RG Nuzzo, DL Allara *Journal of the American Chemical Society*. 1983, 105, 4481-4483.

20 R Maoz, J Sagiv *Thin Solid Films*. 1985, 132, 135.

21 DL Allara, RG Nuzzo *Langmuir*. 1985, 1, 45-52.

22 a) JC Love, LA Estroff, JK Kriebel, RG Nuzzo, GM Whitesides *Chemical Reviews*. 2005, 105, 1103-1169.
b) S Onclin, BJ Ravoo, DN Reinhoudt *Angewandte Chemie - International Edition*. 2005, 44, 6282-6304.

23 A Ulman *Chemical Reviews*. 1996, 96, 1533-1554.

24 a) RJ Walters, RVA van Loon, I Brunets, J Schmitz, A Polman *Nature Materials*. 2010, 9, 21-25.
b) Z Li, P Beck, DAA Ohlberg, DR Stewart, RS Williams *Surface Science*. 2003, 529, 410-418.

25 SP Murarkaa, SW Hymesa *Critical Reviews in Solid State and Materials Sciences*. 1995, 20, 87-124.

26 PE Laibinis, GM Whitesides, DL Allara, YT Tao, A Parikh, RG Nuzzo *Journal of the American Chemical Society*. 1991, 113, 7152-7167.

27 PE Laibinis, GM Whitesides *Journal of the American Chemical Society*. 1992, 114, 9022-9028.

28 SV Dzyadevych, AP Soldatkin, AV El'skaya, C Martelet, N. Jaffrezic-Renault *Analytica Chimica Acta*. 2006, 24, 248-258.

29 PJ Conroy, S Hearty, P Leonard, RJ O'Kennedy *Seminars in Cell Development and Biology*. 2009, 20, 10-26.

30 Y Lei, W Chen, A Mulchandani *Analytica Chimica Acta*. 2006, 24, 200-210.

31 C Hamers-Casterman, T Atarhouch, S Muyldermans, G Robinson, C Hamers, EB Songa, N Bendahman, R Hamers *Nature*. 1993, 363, 446–448.

32 MS Ardejani, NX Li, BP Orner *Biochemistry*. 2011, 50, 4029–4037.

33 RD Heselpoth, DC Nelson *Journal of Visualized Experiments*. 2012, 69, 4216.

34 J Cohen *Science*. 2001, 293, 237.

35 JA Johnson, YY Lu, JA Van Deventer, DA Tirrell *Current Opinions in Chemical Biology*. 2010, 14, 774–780.

36 a) J Homola, SS Yee, G Gauglitz *Sensors and Actuators B*. 1999, 54, 3-15.
b) J Homola *Analytical and Bioanalytical Chemistry*. 2003, 377, 528-539.

CHAPTER 2

Self-Assembled Functional Organic Monolayers on Oxide-Free Copper

ABSTRACT

The preparation and characterization of self-assembled monolayers on copper with *n*-alkyl and functional thiols was investigated. Well-ordered monolayers were obtained, while the copper remained oxide-free. Direct attachment of N-succinimidyl mercaptoundecanoate (NHS-MUA) onto the copper surface allowed for the successful attachment of biomolecules, such as β-d-glucosamine, the tripeptide glutathione, and biotin. Notably, the copper surfaces remained oxide-free even after two reaction steps. All monolayers were characterized by static water contact angle measurements, X-ray photoelectron spectroscopy, and infrared reflection absorption spectroscopy. In addition, the biotinylated copper surfaces were employed in the immobilization of biomolecules such as streptavidin.

This chapter was published as:
Mabel A. Caipa Campos, Anke K. Trilling, Menglong Yang, Marcel Giesbers, Jules Beekwilder, Jos M. J. Paulusse and Han Zuilhof *Langmuir.* 2011, 27, 8126–8133.

2.1 Introduction

The spontaneous organization of organic molecules adsorbed onto metallic (Au, Cu, Ag, Pt, Hg, and Pd) and semiconducting surfaces (Si, SiO_2, GaAs) has been extensively investigated.[1-3] Due to their high packing density, these so-called self-assembled monolayers (SAMs) enable the tailoring of surface properties such as wettability, friction, and adhesion. Moreover, functional moieties may be included, which allow for the development of biosensors and molecular electronics.[4, 5] In particular, self-assembled monolayers (SAMs) formed by chemisorption of thiols onto transition metal surfaces (e.g. Au, Ag, Cu, Zn) are among the most widely studied systems.[1] Due to its high chemical inertness, high affinity for thiols, and compatibility with cells, gold is the most widely employed metal.[6] Ever since the preparation of the first SAM on gold with organic disulfides by Nuzzo and Allara,[7] much research has focused on the modification of gold surfaces with alkanethiols and functional thiols.[3] Apart from gold surfaces, other metal surfaces such as nickel,[8, 9] zinc,[10, 11] iron,[12] silver,[13-15] and copper[14, 16, 17] may also form close-packed monolayers; however, these monolayers are more prone to oxidation. The monolayers so obtained present similar surface wetting properties as those reported for SAMs on gold. In addition, the incorporation of terminal functional groups (e.g. -OH, COOH, $-NH_2$, -CONHR)[13, 18-21] has been mainly demonstrated for gold alkanethiol SAMs, making these assemblies highly suitable for the manipulation of interfacial properties such as wettability, adhesion, and corrosion resistance,[22-24] the selective adsorption of proteins, the immobilization of cells, protein repellence, and microarray applications.[3] Moreover, provided that the alkyl chains are long enough, densely packed SAMs may be obtained, which serve as an excellent protection barrier against, for example, oxygen, water and aqueous ions.[25-28]

Copper metal is characterized by several outstanding properties, such as high thermal and electrical conductivity and high resistance to electromigration.[29, 30] In combination with its ready availability, it is generally the material of choice in replacing aluminum and gold as interconnecting materials in electronic circuits.[31] Although gold is more biocompatible than copper, gold is not semiconductor-compatible, preventing integration with commonly employed silicon. The diffusion of gold into silicon creates deep levels in the silicon band gap, which damages the carrier (electron and hole) properties of silicon-based semiconductor materials. On the contrary, copper is widely used for back-end metallization in silicon-based semiconductor process technology.[31] In contrast to these advantages, copper readily oxidizes upon exposure to air and is easily corroded in aqueous solutions, which drastically affects the functions and lifetime of integrated devices. These disadvantages may, in principle, be overcome by the formation of a passivating SAM.[3]

Laibinis and Whitesides[32] have performed seminal work in the field of self-assembled monolayers of alkanethiols on copper. Although these SAMs exhibit si-

milar wettability as SAMs on silver[33] and gold,[34-38] they differ significantly in chain conformation and surface roughness. Their studies revealed that the adsorbed species is a thiolate moiety, and in the case of copper surfaces, the hydrocarbon chain adopts a quasi-crystalline structure, where the chains are primarily extended in a nearly all-trans conformation and oriented close to the surface normal, at an angle of approximately 12°.[33] These monolayers on copper could in their experiments protect the metal from oxidation to a certain extent.[39, 40] The formation of SAMs on copper was, however, severely hampered by a lack of reproducibility resulting from the substrates' susceptibility toward oxidation upon exposure to air during sample preparation.[32, 33]

Over the past decade, several studies have described the development of new systems to protect the copper surface against oxidation, as well as the effects of copper surface oxidation on SAM quality.[41-48] Different etching procedures have been investigated, such as the use of a series of different etching solutions (aqueous solutions of HNO_3 and HCl) followed by several rinsing steps,[49] the electrochemical reduction of copper electrodes to remove the oxide layer prior to SAM formation,[50] as well as the addition of acetic acid to the thiol solution, which is suggested to act as an *in situ* etching agent during monolayer formation.[42] Employing these techniques in the fabrication of functional monolayers on large copper surfaces while maintaining their oxide-free nature remains challenging. Mechanistic studies and investigations into the stability of SAMs on copper upon exposure to air as a function of chain length also have been reported.[51, 52] The rate of oxidation of copper substrates was investigated by impedance and capacitance measurements, revealing that oxidation of copper is significantly slowed down at room temperature upon increasing alkanethiol chain length. It is suggested that oxidation of copper substrates affects surface roughness and perturbs the hydrocarbon lattice of the SAM into a less crystalline state.[39] In addition, comparative studies have been reported on the use of aliphatic thiols, dithiols, and dithiocarboxylic acids to form SAMs on copper. Although molecular order of the latter two systems is similar as observed for aliphatic thiols, these SAMs degrade rapidly.[53] Recent studies reported on the use of isoelectronic selenium as an alternative linking atom for SAM formation. These systems display greater adsorptivity than analogous thiols, but lower surface coverages were achieved.[54-57] Although it has been suggested that the rich chemistry to form functional monolayers on gold may also be extended to copper,[16, 33] the number of reports is still limited, evidencing the need for a robust and reproducible approach toward functional organic monolayers on copper while maintaining the copper substrate oxide-free, as is relevant for a variety of electronic biosensing schemes.

We describe here a facile and accessible wet-chemical route toward oxide-free copper surfaces, modified with alkanethiols and functional thiols, with carboxylic acid, N-hydroxysuccinimide, and alcohol moieties. Both the carboxylic acid and alcohol functional groups are characterized by their robustness, since they are not

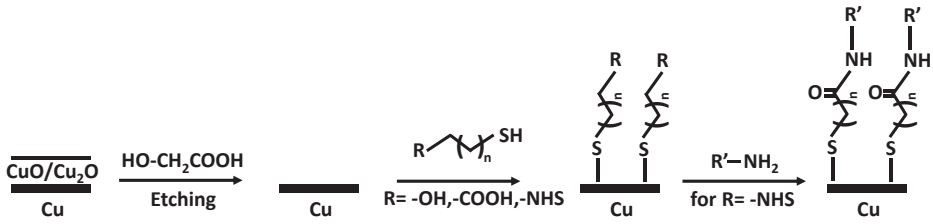

Figure 1. Biofunctionalization of oxide-free copper surfaces via functional thiols.

prone to degradation or side reactions. In addition, they present complementary reactivity, as the carboxylate group is easily activated toward further conjugation with nucleophiles such as amines, while alcohols readily react with a wide range of electrophiles. Hence, immobilizing these moieties onto a copper surface significantly increases its application potential. The activation of acid moieties with N-hydroxysuccinimide (NHS), employing conventional carbodiimide reagents such as 1-ethyl-3-[3-(dimethylamino)propyl]carbodiimide (EDC), has been frequently applied in the synthesis of biofunctional molecules,[58-60] as well as for the immobilization of amine-containing biomolecules on gold and silicon surfaces.[61, 62] Our group recently reported on the covalent one-step attachment of NHS ester functional monolayers onto silicon surfaces using mild photochemical methods, and further biofunctionalization of the resulting surfaces.[63] The successful facile modification of these silicon surfaces prompted us to employ this approach in the functionalization of copper surfaces with (bio)molecules (Fig. 1). Subsequently we detail the conjugation of these functional monolayers with a variety of amine-functional biomolecules while maintaining the copper surface oxide-free, and we present preliminary patterning data.

2.2 Results and Discussion

2.2.1 Monolayer Formation with Alkanethiols

In order to prepare monolayers on copper with alkyl- and functional thiols, the protective benzotriazole layer that is typically present on wafer-quality copper surfaces was first removed with an ethanolic solution of glycolic acid (70 wt %). The freshly etched substrates were immersed in neat thiols or in thiol-containing ethanol or toluene solution under an argon atmosphere for 16 h, as depicted in Figure 1.

Hydrophobic surfaces were obtained when employing *n*-decanethiol, as confirmed by the static water contact angle of 109°. These decanethiol monolayers on copper were further characterized by X-ray photoelectron spectroscopy (XPS) of freshly prepared samples. Wide-scan XPS spectra reveal the presence of copper, carbon, and sulfur, and importantly, no oxygen or nitrogen was observed. Under our experimental conditions, the oxygen content is already, with such short alkyl chains, below the

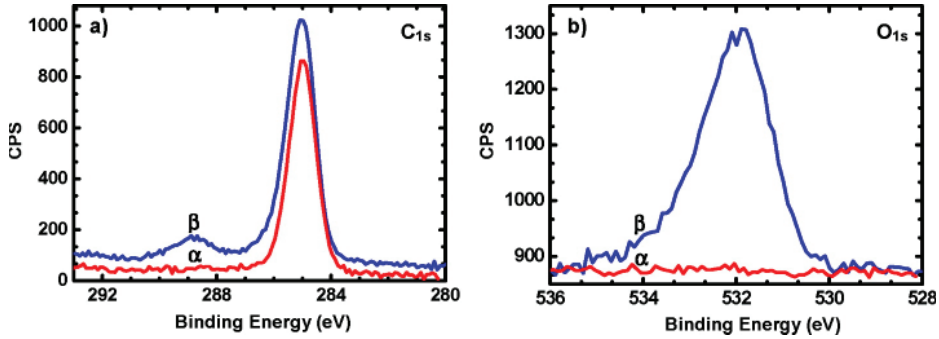

Figure 2. (a) XPS C_{1s} and (b) O_{1s} spectra of *n*-decanethiol (α) and mercaptoundecanoate (MUA) (β) self-assembled monolayers on copper.

detection limits, as observed from the O_{1s} XPS narrow scan of the 530–536 eV region (Fig. 2b). The absence of nitrogen confirms efficient removal of the protective layer of benzotriazole from the copper surface. The C_{1s} XPS narrow scan reveals the presence of carbon-bound carbon (C–C) at 285 eV (Fig. 2a). The absence of signals in the 165–168 eV region in the S_{2p} XPS narrow scan suggests that no oxidation of the thiol took place (Fig. S3, Appendix 1). Only a single spin–orbital doublet with a maximum at 162 eV is observed with an intensity ratio of 1:2, confirming the presence of thiolate bonds attached to the metallic substrate, similar to those reported for gold substrates.[65] When other etching solutions were employed, for instance, hydrochloric acid in ethanol (3.3 wt %), low percentages (in the order of 1%) of oxygen are observed from the wide-scan XPS (Fig. S10, Appendix 1). In addition, the O_{1s} XPS narrow scan in that case shows the presence of several oxidized copper species at 529.5, 530.4, and 531.0 eV and of water at 532.1 eV.[32]

The frequency shifts of the C–H stretching modes as obtained by infrared reflection absorption spectroscopy (IRRAS) provided more insight into the ordering of these monolayers.[66] These C_{10} alkyl monolayers on copper do not yet display a high degree of ordering as indicated by the CH_2 stretching vibrations (ν_{anti} = 2921 cm^{-1}; ν_{symm} = 2851 cm^{-1}), in line with observations of C_{10} thiols on Au. Increasing the length of the alkyl chain in the monolayer is known to increase van der Waals interactions and hence to enhance the ordering. Under the same experimental conditions but employing *n*-octadecanethiol, self-assembled monolayers on oxide-free copper were obtained as observed by XPS (Fig. S11, Appendix 1) and contact angle (110°) information. In addition, these copper monolayers are well-ordered as determined by IRRAS (ν_{anti} = 2918 cm^{-1}; ν_{symm} = 2849 cm^{-1}) (Fig. 3a), which is in good agreement with the analogous all-trans monolayers on gold (typically ν_{anti} = 2918 cm^{-1}; ν_{symm} = 2850 cm^{-1}).[25, 33, 67, 68] The signals at 2954 and 2870 cm^{-1} are assigned to the antisymmetric and symmetric C–H stretching vibrations of the terminal CH_3 group, respectively, as depicted in Figure 3a. This is in agreement with previous infrared studies carried

out on alkanethiols SAMs on copper. For $C_nH_{2n+1}SH$, where $n > 12$, hydrocarbon chains adopt all-trans configurations, with only low percentages of gauche conformers. As a result, well-ordered and more stable monolayers are obtained.[33, 39, 69]

The formation of high-quality monolayers depends on the concentration of the thiol as well as the reaction time. When the assembly reaction was conducted in neat *n*-decanethiol, similar Cu/C ratios (from XPS) were observed after 2 and 16 h (Fig. S2 and S3, Appendix 1). In both cases, the Cu surface displays no indication of oxidation. For solutions in ethanol (500 and 400 mM), only 2 h of reaction is required to reach the same Cu/C ratio (Fig. S4 and S5, Appendix 1). High-quality monolayers were also obtained when the reaction was carried out at a relatively low thiol concentration (50 mM), but the reaction then required 16 h to reach completion (Fig. S8, Appendix 1). At a thiol concentration of 10 mM, formation of the monolayer was not complete after 16 h, as inferred from the low C content in the XPS spectrum (Fig. S9, Appendix 1). This monolayer is also more prone to undergo oxidation, and only in this case the surface showed slight oxidation. A very small signal at 530 eV was observed in the O_{1s} XPS narrow scan, indicating the presence of traces of CuO and Cu_2O.[32]

2.2.2 Functional Monolayers on Oxide-Free Copper

The assembly of monolayers by use of functional thiols was examined next. To this purpose, 11-mercaptoundecanoic acid (MUA) and 10-mercaptodecanol (MD) were selected to be employed in monolayer formation (Fig. 1).

Monolayers were prepared by the same experimental procedure as described for alkanethiols (200 mM, 16 h). The monolayers were first characterized by static water contact angle measurements. Both the acid- and alcohol-terminated monolayers

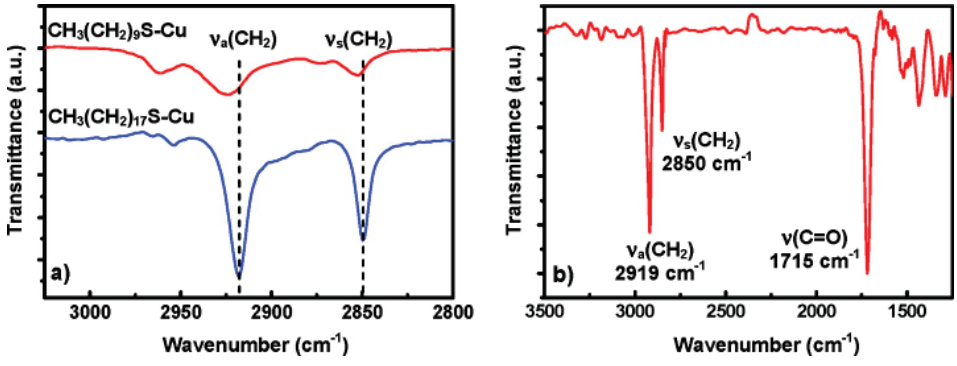

Figure 3. IRRA spectra of (a) *n*-decanethiol and *n*-octadecanethiol (expanded region) and (b) MUA monolayer on copper. The spectra have been offset vertically for clarity. Dashed vertical lines mark the position of the antisymmetric and symmetric $\nu(CH_2)$ mode.

yielded hydrophilic surfaces as confirmed by the respective contact angles of 40° [70] and 40°. These values are similar to what was measured by Laibinis and Whitesides,[16] but could not be reduced further by treatment with trifluoroacetic acid, as has successfully been developed for gold surfaces.[70] Monolayer formation on the copper substrates used may proceed less ideally than on gold samples, leading to a slightly lower packing density and concomitantly increased exposure to CH_2 moieties and higher contact angles. Wide-scan XPS spectra of the acid-terminated monolayer revealed the presence of sulfur and oxygen, while the C_{1s} XPS narrow scan revealed the presence of a COOH carbon atom at 289.2 eV (Fig. 2a), as well as two contributions at lower binding energies (286.0 and 285.0 eV), which are assigned to C–C=O and C–C carbon atoms, respectively (Fig. S12, Appendix 1). The ratio found (1.0:1.0:9.1) is in excellent agreement with the expected ratio (1:1:9). The S_{2p} XPS narrow scan displayed a relatively broad signal in the area of 162–164 eV, which was fit with a single spin–orbital doublet. The broad signal observed in the O_{1s} XPS narrow scan was deconvoluted into two components, which are assigned to the C=O (532.2 eV) and C–OH (533.7 eV) oxygen atoms of the carboxylic acid moiety.[71, 72] Importantly, the narrow scan does not indicate the presence of oxidized Cu atoms, since no signals in the area of 529–531 eV were observed. The IRRA spectrum (Fig. 3b) shows the characteristic C=O stretch of the acid moiety at 1715 cm^{-1} and the CH_2 stretch vibrations at 2919 cm^{-1} and 2850 cm^{-1}, confirming the formation of well-ordered monolayers on copper, as reported for similar monolayers on gold.[73-75] The alcohol-terminated monolayers showed comparable features as the acid-terminated monolayers (Fig. S13, Appendix 1). The S_{2p} XPS narrow scan also shows the presence of a single spin–orbital doublet, and no oxidation of the thiol was observed, since the O_{1s} XPS narrow scan only displays the alcohol signal at 532.6 eV. The C_{1s} XPS narrow scan revealed the presence of the C–O carbon atom at 286.5 eV, and the contribution at 285.0 eV is assigned to C–C carbon atoms. In addition, the ratio found (1.0:9.0) is in excellent agreement with the expected ratio (1:9), confirming the presence of the alcohol monolayer on copper.

2.2.3 NHS Ester-Terminated Monolayers

Aiming for facile conjugation of biomolecules, we investigated the single-step preparation of functional monolayers based on activated esters derived from N-hydroxysuccinimide (NHS). The corresponding monolayers were prepared from N-succinimidyl mercaptoundecanoate (NHS-MUA) in toluene (200 mM, 16 h) following the aforementioned experimental procedure. A hydrophilic monolayer was obtained as indicated by a static water contact angle of 55°, similar to the 52° obtained analogously on Si(111).[63] IRRAS demonstrated the presence of the NHS functionality by the characteristic C=O stretching vibrations at 1817, 1788, and 1745 cm^{-1},

corresponding to the ester carbonyl stretches (Fig. S15 and Table S1, Appendix 1).[63] Furthermore, the signals for the antisymmetric and symmetric CH_2 stretching vibrations observed at 2919 and 2850 cm^{-1}, respectively, again demonstrate the formation of a well-ordered monolayer. Wide-scan XPS data reveal the presence of sulfur and nitrogen, in agreement with the presence of NHS-MUA (Fig. S14, Appendix 1). The N_{1s} XPS narrow scan displays one signal at 402.4 eV, while the S_{2p} XPS narrow scan shows the characteristic spin–orbital doublet (163.9 and 162.6 eV), confirming the successful attachment of NHS-MUA to the copper surface. The C_{1s} XPS narrow scan further corroborates this attachment by the presence of the C=O carbon atom at 289.4 eV (Fig. 4a). The signal was deconvoluted into three components. The experimental ratio found for these three peaks is 9.4:2.8:2.8, which is in close agreement with the theoretical ratio of 9:3:3.[63]

In addition, the O_{1s} XPS narrow scan shows a signal at 535.2 eV, which is assigned to the oxygen of the C–O–N bond of the NHS moiety, and a signal at 532.8 eV that is assigned to the oxygen atoms of the carbonyl groups (Fig. 4b). Importantly, the experimental ratio found (3.1:0.9) indicates that, within experimental error, only O atoms that belong to the NHS-MUA monolayer are found. In addition, no O signals were observed with binding energies in the 529–531 eV range, again demonstrating the oxide-free nature of this copper surface.

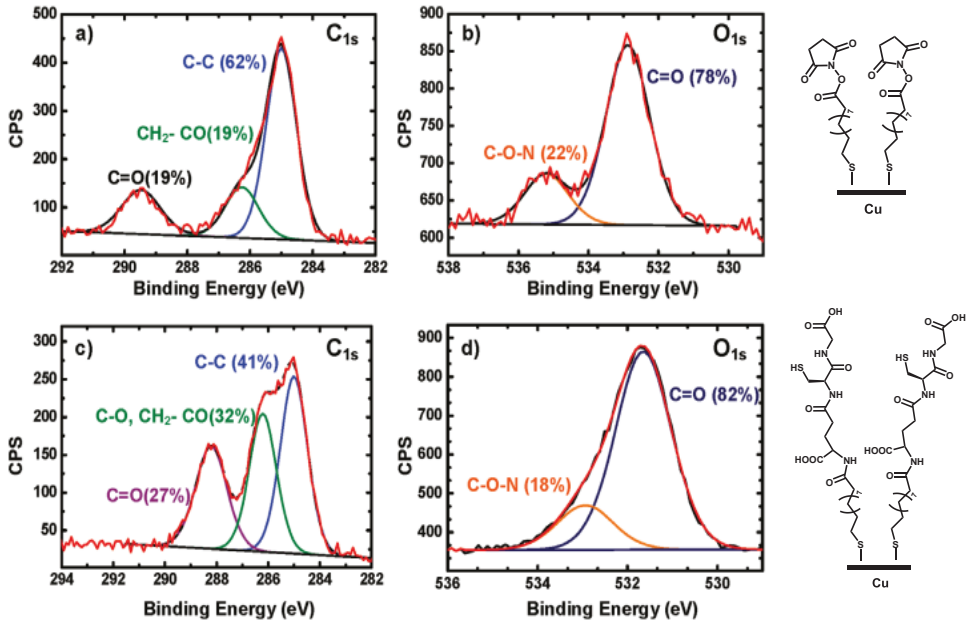

Figure 4. XPS C_{1s} and O_{1s} spectra of a NHS ester-terminated thiol monolayer on oxide-free copper (a, b), and of this monolayer after reaction with glutathione (c, d).

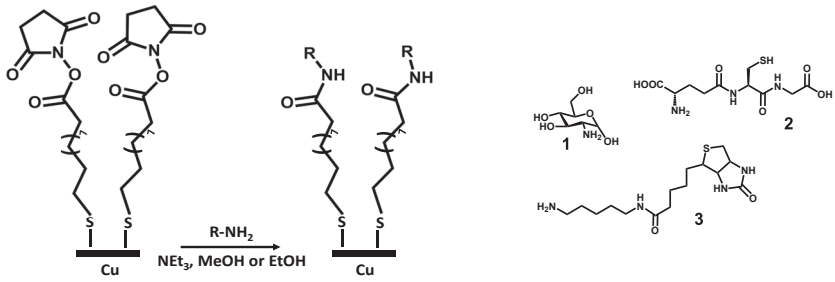

Figure 5. Functionalization of copper surfaces with biomolecules.

2.2.4 Bioconjugation Reactions

Essential in the development of new sensing devices is the selective capture of biomolecules. This can be achieved, for instance, by making use of complex sugars,[76, 77] peptides,[78] or oligo-DNA. After the successful attachment of NHS-MUA, the functionalization of these monolayers with various amines was investigated. Conjugation reactions were carried out at room temperature by immersion of the NHS-functional copper substrates in alcoholic solutions containing the respective amine, as well as triethylamine, under an argon atmosphere at room temperature (Fig. 5).

The reaction of β-d-glucosamine (1) with the NHS ester-terminated monolayer was investigated first. A water contact angle of 76° was measured for the functionalized substrate, indicating the formation of a hydrophilic monolayer, though less hydrophilic than the original NHS-MUA monolayer (55°). The C_{1s} XPS narrow scan displays a broad signal at 288.5 eV due to contributions from unreacted NHS-MUA as well as the newly formed amide bond (Fig. S16, Appendix 1). Shifting of the N signal in the N_{1s} XPS narrow scan to lower binding energies (from 402.4 to 400.0 eV) confirms the formation of an amide bond. A surface coverage of 50% was calculated on the basis of the C_{1s} narrow scan spectrum. Importantly, the S_{2p} XPS narrow scan and the S/Cu ratio did not change, indicating that the Cu–S bond was not affected by the conjugation reaction. In addition, the O_{1s} XPS narrow scan displays a broad signal, but no additional signals were observed in the area of 529–531 eV, demonstrating that the conjugation of the amine did not induce oxidation of the Cu surface.

The versatility of the conjugation approach was further explored for the tripeptide glutathione (Glu-Cys-Gly) (2) as a model peptide. Considering the steric bulk of this tripeptide, a relatively high conversion of 40% was achieved as determined from the C_{1s} XPS narrow scan (Fig. 4c). The O_{1s} XPS narrow scan shows a broad signal, due to the contributions of several different types of oxygen atoms (Fig. 4d). However, again no additional signals were observed in the area of 529–531 eV, confirming the oxide-free nature of the Cu surface (Fig. S17, Appendix 1). After exposure to air under ambient conditions for several hours, the surface was analyzed again by XPS and revealed no significant changes in the C_{1s} and O_{1s} narrow scans. IRRAS analysis

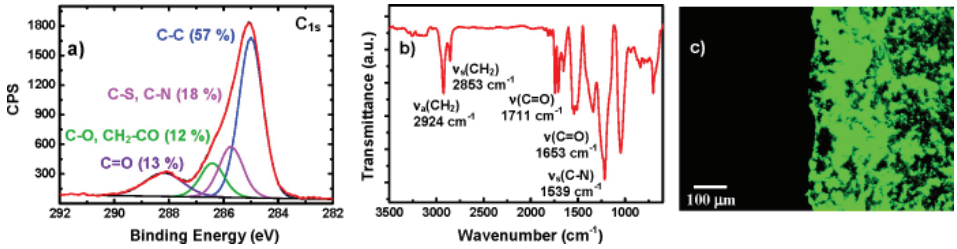

Figure 6. (a) XPS C_{1s} and (b) IRRA spectra of the biotinylated copper surface; (c) attachment of fluorescently labeled streptavidin.

confirmed the presence of the amide moieties at 1742 cm^{-1} as well as the carboxylic acid at 1659 cm^{-1} (Fig. S18 and Table S2, Appendix 1).[79] The antisymmetric C–H stretching vibration is shifted to higher frequencies (2921 cm^{-1}) as compared to the CH_2 stretching vibrations of the NHS ester monolayer (2919 cm^{-1}), suggesting that the alkyl chains become slightly disordered, as can be expected given the fact that the monolayer is now topped with a mixture of amides and unreacted NHS moieties.

Biotinylation provides for a versatile yet highly specific approach toward the attachment of complex biomolecules such as antibodies, via the biotin–streptavidin interaction.[80] Hence, biotin was immobilized onto the copper substrate, by reaction of the NHS ester-terminated monolayer with 5-(biotinamido)pentylamine (3). Successful attachment was confirmed by the narrow scan XPS C_{1s} spectrum, which displayed both biotin and residual NHS ester moieties; careful analysis revealed a biotin yield of 30% (Fig. 6a). The O_{1s} XPS narrow scan corroborated the oxide-free nature of the Cu surface (Fig. S19, Appendix 1). The biotinylated copper surface was characterized by IRRAS. Characteristic signals for the biotin C=O stretching vibrations are observed at 1711 and 1653 cm^{-1}, which correspond to the ureido ring and the amide bonds, respectively (Fig. S20 and Table S4, Appendix 1). The antisymmetric and symmetric C–H stretching vibrations are shifted to higher frequencies (2924 and 2853 cm^{-1}, respectively), as a result of the steric bulk of the biotin moieties that hamper a 100% substitution of the densely packed NHS groups and thus disrupt monolayer ordering.

2.2.5 Binding of Streptavidin

The immobilization of proteins was investigated for the biotinylated copper surface and the tetrameric protein streptavidin. Due to its exceptionally high binding affinity toward biotin and easy functionalization of biomolecules, this well-known streptavidin–biotin system has been applied in a wide variety of diagnostic assays and tagging of molecules for imaging.[80, 81] The biotinylated copper surface was incubated with Alexa Fluor 635-labeled streptavidin in phosphate-buffered saline (PBS, pH 8.0) for 1 h. Confocal laser scanning microscopy was used to visualize the at-

tachment of streptavidin onto the biotinylated surface. Exposure of a part of the biotinylated surface to streptavidin resulted in successful local attachment of the protein as shown in Figure 6c, showing that contact patterning techniques will be easily applicable to this modified surface.

2.3 Conclusion

A variety of alkanethiols and functional thiols was successfully employed in the preparation of SAMs on copper while maintaining the substrate oxide-free. Detailed characterization demonstrated that these monolayers are well-ordered and are readily employed as a platform in the surface attachment of biomolecules. NHS ester-terminated monolayers were conjugated with different amine-functional biomolecules, and in all cases high surface coverages were achieved, while the oxide-free nature of the copper substrate was maintained. The successful attachment of biotin to the copper surface and its binding to streptavidin offers a promising approach toward the immobilization of biomolecules, whereas the use of copper greatly facilitates the implementation of this technique in the development of new biosensors. Current research efforts focus on the applicability of this approach in the binding of target biomolecules such as peptides, antibodies, and DNA to these self-assembled monolayers on copper.

2.4 Materials and Methods

2.4.1 General Information

All materials were obtained from Aldrich and used as received, unless noted otherwise. 5-(Biotinamido)pentylamine was purchased from Thermo Fisher Scientific, and streptavidin (Alexa Fluor 635 conjugate) was from Invitrogen. Dichloromethane, ethanol, and methanol were distilled before use. Toluene (HPLC grade) was stored over 4 Å activated molecular sieves. Nuclear magnetic resonance (^{1}H and ^{13}C NMR) spectra were recorded on a Bruker Avance III 400 MHz spectrometer at room temperature. Chemical shifts are reported in parts per million (δ) relative to $CHCl_3$ (7.26 ppm for ^{1}H and 77.2 ppm for ^{13}C) as internal reference. Static water contact angles were measured with an automated Krüss DSA 100 goniometer under ambient conditions. Small droplets of 3.0 μL deionized water (18.3 MΩ·cm resistivity) were dispensed with a microsyringe. The error in the contact angles is ±1°. X-ray photoelectron spectroscopy (XPS) measurements were performed on a Jeol JPS-9200 system using a standard Al Kα source with X-ray power of 300 W, analyzer pass energy of 10 eV, and energy resolution of <0.65 eV. All C_{1s} (C–C) peaks were calibrated to binding energies of 285.0 eV. Infrared reflection absorption spectroscopy (IRRAS) measurements were collected with a Bruker

spectrometer (model Tensor 27) equipped with liquid-nitrogen-cooled mercury–cadmium–telluride (MCT) detector using a commercial variable-angle reflection unit (Auto Seagull, Harrrick Scientific). A Harrick grid polarizer was placed in front of the reflection unit and was used for measuring spectra with p-polarized (parallel) radiation at an incident angle of 85° with respect to the normal of the sample surface. Single channel transmittance spectra were taken at a resolution of 2 cm^{-1} with 2048 scans and were referenced to a clean copper crystal, sample size 2 × 2 cm. The fluorescence images were recorded on a Zeiss Axiovert 200 M inverted microscope for transmitted light and epifluorescence equipped with a 633 nm laser. Selected images were captured with a 40× or 10× objective. Contrast optimization and color scale of the fluorescence images were performed employing Zen 2008 software.

2.4.2 Synthesis of N-Succinimidyl Mercaptoundecanoate (NHS-MUA)

This compound was synthesized from 11-mercaptoundecanoic acid (MUA) and N-hydroxysuccinimide (NHS) via the standard N,N′-dicyclohexylcarbodiimide (DCC) coupling reported by Warner and co-workers.[64] Under argon atmosphere, MUA (4.8 g, 0.022 mol) was dissolved in dry dioxane (100 mL). To this solution, NHS (2.90 g, 0.025 mol) and DCC (5.22 g, 0.025 mol) were added portionwise. The solution was cooled down to 0 °C and stirred for 2 h. The suspension formed was further stirred at room temperature (rt) for 16 h. The solid was filtered off and the solution was concentrated by rotary evaporation. The resulting residue was purified by column chromatography on silica gel (eluted with ethyl acetate and *n*-heptane, 50:50). The desired compound was isolated as a crystalline powder in 80% yield (5.50 g, 0.017 mol) and a purity of 99.8% (GC-MS). ^{1}H NMR (400 MHz, $CDCl_3$): δ 2.84 (br s, 4 H, $NCOCH_2$), 2.63 (t, J = 7.6 Hz, 2 H, CH_2–C=O), 2.54 (q, 2 H, CH_2-SH), 1.73–1.77 (m, 2 H, CH_2), 1.59–1.61 (m, 2 H, CH_2–CH_2–SH), 1.30–1.40 (m, 12 H, CH_2). ^{13}C NMR (100 MHz, $CDCl_3$): δ 169.11 (N–C=O), 168.64 (C=O), 34.01 (CH_2–CH_2–SH), 30.88 (CH_2–SH), 29.93 (CH_2), 29.21 (CH_2), 29.00 (CH_2), 28.98 (CH_2), 28.72 (CH_2), 28.32 (CH_2), 25.58 ($NCOCH_2$), 24.62 (CH_2), 24.54 (CH_2).

2.4.3 Preparation of Organic Monolayers on Oxide-Free Copper

Polycrystalline copper, electroplated on a silicon substrate, polished by chemo-mechanical polishing (CMP) and coated with benzotriazole (BTA) as a corrosion inhibitor (470–600 nm layer thickness, NXP Semiconductors, The Netherlands), was used as copper source. Samples of copper (1 × 1 cm) were sonicated for 20 min in acetone (semiconductor grade) in an Elma S-40 Elmasonic sonicator. The samples were etched in an argon-saturated 10 % solution of EKC 570 (copper-compatible post-etch residue remover from DuPont, consisting of 70 wt % of glycolic acid in ethanol) in dry ethanol for 5 min under argon. The substrates were washed with dry ethanol (20

mL) and dried with a stream of dry argon. Alkanethiols, neat or in solution (at concentrations ranging from 10 to 500 mM in dry EtOH) were poured in a small three-neck flask equipped with a capillary (for the argon inlet). The solution was degassed for 30 min by bubbling argon through the capillary. The freshly etched Cu substrate was transferred, while maintaining the copper substrate under continuous flow of argon (underneath a tube with argon flowing out), to the reaction flask. After addition of the substrate, the capillary was moved away from the solution to avoid disturbing the forming monolayer. The reaction flask was kept at room temperature with a low argon flow for the indicated time. The copper substrate was removed from the solution, rinsed with dichloromethane, and sonicated for 10 min (in CH_2Cl_2) before being dried with a stream of dry argon. The same experimental procedure was employed for the modification of copper surfaces with functional thiols (MD, MUA, NHS-MUA). In all cases, 200 mM solutions in dry toluene (2.0 mL) were employed, as this was found to give optimum monolayer quality. The modified copper substrates were characterized by static water contact angle measurements, XPS and IRRAS. The formation of these monolayers is fully reproducible, but only if all modification steps are performed under argon and all samples are stored under vacuum or argon to prevent oxidation of the copper surface.

2.4.4 Conjugation Reactions

In a small three-neck flask equipped with a capillary (for the argon inlet), a solution containing triethylamine (0.1 mL) and the dry amine (0.1 M) in MeOH or EtOH (1.9 mL) was degassed for 30 min by bubbling argon through the capillary. To this solution, a freshly functionalized (NHS-MUA) copper substrate (previously washed with dry toluene and dried with a stream of argon) was added. After the solution was bubbled with argon for 5 min, the capillary was moved away. The reaction flask was kept at room temperature for 16 h under argon. The copper substrates were rinsed and sonicated with dry ethanol and dried with a stream of argon. The modified copper substrates were characterized by static water contact angle measurements and XPS and IRRAS.

2.4.5 Binding of Fluorescently Labeled Streptavidin

A freshly biotinylated surface was rinsed with dry ethanol and dried with a stream of argon. Subsequently, the copper substrate was immersed in a solution containing 0.5 mg/mL fluorescently labeled streptavidin (excitation 633 nm, emission 647 nm) in phosphate-buffered saline (PBS; 137 mM NaCl, 2.7 mM KCl, 10 mM Na_2HPO_4 and 2 mM KH_2PO_4, pH 8.0) for 1 h at room temperature. The copper substrate was dried with a stream of argon and rinsed with Tween-20 solution (5.0 mL, 0.05% in PBS, pH 8.0) and 5.0 mL of PBS. The copper substrate was dried with a

stream of dry argon before characterization by confocal fluorescence microscopy.

2.5 ACKNOWLEDGEMENTS

This research was financially supported by MicroNed, funded by the Dutch Ministry of Economic Affairs (project C-II) (to M.A.C.C.), by the EU through the Marie Curie ITN Project Hierarchy (Contract PITN-2007-215851) as well as IPOP (The Wageningen UR strategic research program BioNanotechnology 2007–2011) (to A.K.T.), and by NXP Semiconductors (postdoctoral fellowship to M.Y.); NXP is also thanked for generous supply of Cu wafers. Finally, Barend van Lagen, Dimitri Ershov, and Radostina Manova (Wageningen University) and Dr. Frans Widdershoven (NXP) are kindly acknowledged for stimulating discussions and instrumental assistance.

2.6 REFERENCES

1 F Schreiber *Progress in Surface Science*. 2000, 65, 151-256.
2 A Salomon, D Cahen, S Lindsay, J Tomfohr, VB Engelkes, CD Frisbie *Advanced Materials*. 2003, 15, 1881-1890.
3 JC Love, LA Estroff, JK Kriebel, RG Nuzzo, GM Whitesides *Chemical Reviews*. 2005, 105, 1103–1169 and references therein.
4 A Sassolas, BD Leca-Bouvier, LJ Blum *Chemical Reviews*. 2008, 108, 109-139.
5 I Ron, L Sepunaru, S Itzhakov, T Belenkova, N Friedman, I Pecht, M Sheves, D Cahen *Journal of American Chemical Society*. 2010, 132, 4131-4140.
6 A Ulman *Chemical Reviews*. 1996, 96, 1533–1554.
7 R Nuzzo, D Allara *Journal of American Chemical Society*. 1983, 105, 4481-4483.
8 Z Mekhalif, J Riga, J Pireaux, J Delhalle *Langmuir*. 1997, 13, 2285-2290.
9 Z Mekhalif, F Laffineur, N Couturier, L Delhalle *Langmuir*. 2003, 19, 637-645.
10 AR Noble-Luginbuhl, RG Nuzzo *Langmuir*. 2001, 17, 3937-3944.
11 H Zhang, S Baldelli *Journal of Physical Chemistry B*. 2006, 110, 24062- 24069.
12 M Volmer, M Stratmann, H Viefhuis *Surface and Interface Analysis*. 1990, 16, 278-282.
13 CED Chidsey, CR Bertozzi, TM Putvinski, AM Mujsce *Journal of American Chemical Society*. 1990, 112, 4301-4306.
14 PE Laibinis, CD Bain, GM Whitesides *Journal of Physical Chemistry*. 1991, 95, 7017-7021.
15 PE Laibinis, MA Fox, JP Folkers, GM Whitesides *Langmuir*. 1991, 7, 3167-3173.
16 PE Laibinis, GM Whitesides *Journal of American Chemical Society*. 1992, 114, 1990-1995.
17 G Li, H Ma, Y Jiao, S Chen *Journal of the Serbian Chemical Society*. 2004, 69, 791-805.
18 JJ Hickman, D Ofer, PE Laibinis, GM Whitesides, MS Wrighton *Science*. 1991, 252, 688-691.
19 DM Collard, MA Fox *Langmuir*. 1991, 7, 1192-1197.
20 CED Chidsey *Science*. 1991, 251, 919-922.
21 SV Atre, B Liedberg, DL Allara *Langmuir*. 1995, 11, 3882-3893.
22 GM Whitesides, PE Laibinis *Langmuir*. 1990, 6, 87-96.

23 CD Bain, GM Whitesides *Journal of American Chemical Society*. 1988, 110, 5897-5898.
24 A Ulman, SD Evans, Y Shnidman, R Sharma, JE Eilers, JC Chang *Journal of American Chemical Society*. 1991, 113, 1499-1506.
25 MD Porter, TB Bright, DL Allara, CED Chidsey *Journal of American Chemical Society*. 1987, 109, 3559-3568.
26 KA Groat, SE Creager *Langmuir*. 1993, 9, 3668-3675.
27 FP Zamborini, JK Campbell, RM Crooks *Langmuir*. 1998, 14, 640-647.
28 P Srivastava, WG Chapman, PE Laibinis *Langmuir*. 2009, 25, 2689-2695.
29 K Iguchi, A Tachibana *Applied Surface Science*. 2000, 159, 167-173.
30 J Rickerby, JHG Steinke *Chemical Reviews*. 2002, 102, 1525-1550.
31 SP Murarka, SW Hymes *Critical Reviews in Solid State and Materials Sciences*. 1995, 20, 87-124.
32 PE Laibinis, GM Whitesides *Journal of American Chemical Society*. 1992, 114, 9022-9028.
33 PE Laibinis, GM Whitesides, DL Allara, YT Tao, AN Parikh, RG Nuzzo *Journal of American Chemical Society*. 1991, 113, 7152-7167.
34 PE Laibinis, JJ Hickman, MS Wrighton, GM Whitesides *Science*. 1989, 245, 845-847.
35 CD Bain, J Evall, GM Whitesides *Journal of American Chemical Society*. 1989, 111, 7155-7164.
36 CD Bain, EB Troughton, YT Tao, J Evall, GM Whitesides *Journal of American Chemical Society*. 1989, 111, 321-335.
37 L Strong, GM Whitesides *Langmuir*. 1988, 4, 546-558.
38 CD Bain, GM Whitesides *Angewandte Chemie - International Edition*. 1989, 101, 522-528.
39 GK Jennings, JC Munro, TH Yong, PE Laibinis *Langmuir*. 1998, 14, 6130-6139.
40 GK Jennings, JC Munro, PE Laibinis *Advanced Materials*. 1999, 11, 1000-1003.
41 J Rodriguez, J Kim, J Hanson, M Perez, A Frenkel *Catalysis Letters*. 2003, 85, 247-254.
42 D Hutt, C Liu *Applied Surface Science*. 2005, 252, 400-411.
43 E Abelev, D Starosvetsky, Y Ein-Eli *Langmuir*. 2007, 23, 11281-11288.
44 E Abelev, D Starosvetsky, Y Ein-Eli *Electrochimica Acta*. 2007, 52, 1975-1982.
45 I Platzman, R Brener, H Haick, R Tannenbaum *Journal of Physical Chemistry C*. 2008, 112, 1101-1108.
46 I Platzman, C Saguy, R Brener, R Tannenbaum, H Haick *Langmuir*. 2010, 26, 191-201.
47 F Caprioli, F Decker, AG Marrani, M Beccari, VD Castro *Physical Chemistry Chemical Physics*. 2010, 12, 9230-9238.
48 F Caprioli, M Beccari, A Martinelli, VD Castro, F Decker *Physical Chemistry Chemical Physics*. 2009, 11, 11624-11630.
49 Y Feng, WK Teo, KS Siow, Z Gao, KL Tan, AK Hsieh *Journal of Electrochemical Society*. 1997, 144, 55-64.
50 R Haneda, K Aramaki *Journal of Electrochemical Society*. 1998, 145, 1856-1861.
51 CA Calderon, C Ojeda, VA Macagno, P Paredes-Olivera, EM Patrito *Journal of Physical Chemistry C*. 2010, 114, 3945-3957.
52 MM Sung, K Sung, CG Kim, SS Lee, Y Kim *Journal of Physical Chemistry B*. 2000, 104, 2273-2277.
53 J Denayer, J Delhalle, Z Mekhalif *Journal of Electroanalytical Chemistry*. 2009, 637, 43-49.

54 A Shaporenko, A Ulman, A Terfort, M Zharnikov *Journal of Physical Chemistry.* 2005, 109, 3898-3906.

55 LV Protsailo, WR Fawcett, D Russell, R Meyer *Langmuir.* 2002, 18, 9342-9349.

56 G Fonder, J Delhalle, Z Mekhalif *Applied Surface Science.* 2010, 256, 2968-2973.

57 MH Dishner, JC Hemminger, FJ Feher *Langmuir.* 1997, 13, 4788-4790.

58 TP Sullivan, WTS Huck *Europeen Journal of Organic Chemistry.* 2003, 1, 17-29.

59 Bioconjugate Techniques, 2nd edition *Publisher: Academic Press/Elsevier: Burlington, MA,* 2008; pp 169179.

60 Surface Plasmon Resonance: Methods and Protocols; Springer Protocols: Methods in Molecular Biology, Vol. 627; *Publisher: Humana Press: Totowa, NJ,* 2010; pp 5573.

61 J Lahiri, L Isaacs, J Tien, GM Whitesides *Analytical Chemistry.* 1999, 71, 777-790.

62 T Bocking, M James, HGL Coster, TC Chilcott, KD Barrow *Langmuir.* 2004, 20, 9227-9235.

63 M Yang, RLM Teeuwen, M. Giesbers, J Baggerman, A Arafat, FA de Wolf, JCM van Hest, H Zuilhof *Langmuir.* 2008, 24, 7931-7938.

64 J Macossay, S Shamsi, I Warner *Tetrahedron Letters.* 1999, 40, 577-580.

65 M Wirde, U Gelius, L Nyholm *Langmuir.* 1999, 15, 6370-6378.

66 IR Hill, IW Levin *Journal of Chemical Physics.* 1979, 70, 842-851.

67 CED Chidsey, DN Loiacono *Langmuir.* 1990, 6, 682-691.

68 PE Laibinis, RG Nuzzo, GM Whitesides *Journal of Physical Chemistry.* 1992, 96, 5097-5105.

69 P Srivastava, WG Chapman, PE Laibinis *Journal of Physical Chemistry B.* 2009, 113, 456-464.

70 The acid-terminated monolayer on copper was also formed in the presence of trifluoroacetic acid (TFA); however, this procedure also gave a relatively high contact angle (~40°), in contrast to prior work by Jiang and co-workers for the analogous acid-terminated monolayer on gold, which reported a contact angle <10°; H Wang, S Chen, L Li, S Jiang *Langmuir.* 2005, 21, 2633-2636.

71 AD Vogt, T Han, TP Jr Beebe *Langmuir.* 1997, 13, 3397-3403.

72 EB Troughton, CD Bain, GM Whitesides, RG Nuzzo, DL Allara, MD Porter *Langmuir.* 1988, 4, 365-385.

73 JP Folkers, PE Laibinis, GM Whitesides *Langmuir.* 1992, 8, 1330-1341.

74 CE Jordan, BL Frey, S Kornguth, RM Corn *Langmuir.* 1994, 10, 3642-3648.

75 H Saavedra, C Thompson, J Hohman, V Crespi, P Weiss *Journal of American Chemical Society.* 2009, 131, 2252-2259.

76 S Park, M Lee, S Pyo, I Shin *Journal of American Chemical Society.* 2004, 126, 4812-4819.

77 M Kohn, R Wacker, C Peters, H Schroder, L Soulere, R Breinbauer, CM Niemeyer, H Waldmann *Angewandte Chemie - International Edition.* 2003, 42, 5830-5834.

78 E Ostuni, BA Grzybowski, M Mrksich, CS Roberts, GM Whitesides *Langmuir.* 2003, 19, 1861-1872.

79 M Bieri, T Burgi *Langmuir.* 2005, 21, 1354-1363.

80 NM Green *Advances in Protein Chemistry.* 1975, 29, 85-133.

81 PC Weber, DH Ohlendorf, JJ Wendoloski, FR Salemme *Science.* 1989, 243, 85-88.

CHAPTER 3

Antibody Orientation on Biosensor Surfaces: a Minireview

ABSTRACT

Detection elements play a key role for analyte recognition in biosensors. Therefore, detection elements with high analyte specificity and binding strength are required. While antibodies (Abs) have been increasingly used as detection element in biosensors, a key challenge remains the immobilization on the biosensor surface. This minireview highlights recent approaches to immobilize and study Abs on surfaces. We first introduce Ab species used as detection elements, and discuss techniques recently used to elucidate Ab orientation by determination of layer thickness or surface topology. Then, several immobilization methods will be presented: non-covalent and covalent surface attachment, yielding oriented or random coupled Abs. Finally, protein modification methods applicable for oriented Ab immobilization are reviewed with an eye to future application.

This chapter was published as:
Anke K. Trilling, Jules Beekwilder and Han Zuilhof. *Analyst.* 2013, 138, 1619-1627.

3.1 Introduction

In the last decade, a wide variety of different biosensors emerged. Sensor specificity relies strongly on the properties of the immobilized detection element, which has stimulated the use of antibodies (Abs) or fragments thereof. In 1971,[1] Abs were used for the first time in an enzyme-linked immunosorbent assay (ELISA) to quantitatively detect analytes. Nowadays, antigen–Ab interactions can be detected by a variety of techniques, including quartz crystal microbalance (QCM), surface plasmon resonance (SPR) and electrochemical impedance spectroscopy (EIS).

Abs with better affinities and higher stabilities have been selected to improve biosensor performance. Further sensor optimization was directed towards surface preparation of biosensors aiming to promote specific binding and suppress non-specific binding. For this purpose site-specific coupling and immobilization of proteins are of great interest.[2–4]

Here, we review recently applied Ab immobilization strategies. In the field of proteins, Abs represent a small class of glycoproteins with a well-defined structure. Since Abs possess only one binding site, it can be highly advantageous to orient these molecules to improve biosensor performance, with improvement factors as high as 220 being reported upon orientation.[5] Similar, albeit smaller, effects have also been reported by several other groups.[6–14] The first section of this minireview presents different types of Abs applied as detection elements. Next, methods are reviewed that are used to elucidate the orientation of immobilized Abs. Then, various recently applied non-covalent and covalent methods for Ab immobilization are summarized, including oriented and random immobilization of both native and engineered Ab species. Finally, we explore to what extent protein modification techniques have already been implemented for Abs, and where new opportunities open up to bring the advantages of protein orientation closer to application in future biosensors.

3.2 Abs as Detection Elements

There are several types of Ab structures that are currently being focused on in biosensing (Fig. 1). Immunoglobulin Gs (IgGs, 150 kDa, 143 x 77 x 40 Å^3)[15] consist of two light and two heavy chains, linked by disulfide bonds to form the characteristic Y-shape. The chains are divided into constant (C) and variable (V) regions. On the second heavy chain constant region (C_H2), IgGs have carbohydrate moieties (Fig. 1).[16] The variable domain bears three hypervariable regions, known as complementarity-determining regions (CDRs), which are responsible for the specific Ab–antigen interaction. The diversity in this area allows the endless supply of Abs with different specificity and binding strength (affinity).

Molecular engineering enabled the minimization of conventional Abs into smaller and more stable Ab-derived fragments. Examples include Fabs (antigen bin-

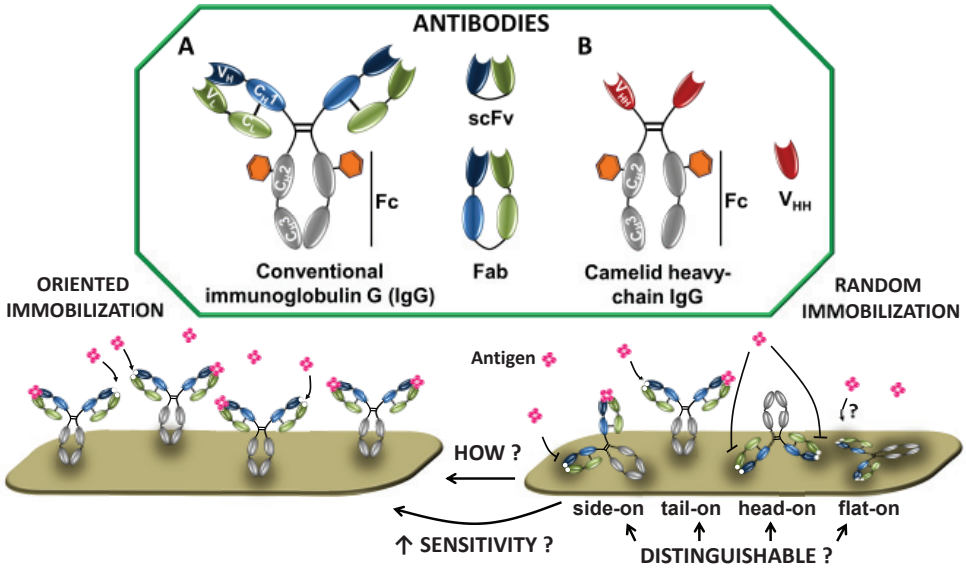

Figure 1. Schematic depiction of natural Abs. (A) Immunoglobulin G (IgG) consists of 2 heavy chains (gray/blue) and 2 light chains (green). Antigens bind to the variable regions V_L and V_H. The C_H2 domain bears a carbohydrate moiety (orange hexagon); scFv = single-chain variable fragment composed of V_L and V_H; Fab = antigen binding Ig fragment. (B) Camelid heavy-chain Ab contains only 2 heavy chains, which are composed of one variable (V_{HH}; antigen-binding unit) and two constant (C_H2 and C_H3) domains. Abs can be immobilized in an oriented or random fashion (see example for IgG).

ding fragment), or the even smaller single-chain variable fragments (scFv, 27 kDa), both of which still retain antigen-binding specificity. Further size reduction into monomeric single domain Abs (sdAbs), the V_H or V_L, resulted in loss of affinity towards the antigen,[17] making time-consuming selection and affinity maturation necessary.

Apart from IgGs, two other Ab classes are becoming important. First, camelid Abs (found in dromedary, llama, alpaca and camel) (Fig. 1).[18] These Abs lack the light chain and the first constant domain of the heavy chain (C_H1), leaving one single domain for effective antigen binding, known as V_{HH} or nanobody. In V_{HH}, the C-terminus is situated at the opposite site of the antigen binding region and represents an optimal target for functionalization. Second, another novel immunoglobulin with one variable domain (V_{NAR}), called novel antigen receptor (IgNAR), was discovered in cartilaginous fish, such as sharks.[19]

V_{HH}, V_{NAR} and sdAbs possess superior stability, and are highly soluble, small (15 kDa) monomeric binding domains that are very useful as detection elements in biosensors. Their value for biotechnological applications has been recently reviewed.[20–22] Antigen-specific Ab fragments can be selected from large libraries by a variety of methods, reviewed in the literature.[23,24]

3.3 Techniques to Study Antibody Orientation

Providing information of Ab orientation on the surface is of fundamental interest. Immobilized IgG can adopt four exemplary molecular orientations: side-on (one Fc and one Fab attached to the surface), tail-on (Fc attached to the surface), head-on (both Fabs attached to the surface) or flat-on (all three fragments attached to the surface) (Fig. 1). For the highest analyte binding, Abs should display free antigen-binding regions after immobilization. Controlling the orientation will therefore lead to better analyte binding resulting in improved biosensor sensitivity.

Many techniques have been used to elucidate the presence and binding function of immobilized Abs. Fourier transform infrared reflection (FTIR) spectroscopy is used to characterize the presence of specific chemical groups, and various fluorescence microscopies help to visualize efficient binding of analyte to Ab-functionalized surfaces.[25,26] In fact, spectroscopic techniques are predominately used to roughly confirm an effective Ab orientation, with only a relatively small set of studies that investigate the orientation of Abs by comparing Abs immobilized in different directions. For example, SPR can be used to calculate the Ab coverage, and the relationship between the adsorbed amount and molecular orientation on the surface has been used earlier to distinguish between tail/head-on and side/flat-on orientation.[27] But minimal direct information about Ab orientation can be deduced with such approaches. Here we present a selection of the techniques recently applied to characterize Ab orientation in a more direct manner by measuring the layer thickness or by scanning of the surface (Fig. 2). It should be kept in mind that this list is not comprehensive, that it focuses due to space considerations on a few representative recent cases, and that each of these techniques still provides only limited information; to get the full picture, several techniques are ideally combined.

3.3.1 Atomic Force Microscopy (AFM)

In atomic force microscopy (AFM), surfaces are scanned by a nano-scale tip, immobilized at the end of a cantilever, yielding resolutions below a nanometer. 3-D structures of soft biomaterials such as proteins can be visualized by AFM, resulting in a topographical surface map.[28] From this information, local properties of the surface such as the degree of coverage, the thickness of the layer, and the shape of the proteins can be deduced (Fig. 2).

AFM is often used to deduce Ab orientation by determining the dimensions of the Abs. Sarkar and co-workers[29] employed non-contact mode AFM to measure the total thickness of a surface coating before and after immobilization of IgG onto a protein A-coated surface. The measured change of height after IgG incubation corresponded roughly to the long axis of IgG, suggesting tail-on position of IgG.[30] Chen et al.[27] used AFM to measure the height of the Ab layer immobilized on a calixare-

ne monolayer to distinguish between tail-on and side-on orientation. AFM has also been used to investigate Ab orientation by scanning 5 nm Au nanoparticles on surfaces as size standard,[31] and to measure the width of the IgG arms.[32]

Likewise, AFM can be used to elucidate the surface topology. Kim et al.[33] compared the surface roughness of Abs captured by cysteine-functionalized protein G (Cys-protein G) to that of a surface that captured Abs by native protein G. The more uniform height image obtained for Cys-protein G-modified surfaces was interpreted

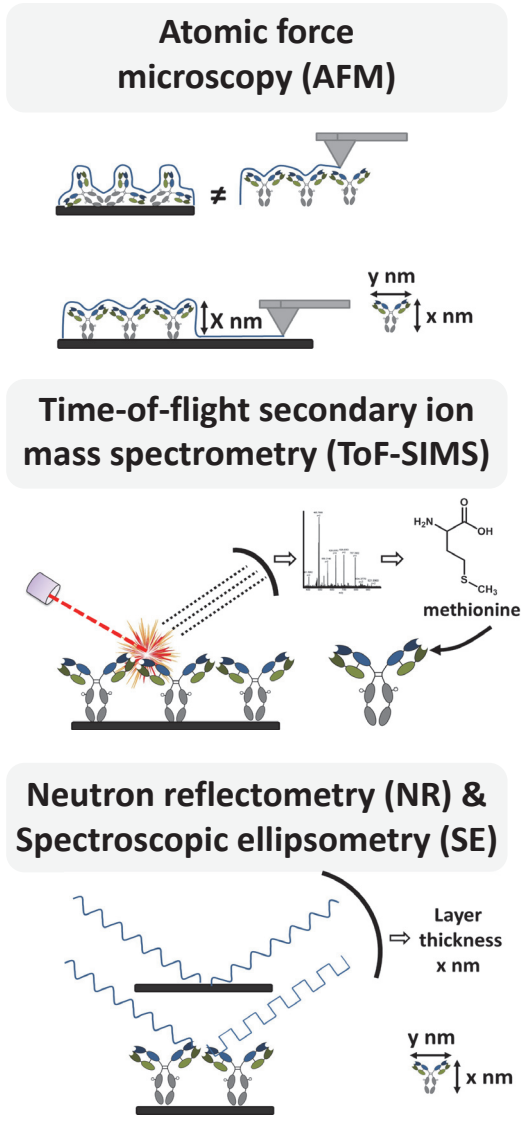

Figure 2. Selection of techniques to study antibody orientation. For detailed information see text.

as more uniformly oriented Abs. AFM was also used to study the time-dependent conformational change of Fabs immobilized on gold in the absence and presence of stabilizing polyethylene glycol (PEG) layers.[34] Directly immobilized Fab fragments showed a fast decrease in height accompanied by a decrease of the antigen-binding ability. In contrast, Fabs stabilized by the PEG layer displayed a diminished height decrease and better antigen binding abilities, suggesting a slowed down change of conformation or/and orientation by the co-immobilized PEG-layer.

3.3.2 Time-of-Flight Secondary Ion Mass Spectrometry (ToF-SIMS)

High-resolution time-of-flight secondary ion mass spectrometry (ToF-SIMS) emerged as a powerful method to obtain evidence about the structure of the surface by providing biophysical information about the molecular structure. This technique combines a high chemical specificity with a good surface sensitivity (sampling depth 1–3 nm) by ion bombardment of a surface with a pulsed primary ion beam.[35] The resulting positively or negatively charged ions are analyzed by a time-of-flight mass analyzer, yielding a fingerprint of the proteins (Fig. 2). As the sampling depth is very shallow, these data can be used to interpret the orientation of immobilized proteins, and the more recently developed milder bombardments with Ar clusters may improve this further.

ToF-SIMS was used by Baio et al.[7] to show intensity differences of secondary ions originating from asymmetrically located amino acids in the protein. Distinct orientations of a variable fragment (HuLys Fv) were achieved on two different substrates – each reacting with a specific, tailor-made moiety at one of the termini. Comparison of the intensity ratios of specific secondary ions suggested that HuLys Fv was indeed oriented in different ways on the two different substrates, although it is difficult to specify any of these orientations based on the data. In another study ToF-SIMS was used to characterize the orientation of randomly biotinylated and site-specifically biotinylated Abs (IgGs, $F(ab')_2$ and Fabs) on streptavidin surfaces.[8] ToF-SIMS results could not be linked to specific locations near the analyte binding site of site-specific biotinylated Abs, but unique peaks were observed in oriented Abs that were absent in randomly immobilized controls. This indicated that sites-pecific and randomly biotinylated Abs were assembled in distinct orientations. The data analysis can be greatly facilitated by principal component analysis (PCA), as shown in an analogous study by the group of Lee.[36] They showed that random biotinylated IgGs at high concentrations yield the same ToF-SIMS spectra as site-specific biotinylated IgGs. This suggests that with high concentrations orientation was achieved for both biotinylated Abs. At the same time Liu et al.[37] showed that head-on orientation (by immobilizing protein A on the surface) can be distinguished from tail-on orientation (by immobilizing the antigen on the surface) of immobilized Abs by combining ToF-SIMS with PCA. Amino acids characteristic of the Fab and Fc fragments could

be used to provide an image ´map` of Ab orientations across the patterned surfaces.

3.3.3 Dual Polarization Interferometry (DPI)

Dual polarization interferometry (DPI), an optical wave-guide based analytical technique, can be used to obtain information on molecular dimensions (layer thickness), packing (layer refractive index, density) and stoichiometry (mass). The measured layer thickness can provide information on the arrangement of Abs on surfaces when combined with known dimensions of the molecule.

Song et al.[38] used dimensions of Abs as determined by X-ray crystallography in correlation with layer thickness and surface coverage (or mass) to distinguish between possible Ab orientations. The surface coverage of random immobilized Abs on a monolayer and oriented Abs on protein G surfaces was determined by DPI and compared to the reference values of ´theoretical` saturated surface coverages for random and oriented Abs. Tail-on orientation of IgG Abs on a protein G layer was further suggested by determining the layer thickness by DPI, which revealed a thickness of the Ab layer on protein G corresponding to the long axis of the Y-shaped Ab.

3.3.4 Neutron Reflectometry (NR)

Neutron reflectometry (NR) is a neutron diffraction technique to determine the thickness and composition of molecular layers on surfaces with a sensitivity of 2–3 Å.[39] The technique involves directing a beam of neutrons onto a flat surface, and measurement of the intensity of the reflected radiation as a function of angle or neutron wavelength. Comparison of layer thickness with the molecular dimensions of Abs allows differentiation between flat-on, side-on and head-on/tail-on orientations of the Abs (Fig. 2).

Using NR Zhao et al.[40] determined the orientation of Abs adsorbed on silicon wafers at low concentration. The observed thickness of adsorbed Abs corresponded to the short axial length of the Ab, suggesting a flat-on orientation. In contrast, Abs immobilized via the Fc region onto an engineered protein A-like (ZZctOmpA) surface adopt a tail-on orientation.[15]

3.3.5 Spectroscopic Ellipsometry (SE)

Spectroscopic ellipsometry (SE) analyses the state of polarized light reflected from multilayer reflective samples. The layer thickness can be deduced by a model-based analysis based on how the light interacts with the surface (Fig. 2). This makes SE a valuable tool to investigate optical parameters and deposition kinetics of thin film structures.

Bae et al.[41] determined the thickness of protein layers consisting of Abs bound to thiolated protein G oriented on gold. The measured thickness suggested that Abs are immobilized in such a manner that the Fc domain is bound to the protein G surface.

3.4 Immobilization Strategies

Strategies for immobilization may result in specific or random orientation of the Abs. The orientation is dependent on the self-organizing capacity of the antibodies, which may be steered by specific reactive groups on the surface, on the antibody, or on both. Specific orientation of immobilized Abs is not easily achieved, since Abs usually carry several copies of reactive groups.

It is essential to immobilize Abs on surfaces without changing their binding activity and specificity. Therefore immobilization strategies should be mild. These strategies can usually be made compatible with the surfaces of various materials, by functionalizing the surface with specific groups. Surfaces can be used either directly or functionalized with (mono)layers, either as two-dimensional surfaces or as three-dimensional matrices. Gold, glass, copper, silicon nitride and silicon surfaces or magnetic beads represent only a small selection of surfaces used for Ab immobilization.[29,32,42–45] Below we will review several strategies of Ab immobilization. They can be distinguished by non-covalent or covalent coupling chemistry.

3.4.1 Non-covalent Immobilization

Immobilization of untreated Abs can be mediated by an intermediate protein directly coupled to the surface, such as protein A and protein G. These proteins display five and two binding domains specific to the Fc portion of Abs, respectively. This results predominantly in tail-on orientation. Improvement of biosensor performance by orienting Abs with protein A or protein G has been shown in several studies when compared to their randomly immobilized counterparts.[10,25,26,43,46] Further improvements have been achieved by orientation of protein A or G. Feng et al.[47] optimized the approach by forming highly organized aggregates of IgG and protein A. Immobilized IgG-protein A aggregates yielded three-dimensional structures on the surface with IgGs exposing their analyte binding sites. Johnson and Mutharasan[48] showed that the pH used for protein G adsorption on gold surfaces influences the protein G orientation and subsequent Ab binding. Often, exposed Cys residues are used for oriented immobilization of protein A or G. Thiolated protein G was used for immobilization onto a copper surface.[42] Lee et al.[49] prepared cysteine-functionalized protein G multimers to improve Ab immobilization on magnetic silica nanoparticles. Recombinant Cys-protein G trimers were engineered by repeated linking of protein G monomers via a flexible linker. The use of such Cys-protein G trimers improved

Ab immobilization and enhanced the biosensor sensitivity by 10-fold compared to a Cys-protein G monomer setup. Brun et al.[15] fused protein A domains genetically to a Cys-exposing variant of *E. coli* protein OmpA, which was embedded in a PEG monolayer on a gold surface, and allowed oriented binding and presentation of antibodies. Ko et al.[50] fused a gold-binding protein (GBP) to protein A, resulting in GBP–ProtA. Compared to native protein A, this fusion protein self-assembled at a higher density on gold surfaces and bound more IgG. Tajima et al.[11] enzymatically conjugated protein A onto a substrate to achieve a ´super-oriented IgG` bound to oriented protein A. The strict control of the IgG orientation resulted in an approximately 100-fold higher affinity than the partially oriented IgG, when protein A was physisorbed on the surface.

Classically, non-covalent binding of Abs on surfaces is achieved by physical adsorption, avoiding an intermediate protein. Making use of ionic bonds, electrostatic and hydrophobic interactions and van der Waals forces results in non-covalent immobilization. Physical adsorption gives low control over the orientation of the Abs, even though immobilization of Abs using a pneumatic nebulizer is fast and reproducible.[51] Zhao et al.[52] studied how solution pH, salt concentration and surface chemistry affect Ab adsorption onto silica surfaces. The salt concentration and pH did influence the amount of adsorbed Ab and analyte binding, but did not influence the orientation of immobilized Abs. Abs predominantly adopted flat-on orientation on the investigated surfaces. Um et al.[53] introduced tail-on orientation in bound Abs by the electrochemical immobilization onto poly-(2-cyano-ethylpyrrole)-coated gold electrodes. Induction by cyclic voltammetry favored electrostatic interactions between the cyano group on the surface and the hydroxyl group of the Ab present in the Fc region. Electrochemically immobilized Abs showed an improved analyte binding compared to physisorbed Abs, which was attributed to orientation effects. Abs adsorbed on hydroxyapatite nanoparticles mainly orient themselves in the tail-on position due to steric hindrance on the round surface.[54] The group of Harmsen[14] showed improved orientation of adsorbed V_{HH}s due to genetic fusion of peptide tags to the C-terminus, situated opposite to the analyte binding site. It was suggested that these tags trigger oriented binding on polystyrene surfaces by hydrophobic interactions with the surface. Nevertheless, physical interactions are generally weak and sensitive to changes in condition such as pH, temperature or salt concentration. Typically, biosensors using non-covalent binding may therefore suffer from poor analytical performance due to lower operational and storage stability. Specific directional interactions between the surface and part of the Ab therefore provide a step forward, and are an intermediate towards covalent and fully irreversible immobilization. As an example, a more stable immobilization resulting in orientation can be achieved when the thiol group is utilized for Ab immobilization on surfaces such as gold. Disulfide bonds are a common feature of intact Abs and thiol groups can

be obtained under mild reduction conditions (Fig. 3). Balevicius et al.[55] showed that oriented Ab fragments can bind 2.5 times more analyte than the intact Ab immobilized in a random fashion using amine groups. An elegant light-assisted approach for Ab immobilization was shown by Ventura et al.[56] Disulfide bonds were broken upon absorption of UV light by nearby aromatic amino acids, yielding reactive thiol groups that are effective for oriented binding onto gold electrodes.

Adsorption of thiol-exposing Fab fragments onto gold was also used to show that co-immobilization of densely packed polyethylene glycol layers improved the time-dependent analyte binding ability of immobilized Fab fragments.[34] Albeit being site-specific, this method yields monovalent Abs, and too harsh reduction conditions might inactivate Ab fragments due to the unintentional reduction of internal disulfide bonds. Another immobilization method introducing orientation involves the fusion of a polyhistidine (His_6) affinity-tag on the C- or N-terminus of the recombinant protein. The His_6 tag shows a high affinity ($K = 10^7\ M^{-1}$) to Ni^{2+}, Co^{2+} and Cu^{2+} surfaces. The tetradentate ligand nitriloacetate (NTA) forms hexagonal complexes with divalent metal ions, leaving two binding sites available for chelation with a histidine residue. The His_6 tag on the C-terminus of a variable fragment (HuLys Fv) was used to control orientation onto a gold substrate.[7] When compared to HuLys Fv immobilized onto maleimide-terminated monolayers via an N-terminal cysteine, binding via the C-terminal His_6 tag to Ni-loaded NTA-terminated monolayers showed a 10-fold higher SPR signal upon analyte binding. However, because the binding affinity of the His_6 tag is for several approaches still not high enough, these experiments might suffer from undesired protein dissociation.

Stronger non-covalent protein immobilization can be achieved by the use of the streptavidin–biotin interaction, one of the strongest non-covalent interactions known in biology. Depending on the applied biotinylation method, Abs can be immobilized in a random or oriented fashion. Abs randomly biotinylated at the amine groups were compared to oriented Abs, site-specifically biotinylated at the hinge region.[36] With increased immobilization concentration both biotinylated Abs adopted tail-on orientation, while site-specific biotinylated IgG became oriented at a slightly faster rate. Cho et al.[8] compared the binding signal of random and site-specific biotinylated IgG and Fab on distinct streptavidin-coated surfaces. In a sandwich-type immunoassay, the group reported a 2 to 3 times higher binding signal for site-specifically biotinylated Ab species. Several other approaches to add a biotin moiety site-specifically to Abs have been employed lately. Biotinylation specifically at the C-terminus of the Ab was achieved using the enzyme carboxypeptidase Y.[57] Kang and co-workers[58] achieved site-specific biotinylation of Abs using a sugar moiety. Oxidation of sugar chains yielded aldehydes reactive towards hydrazine-biotin. Further, in vivo biotinylation of V_{HH} was successfully explored by our group using the Avi-tag.[5] This tag is recognized by the BirA enzyme, and biotinylation occurs at the lysine position of the tag. This in vivo biotinylation is somewhat time consuming, but is also extre-

mely effective as it improved the analyte binding by more than a 200-fold.

3.4.2 Covalent Immobilization

Covalent immobilization does, in principle, provide the best entry point to combine longevity of the Ab-modified surface with a high sensitivity due to a specific orientation. Therefore, a lot of efforts are currently undertaken to investigate and improve this area, including both by now well-known reactions of naturally present moieties and the developments of tailor-made, i.e. man-made, modifications thereof.

So far the chemistry deployed to immobilize Abs has been limited to classical protein chemistries. Amine (NH_2) groups present in the lysine amino acid side-chain on the Ab surface can be used for covalent immobilization in a random fashion (Fig. 3). Widely used, e.g. for SPR studies, is the immobilization of Abs onto carboxymethylated dextran layers on gold surfaces.[5,46,55] Recently, it has been shown that this immobilization is not completely random. Prior to covalent conjugation, Abs need to undergo physisorption. Orientation during physisorption depends on the surface pKa, isoelectric point of the Ab and the pH of the used immobilization buffer, by optimizing the conditions one orientation can be favored.[59,60] By attaching antibodies via the amine group to protein-repellent zwitterionic polymer brushes Nguyen et al.[44] prepared surfaces recognizing the antigen while preventing non-specific adsorption of other proteins. Epoxide-functionalized polymer brushes allow another possibility to immobilize Abs via the amine group.[61] Similarly, immobilization via the amine group can be achieved by the use of glutaraldehyde-functionalized surfaces.[13,26]

Another covalent approach to orientation makes use of a unique carbohydrate moiety at the Fc part of Abs (Fig. 3). Specific oxidation on the carbohydrate vicinal hydroxyl group via the use of periodate sodium generates aldehydes. These aldehydes are reactive towards aminated surfaces[13] or hydrazine-functionalized dendrimers on surfaces,[62] resulting in oriented covalent Ab coupling. Ho et al.[63] used a boronic acid presenting surface to orient Abs via the carbohydrate moiety. Boronic acids form cyclic boronate esters with 1,2- and 1,3-diols present in carbohydrates of Abs, and thus provide an additional anchoring point, with chemistry that is largely orthogonal to other methods discussed in here.

Also the Fc region itself is used for oriented immobilization. Batalla et al.[64] used heterofunctionally activated agarose matrices displaying metal chelate groups. These lead to oriented non-covalent attachment of the Ab via the histidine rich Fc portion of the Ab. Then, reaction of exposed amine groups with matrix-bound glyoxyl groups was promoted by a change of pH. The formed reversible Schiff's base bonds can then be mildly reduced by e.g. $NaB(CN)H_3$ to obtain irreversible oriented and covalently attached Abs. Another possibility to immobilize Abs via the Fc part makes use of intermediate proteins described before. To circumvent stability prob-

lems of the non-covalent interaction between protein A/protein G and the Fc region, chemical crosslinking was successfully applied using cyanamide,[65] dimethyl pimelimidate (DMP)[66] or the homobifunctional linker bis(sulfosuccinimidyl) suberate.[38] Analogously, thiol groups were explored for covalent oriented coupling of Abs, via reduction of the disulfide group present in the hinge region of Abs (Fig. 3), and subsequent coupling to a maleimide-functionalized surface.[67]

Another possibility to covalently immobilize Abs in an oriented manner makes use of the conserved nucleotide binding site (NBS) present in the conserved region of the variable domain of all Ab isotypes. This region, which has not been removed so far from the antigen-binding site, is rich in specific aromatic amino acids, and displays an affinity for indole-3-butyric acid. Exposure to 254 nm light allows irreversible photo-cross-linking of Abs onto an indole-3-butyric acid-terminated surface, while leaving the antigen binding site unaffected.[68]

These examples show the success of covalently attached Abs, but also point to the potential of using and developing milder (non-denaturing), bio-orthogonal reactions that allow control over the Ab direction. Today, protein coupling can be achieved by a range of highly reliable chemistries. However, most of these have not been deployed for Abs since they rely on protein engineering and recombinant production. Currently, bioorthogonal chemistries such as Diels–Alder reaction or Staudinger ligation are widely applied for protein immobilization or functionalization, but

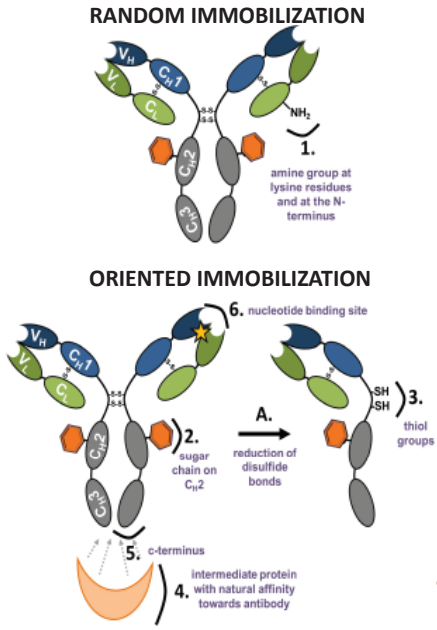

		reacted with:
1.	**amine group**	carboxy-methylated dextran layers[5, 46]
		glutaraldehyde exposing surfaces[13, 26]
		epoxide-functionalized polymer brushes[61]
		NHS-activated biotin*[36]
2.	**sugar chain**	boronic acid presenting surfaces[63]
	oxidated sugar chain (reactive aldehyde)	hydrazine-biotin*[58]
		aminated surfaces[13]
		hydrazine-functionalized dendrimers on surfaces[62]
3.	**C-terminus**	enzyme yielding biotinylation*[57]
4.	**intermediate protein**	protein A and G (non-covalent) [6, 9, 15, 25, 26, 42, 43, 46, 47, 49, 50]
		protein A and G, then chemical-crosslinking (covalent)[38, 65, 66]
5.	**thiol group**	gold[34, 55, 56]
		maleimide-functionalized biotin*[36]
		maleimide-functionalized surfaces[7]
6.	**nucleotide binding site**	Indole-3-butyric acid followed by photo-cross-linking with UV-light[68]

*followed by immobilization on streptavidin-functionalized surfaces

		reduced with:
A.	**disulphide bond**	2-mercaptoethanol[55]
		UV-light adsorption by nearby aromatic amino acids[56]

Figure 3. Functional groups used for random and oriented Ab immobilization onto surfaces.

functional groups are often introduced via the amine group of lysine side-chains or the thiol group of cysteines, making such approaches unsuitable for the site-specific immobilization of Abs. Here we will limit the discussion to a selection of methods that would lead to site-specific introduction of functional groups.

Stamos et al.[69] immobilized various proteins site specifically via the Diels–Alder cycloaddition reaction[70] between an O-iminoquinone group in the protein and an acryloyl linker on the surface. To this end, site-specific genetic incorporation of the 3-NH_2Tyr amino acid into proteins was performed.

The Staudinger ligation reported by Saxon and Bertozzi involves the reaction between an azide and a phosphine containing ester or thioester yielding a covalent amide bond.[71] Introduction of a functional azide-group into the protein can be achieved by the use of the methionine analogue azidohomoalanine.[72] Unfortunately, this approach is only site-specific if no more than one methionine is surface accessible. To guarantee specificity, engineering of the protein is often required. Another technology to truly site-specifically incorporate azides was developed by the group of Schulz.[73] Functionally unique unnatural amino acids such as p-azido-L-phenylalanine can be incorporated into proteins such as green fluorescent protein by expressing orthogonal tRNAs and aminoacyl-tRNA synthetases.[74] Using this approach azides can be incorporated into antibodies in response to amber nonsense codons at the preferred protein position. Another approach to introduce an azide specifically at the N- or C-terminus uses expressed protein ligation (EPL).[75] EPL generates recombinant protein thioesters by thiolysis of intein fusion proteins reactive towards synthetic peptides bearing an N-terminal cysteine, which yields a native amide bond. EPL has been employed in combination with a synthetic azide-containing reagent to produce azide-functionalized RNase A (azido-RNase A).[76] Azido-RNase A was then site-specifically immobilized onto phosphine-terminated surfaces by a Staudinger ligation.

Sulfonylazides react with terminal alkynes under the catalysis of Cu(I) to form N-acylsulfonamides. This ´click sulfonamide reaction` (CSR)[77,78] is related to the Cu(I)-catalyzed [3 + 2] azide–alkyne cycloaddition (CuAAC). Both reactions displayed specificity during protein immobilization using alkyne-modified mCerry-Ypt7 protein (at the C-terminus by ELP) on sulfonylazide- and azide-functionalized surfaces, respectively.[79] A potential disadvantage of CuAAC is the used copper(I) catalyst. In contrast, the strain-promoted alkyne–azide cycloaddition (SPAAC) with cyclooctynes requires no additional reagent, but reacts spontaneously with azides. Different cyclooctyne variants used for surface functionalization and/or bioconjugation have been reviewed.[80–82] Taking advantage of these mild and bioorthogonal reactions will most likely open up new approaches for the site-specific immobilization of Abs on surfaces. For example, Witte et al.[83] prepared anti-GFP V_{HH} with azide or cyclooctyne moieties at the C-terminus using a combined shortage-click strategy to prepare V_{HH} dimers. Such functionalized V_{HH}s could also be covalently immobilized using

SPAAC onto cyclooctyne- or azide-functionalized surfaces, respectively.

3.5 Outlook

The approaches for Ab immobilization as presented in this chapter show that a wide variety of immobilization methods are available for various surfaces and different Ab species. However, the variety of available methods also illustrates that a universal method is not yet available.

The limited amount of studies in which oriented Ab immobilization was quantitatively compared to random Ab immobilization shows that orientation can significantly (up to two orders of magnitude) improve the analyte binding signal. Therefore, the ever increasing demands in sensitivity should lead future efforts to oriented immobilization of Abs. The currently most widely used method, adsorption onto protein-coated surfaces, is effective, but also limited given the heterogeneous nature of such surfaces. Further improvements in orientation and therefore likely in sensor sensitivity will require involvement of tailor-made Ab modifications and/or novel bioorthogonal surface-bound or Ab-directed chemistries. Specifically the ongoing exploration in protein coupling techniques is expected to hold significant promises for the field of Ab orientation in the future.

3.6 References

1 E Engvall, P Perlmann *Immunochemistry*. 1971, 8, 871-874.
2 P Jonkheijm, D Weinrich, H Schröder, CM Niemeyer, H Waldmann *Angewandte Chemie - International Edition.* 2008, 47, 9618-9647.
3 PC Lin, D Weinrich, H Waldmann *Macromolecular Chemistry and Physics.* 2010, 211, 136-144.
4 K Hernandez, R Fernandez-Lafuente *Enzyme and Microbial Technology.* 2011, 48, 107-122.
5 AK Trilling, MM Harmsen, VJB Ruigrok, H Zuilhof, J Beekwilder *Biosensors & Bioelectronics.* 2013, 40, 219-226.
6 A Kausaite-Minkstimiene, A Ramanaviciene, J Kirlyte, A Ramanavicius *Analytical Chemistry*. 2010, 82, 6401-6408.
7 JE Baio, F Cheng, DM Ratner, PS Stayton, DG Castner *Journal of Biomedical Materials Research Part A.* 2011, 97, 1-7.
8 IH Cho, JW Park, TG Lee, H Lee, SH Paek *Analyst.* 2011, 136, 1412-1419.
9 M Park, J Jose, JC Pyun *Sensors and Actuators B.* 2011, 154, 82-88.
10 G Shen, C Cai, K Wang, J Lu *Analytical Biochemistry*. 2011, 409, 22-27.
11 N Tajima, M Takai, K Ishihara *Analytical Chemistry*. 2011, 83, 1969-1976.
12 G Yoo, M Park, EH Lee, J Jose, JC Pyun *Analytica Chimica Acta.* 2011, 707, 142-147.
13 Y Yuan, M Yin, J Qian, C Liu *Soft Matter.* 2011, 7, 7207-7216.
14 MM Harmsen, HPD Fijten *Journal of Immunoassay and Immunochemistry*. 2012, 33, 234-251.
15 AP Le Brun, SA Holt, DSH Shah, CF Majkrzak, JH Lakey *Biomaterials.* 2011, 32,

3303-3311.
16 EM Yoo, KR Chintalacharuvu, ML Penichet, SL Morrison *Journal of Immunological Methods*. 2002, 261, 1-20.
17 CA Borrebaeck, AC Malmborg, C Furebring, A Michaelsson, S Ward, L Danielsson, M Ohlin *Biotechnology*. 1992, 10, 697-698.
18 TAC Hamers-Casterman, S Muyldermans, G Robinson, C Hammers, E Bajyana-Songa, N Bendahman, R Hammers *Nature*. 1993, 363, 446-448.
19 AS Greenberg, D Avila, M Hughes, A Hughes, EC McKinney, MF Flajnik *Nature*. 1995, 374, 168-173.
20 L Huang, S Muyldermans, D Saerens *Expert Review of Molecular Diagnostics*. 2010, 10, 777-785.
21 D Saerens, L Huang, K Bonroy, S Muyldermans *Sensors*. 2008, 8, 4669-4686.
22 CAK Borrebaeck, C Wingren *Methods in Molecular Biology*. 2011, 785, 247-262.
23 PJ Conroy, S Hearty, P Leonard, RJ O'Kennedy *Seminars in Cell & Developmental Biology*. 2009, 20, 10-26.
24 X Zeng, Z Shen, R Mernaugh *Analytical and Bioanalytical Chemistry*. 2012, 402, 3027-3038.
25 TQ Huy, NTH Hanh, NT Thuy, PV Chung, PT Nga, MA Tuan *Talanta*. 2011, 86, 271-277.
26 TQ Huy, NTH Hanh, PV Chung, DD Anh, PT Nga, MA Tuan *Applied Surface Science*. 2011, 257, 7090-7095.
27 H Chen, J Huang, J Lee, S Hwang, K Koh *Sensors and Actuators B*. 2010, 147, 548-553.
28 PJM Murphy, M Shannon, J Goertz *Journal of Visualized Experiments*. 2011, 53, 1-5.
29 P Dutta, S Sawoo, N Ray, O Bouloussa, A Sarkar *Bioconjugate Chemistry*. 2011, 22, 1202-1209.
30 MC Coen, R Lehmann, P Gröning, M Bielmann, C Galli, L Schlapbach *Journal of Colloid and Interface Science*. 2001, 233, 180-189.
31 LR Farris, MJ McDonald *Analytical and Bioanalytical Chemistry*. 2011, 401, 1-9.
32 S Kumar, R Ch, D Rath, S Panda *Materials Science and Engineering C*. 2011, 31, 370-376.
33 ES Kim, CK Shim, JW Lee, JW Park, KY Choi *Analyst*. 2012, 137, 2421-2430.
34 K Yoshimoto, M Nishio, H Sugasawa, Y Nagasaki *Journal of the American Chemical Society*. 2010, 132, 7982-7989.
35 MS Wagner, DG Castner *Applied Surface Science*. 2004, 231, 366-376.
36 JW Park, IH Cho, DW Moon, SH Paek, TG Lee *Surface and Interface Analysis*. 2011, 43, 285-289.
37 F Liu, M Dubey, H Takahashi, DG Castner, DW Grainger *Analytical Chemistry*. 2010, 82, 2947-2958.
38 HY Song, X Zhou, J Hobley, X Su *Langmuir*. 2011, 28, 997-1004.
39 JR Lu, EM Lee, RK Thomas *Acta Crystallographica Section A: Foundations of Crystallography*. 1996, 52, 11-41.
40 X Zhao, F Pan, B Cowsill, JR Lu, L Garcia-Gancedo, AJ Flewitt, GM Ashley, J Luo *Langmuir*. 2011, 27, 7654-7662.
41 YM Bae, BK Oh, W Lee, WH Lee, JW Choi *Biosensors & Bioelectronics*. 2005, 21, 103-110.
42 X Liu, X Wang, J Zhang, H Feng, X Liu, D Wong *Biosensors & Bioelectronics*. 2012, 35, 56-62.

43 Y Ryu, Z Jin, M Kang, HS Kim *BioChip Journal*. 2011, 5, 193-198.
44 AT Nguyen, J Baggerman, JMJ Paulusse, H Zuilhof, CJM van Rijn *Langmuir*. 2012, 28, 604-610.
45 AT Nguyen, R Van Doorn, J Baggerman, JMJ Paulusse, M Klerks, H Zuilhof, CJM Rijn *Chemical Communications*. 2012, submitted.
46 SK Vashist, CK Dixit, BD MacCraith, R O'Kennedy *Analyst*. 2011, 136, 4431-4436.
47 B Feng, S Huang, F Ge, Y Luo, D Jia, Y Dai *Biosensensors & Bioelectronics*. 2011, 28, 91-96.
48 BN Johnson, R Mutharasan *Langmuir*. 2012, 28, 6928-6934.
49 JH Lee, HK Choi, SY Lee, MW Lim, JH Chang *Biosensensors & Bioelectronics*. 2011, 28, 146-151.
50 S Ko, CJ Kim, DY Kwon *NSTI-Nanotech*. 2010, 3, 129–136.
51 J Figueroa, S Magaña, DV Lim, R Schlaf *Journal of Immunological Methods*. 2012, 386, 1-9.
52 X Zhao, F Pan, L Garcia-Gancedo, AJ Flewitt, GM Ashley, J Luo, JR Lu *Journal of the Royal Society Interface*. 2012, 9, 2457-2467.
53 HJ Um, M Kim, SH Lee, J Min, H Kim, YW Choi, YH Kim *Talanta*. 2011, 84, 330-334.
54 M Iafisco, E Varoni, M Di Foggia, S Pietronave, M Fini, N Roveri, L Rimondini, M Prat *Colloids Surfaces B*. 2012, 90, 1–7.
55 Z Balevicius, A Ramanaviciene, I Baleviciute, A Makaraviciute, L Mikoliunaite, A Ramanavicius *Sensors and Actuators B*. 2011, 160, 555–562.
56 BD Ventura, L Schiavo, C Altucci, R Esposito, R Velotta *Biomedical Optics Express*. 2011, 2, 3223–3231.
57 EJ Franco, H Hofstetter, O Hofstetter *Journal of Separation Science*. 2006, 29, 1458–1469.
58 JH Kang, HJ Choi, SY Hwang, SH Han, JY Jeon, EK Lee J*ournal of Chromatography A*. 2007, 1161, 9-14.
59 X Yuan, D Fabregat, K Yoshimoto, Y Nagasaki *Colloids and Surfaces B*. 2012, 99, 45–52.
60 Z Pei, H Anderson, A Myrskog, G Duner, B Ingemarsson, T Aastrup *Analytical Biochemistry*. 2010, 398, 161–168.
61 Y Liu, CX Guo, W Hu, Z Lu, CM Li *Journal of Colloid and Interface Science*. 2011, 360, 593–599.
62 HJ Han, RM Kannan, S Wang, G Mao, JP Kusanovic, R Romero *Advanced Functional Materials*. 2010, 20, 409–421.
63 JA Ho, WL Hsu, WC Liao, JK Chiu, ML Chen, HC Chang, CC Li *Biosensors & Bioelectronics*. 2010, 26, 1021–1027.
64 P Batalla, JM Bolıvar, F Lopez-Gallego, JM Guisan, *Journal of Chromatography A*. 2012, 1262, 56–63.
65 N Bereli, G Sxener, H Yavuz, A Denizli *Materials Science and Engineering C*. 2011, 31, 1078–1083.
66 G Bergstroem, CF Mandenius *Sensors and Actuators B*. 2011, 158, 265–270.
67 MM Billah, CS Hodges, HCW Hays, PA Millner *Bioelectrochemistry*. 2010, 80, 49–54.
68 NJ Alves, T Kiziltepe, B Bilgicer *Langmuir*. 2012, 28, 9640–9648.
69 B Stamos, L Loredo, S Chand, TV Phan, Y Zhang, S Mohapatra, K Rajeshwar, R Perera *Analytical Biochemistry*. 2012, 424, 114–123.
70 UM Lindstrom *Chemical Reviews*. 2002, 102, 2751–2772.

71 E Saxon, CR Bertozzi *Science*. 2000, 287, 2007–2010.
72 KL Kiick, E Saxon, DA Tirrell, CR Bertozzi *Proceedings of the National Academy of Sciences*. 2002, 99, 19–24.
73 JW Chin, SW Santoro, AB Martin, DS King, L Wang, PG Schultz *Journal of the American Chemical Society*. 2002, 124, 9026–9027.
74 BC Bundy, JR Swartz *Bioconjugate Chemistry*. 2010, 21, 255–263.
75 TW Muir, D Sondhi, PA Cole *Proceedings of the National Academy of Sciences*. 1998, 95, 6705–6710.
76 J Kalia, NL Abbott, RT Raines *Bioconjugate Chemistry*. 2007, 18, 1064–1069.
77 IH Cho, EH Paek, H Lee, JY Kang, TS Kim, SH Paek *Analytical Biochemistry*. 2007, 365, 14–23.
78 MP Cassidy, J Raushel, VV Fokin *Angewandte Chemie - International Edition*. 2006, 45, 3154–3157.
79 T Govindaraju, P Jonkheijm, L Gogolin, H Schroeder, CFW Becker, CM Niemeyer, H Waldmann *Chemical Communications*. 2008, 32, 3723–3725.
80 R Manova, TA van Beek, H Zuilhof *Angewandte Chemie - International Edition*. 2011, 50, 5428–5430.
81 JC Jewett, CR Bertozzi *Chemical Society Reviews*. 2010, 39, 1272–1279.
82 MF Debets, SS van Berkel, J Dommerholt, AJ Dirks, FPJT Rutjes, FL van Delft *Accounts of Chemical Research*. 2011, 44, 805–815.
83 MD Witte, JJ Cragnolini, SK Dougan, NC Yoder, MW Popp, HL Ploegh *Proceedings of the National Academy of Sciences*. 2012, 109, 11993–11998.

CHAPTER 4

A Broad Set of Different Llama Antibodies Specific for a 16 kDa Heat Shock Protein of *Mycobacterium tuberculosis*

ABSTRACT

Background: Recombinant antibodies are powerful tools in engineering of novel diagnostics. Due to the small size and stable nature of llama antibody domains selected antibodies can serve as a detection reagent in multiplexed and sensitive assays for *Mycobacterium tuberculosis* (*M. tb*).

Methodology/Principal Findings: Antibodies for *M. tb* recognition were raised in Alpaca, and, by phage display, recombinant variable domains of heavy-chain antibodies (V_{HH}) binding to *M. tb* antigens were isolated. Two phage display selection strategies were followed: one direct selection using semi-purified protein antigen, and a depletion strategy with lysates, aiming to avoid cross-reaction to other mycobacteria. Both panning methods selected a set of binders with widely differing complementarity determining regions. Selected recombinant V_{HH}s were produced in *E. coli* and shown to bind immobilized lysate in direct Enzymelinked Immunosorbent Assay (ELISA) tests and soluble antigen by surface plasmon resonance (SPR) analysis. All tested V_{HH}s were specific for tuberculosis-causing mycobacteria (*M. tuberculosis, M. bovis*) and exclusively recognized an immunodominant 16 kDa heat shock protein (hsp). The highest affinity V_{HH} had a dissociation constant (K_D) of 4×10^{-10} M.

Conclusions/Significance: A broad set of different llama antibodies specific for 16 kDa heat shock protein of *M. tuberculosis* is available. This protein is highly stable and abundant in *M. tuberculosis*. The V_{HH} that detect this protein are applied in a robust SPR sensor for identification of tuberculosis-causing mycobacteria.

This chapter was published as:
Anke K. Trilling, Hans de Ronde, Linda Noteboom, Adele van Houwelingen, Margriet Roelse, Saurabh K. Srivastava, Willem Haasnoot, Maarten A. Jongsma, Arend Kolk, Han Zuilhof and Jules Beekwilder. *PLoS ONE.* 2011, 6, e26754.

4.1 INTRODUCTION

For centuries, Tuberculosis (TB) has been a severe health problem all over the world. Currently, it is estimated that the microbe *Mycobacterium tuberculosis* causes 9.4 million new cases of TB each year.[1] Recent and alarming developments around TB comprise the appearance of multidrug-resistant strains and co-infection with HIV, both of which reduce the lifetime of tuberculosis patients significantly. Accurate and rapid diagnosis of active TB is essential for both control of disease epidemic, and treatment of infected patients. Current diagnostic methods for TB include DNA-based, biochemical and serological approaches,[2-6] but none of these methods is yet appropriate for the high-throughput, rapid, reliable and low-cost detection of TB in an affordable near-patient test.

Classical detection methods for infectious diseases such as TB rely on rapid immunological detection. Use of recombinant antibodies may facilitate multiplex design of protein chips for diagnosing several potential pathogens in parallel.[7] Furthermore, they can be deployed in novel bio-sensing systems such as nanowires with very high sensitivity and potential for near patient testing.[8] Llama antibody fragments (V_{HH}s) are particularly suited for these applications due to their compact size (15 kDa)[9] and remarkable physicochemical stability.[10-12] Furthermore, they were shown to display many additional advantages over other recombinant antibodies, regarding cost of production, specificity, affinity, and especially stability under conditions of diagnosis in the field, which would make them suitable as detection units in biosensors.[13]

In the present study, our objective was to select and produce V_{HH}s capable of recognizing *Mycobacterium tuberculosis* antigens. V_{HH}s were selected by phage display from a library generated from an immunized alpaca, and characterized. All characterized V_{HH}s bound to the same target - the immunodominant 16 kDa heat shock protein of *M. tuberculosis* - despite having highly diverse sequence profiles. The utility of the selected V_{HH}s in sensor devices were demonstrated using a surface plasmon resonance set-up as model biosensor.

4.2 RESULTS

4.2.1 Generation of Recombinant Antibodies

Recombinant antibodies for *M. tuberculosis* detection were obtained by phage display. A V_{HH} phage display library with 10^7 clones was constructed from the lymphocyte RNA of an alpaca immunized with *M. tuberculosis* lysate. This library was subjected to two different methods of phage display selection: The first method deployed a direct selection on *M. tuberculosis* protein, enriched for 16 kDa, 24 kDa

and 70 kDa proteins (Fig. 1). The second method used a depletion strategy, where non-specific phages were removed using total protein of non-tuberculosis mycobacteria, and positive binders were selected on lysate of *M. tuberculosis*. Both selection methods were carried out for three selection rounds. After the last selection, V_{HH}-encoding DNA inserts from both selection methods were mass-excised and transferred into an expression vector.

For each selection method DNA sequences of 96 clones were analyzed. Ninety-two of the 192 sequences were rejected because they suffered from premature stop codons or the technical quality of the sequencing reactions was poor. After removal of redundant sequences, 62 unique protein sequences remained, which are shown in Figure 2.

Based on protein similarity, V_{HH} sequences could be clustered into 6 groups (A, B, C, D, E and F) consisting of 29, 8, 6, 5, 2 and 3 members respectively (Fig. 2), while 9 sequences could not be grouped. Both panning methods raised antibodies belonging to the groups A, B and D, suggesting the presence of a dominant antigen either during alpaca immunization or in vitro selection. Grouping was mainly based on the antigen binding regions (CDRs), where most sequence variation occurs. The length of the CDR3 region represents the dominant difference between all single sequences and sequence groups, ranging from five residues in group A to 27 residues in sequence B-B2 (Fig. 2). The variations in protein sequence and length of the antigen

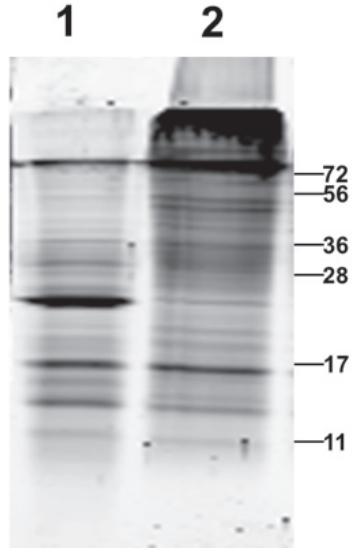

Figure 1. Whole and enriched protein lysate of *M. tuberculosis*. Lysate enriched for 16 kDa, 24 kDa and 70 kDa *M. tuberculosis* protein (lane 1) and whole *M. tuberculosis* lysate (lane 2). Shown is a 15% SDS PAGE gel, stained by SYPRO ruby. Indicated are the positions of relevant size markers in kDa.

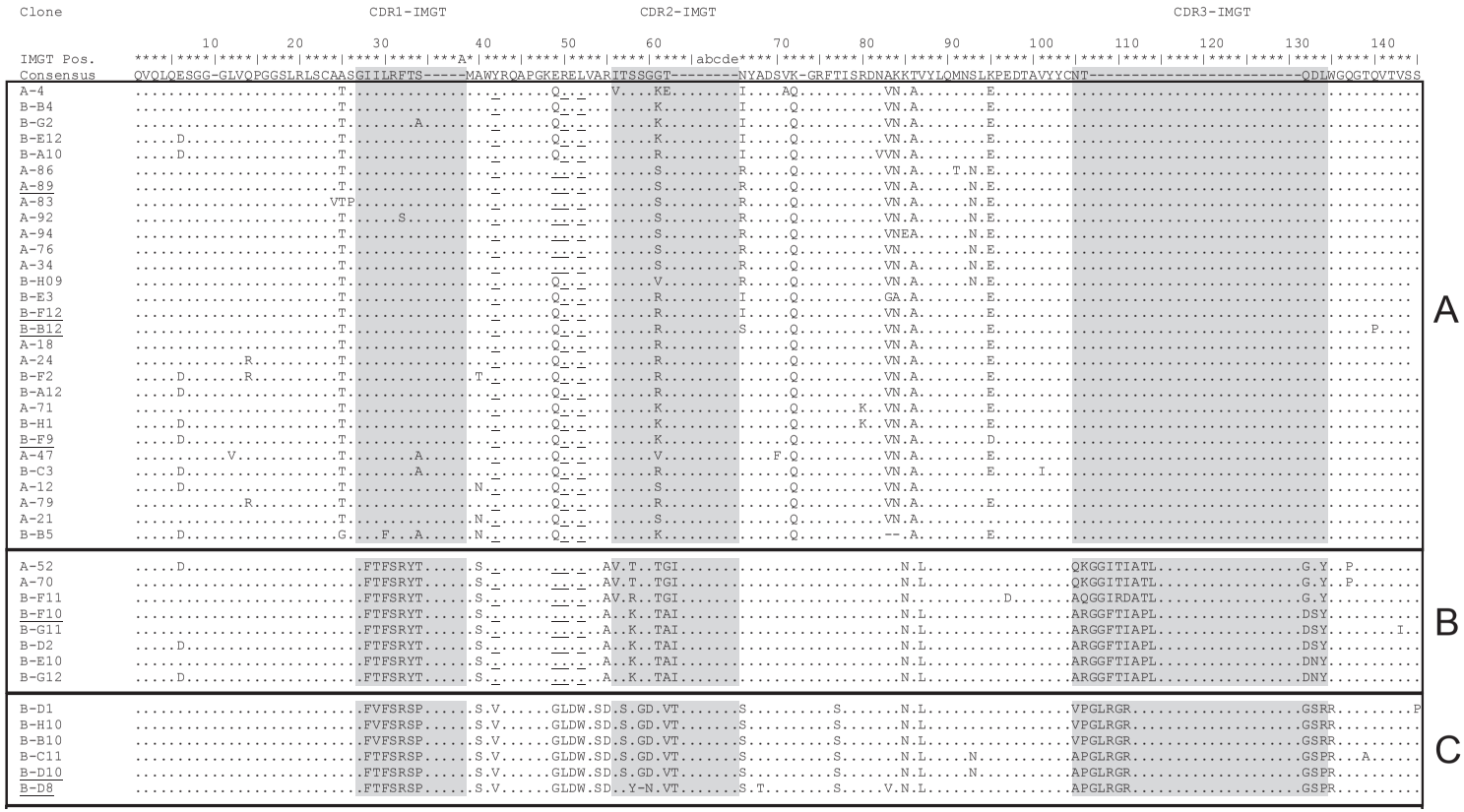
Clone
CDR1-IMGT
CDR2-IMGT
CDR3-IMGT
IMGT Pos.
Consensus
QVQLQESGG-GLVQPGGSLRLSCAASGIILRFTS-----MAWYRQAPGKERELVARITSSGGT--------NYADSVK-GRFTISRDNAKKTVYLQMNSLKPEDTAVYYCNT----------QDLWGQGTQVTVSS
A-4
B-B4
B-G2
B-E12
B-A10
A-86
A-89
A-83
A-92
A-94
A-76
A-34
B-H09
B-E3
B-F12
B-B12
A-18
A-24
B-F2
B-A12
A-71
B-H1
B-F9
A-47
B-C3
A-12
A-79
A-21
B-B5
A-52
A-70
B-F11
B-F10
B-G11
B-D2
B-E10
B-G12
B-D1
B-H10
B-B10
B-C11
B-D10
B-D8
A
B
C

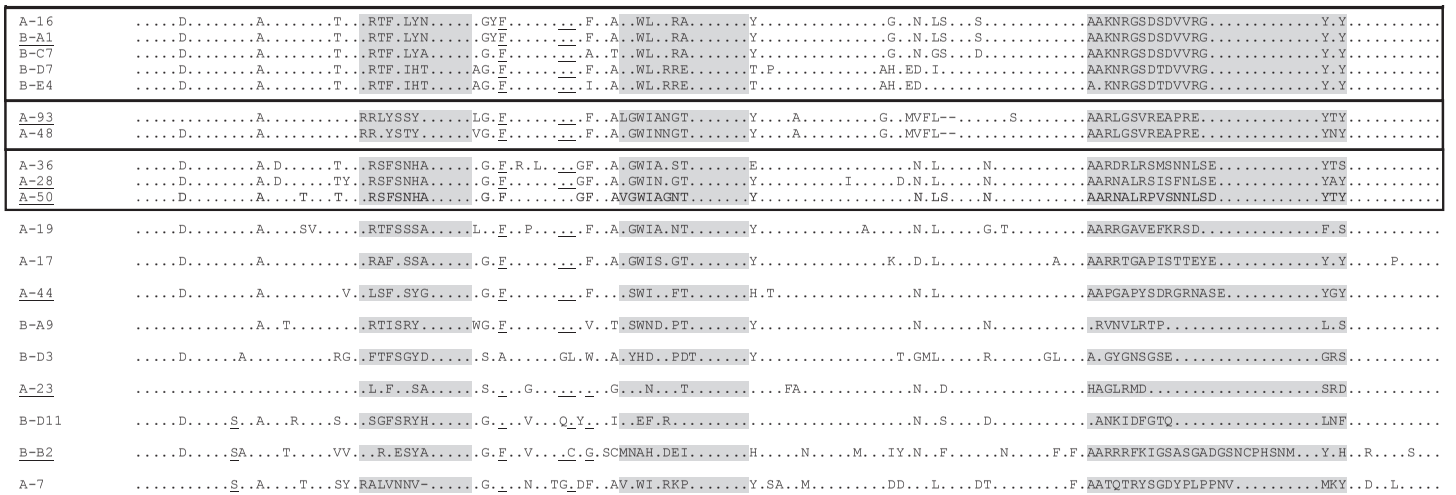

Figure 2. ***M. tuberculosis*** **binding V_{HH} antibody fragments. Protein sequence of 62 selected V_{HH} antibody fragments selected by phage display for binding to *M. tuberculosis*. Dots indicate sequence identity, and dashes indicate gaps. The three complementarity determining regions CDR1, CDR2 and CDR3 are shaded. Characteristic V_H-V_{HH} hallmark substitutions (Leu12Ser, Val42Phe or Val42Tyr, Gly49Glu, Leu50Arg or Leu50Cys and Trp52Gly or Trp52Leu [the last substitution is less well conserved], the ImMunoGeneTics system[52] was followed)[15] are underlined. The 12 clones selected for further investigations are underlined. V_{HH} protein sequences labeled A-x (with x = 1–96) resulted from direct selection using semi-purified protein antigen, protein sequences labeled B-yx (with y = A–F and x = 1–12) were achieved by depletion method.**

binding regions suggests that proteins from different origins with a broad range of sequence diversity were selected.

Sequence groups were inspected for amino acid substitutions which could classify them as V_{HH}s, and distinguish them from canonical antibodies with heavy and light chain. Most of these substitutions (at positions 42, 49, 50 and 52: underlined in Fig. 2) could be regarded as adaptations to the absence of a light chain[14, 15] resulting in a more soluble V_{HH} fragment. Most prominently, the hydrophobic leucine at position 50 has changed to a water-soluble arginine in 87% of the inspected sequences. Other typical V_{HH} substitutions occur at a lower frequency (15% V42->F; 64% V42->Y; 50% G49->E; 1.6% L50->C; 63% W52->L and 1.6% W52->G).

4.2.2 Specificity of the Selected Antibodies

To characterize their properties into more detail, 12 clones (A-23, A-28, A-44, A-50, A-89, A-93, B-A1, B-B12, B-D8, B-D10, B-F9 and B-F10), representing the 6 groups and 3 single sequences, were expressed in *E. coli* at 1 liter scale. Reactivity to *M. tuberculosis* protein - already used for coating in phage display - was assessed in a direct ELISA. All tested V_{HH}s reacted with *M. tuberculosis* protein, but not with *E. coli* protein (not shown), indicating that the selected antibodies could specifically recognize *M. tuberculosis*. The four clones with highest binding capability in ELISA (A-23, A-44, A-50 and B-F10) were used for further analysis.

To investigate the capability of the V_{HH} antibody fragments to distinguish *M. tuberculosis* from other mycobacteria, further direct ELISA experiments were carried out. For this purpose different lysates of *M. tuberculosis* substrains as well as other *Mycobacterium* species and respiratory pathogens were tested. V_{HH} antibody fragments reacted well with all *M. tuberculosis* substrains and *M. bcg* in different intensities, but not with *M. avium, M. kanssasi, M. smegmatis, S. pneumoniae* and *H. influenzae* (Fig. 3B). Thus, the selected antibodies displayed selectivity for *M. tuberculosis*.

4.2.3 Characterization of V_{HH} Antibody

The subcellular localization of the antigen recognized by the four selected V_{HH}s (A-23, A-44, A-50 and B-F10) was further investigated. To this end, *M. tuberculosis* whole cells, *M. tuberculosis* cell lysate and the media in which *M. tuberculosis* bacteria had grown was tested in direct ELISA. In all experiments signal was calibrated with those of the media (Middlebrook 7H9) or the buffer (phosphate-buffered saline). It appeared that the V_{HH}s bind most strongly to the *M. tuberculosis* protein lysate (Fig. 3A), indicating that they recognize an intracellular antigen.

To identify the target protein of the four selected V_{HH} antibody fragments, western blot analysis of *M. tuberculosis* lysate was carried out. As exemplified in Figure

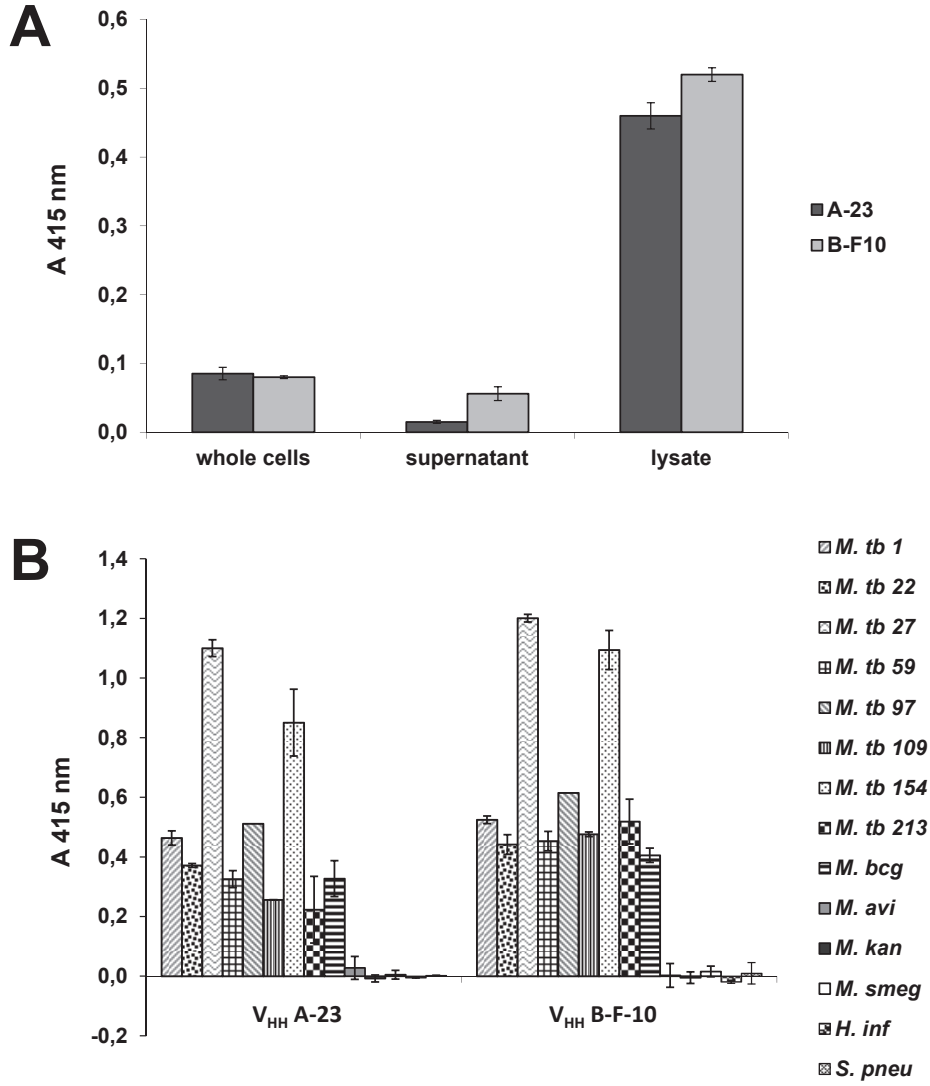

Figure 3. Direct ELISA to confirm specific binging of V_{HH} antibody fragments to tuberculosis lysate. V_{HH} antibody fragments A-23 and B-F10 with A) *M. tuberculosis* whole cells, *M. tuberculosis* cell lysate and media in which *M. tuberculosis* bacteria were grown. B) different *M. tuberculosis* lysates as well as lysates of *M. bcg*, *M. avium*, *M. kansasii*, *M. smegmatis*, *S. pneumoniae* and *H. influenzae*. Measurements were performed in duplicate, expressed as means ± SD.

4A for V_{HH} A-23, all four tested clones (A-23, A-44, A-50 and B-F10) showed binding to a protein of 16 kDa size. Testing of a number of other selected V_{HH} antibodies (A-28, A-89, A-93, B-A1, B-B12, B-D8, B-D10 and B-F9) revealed that all V_{HH}s bind to a 16 kDa protein (data not shown).

A 16 kDa heat shock protein of *M. tuberculosis* has been reported before to re-

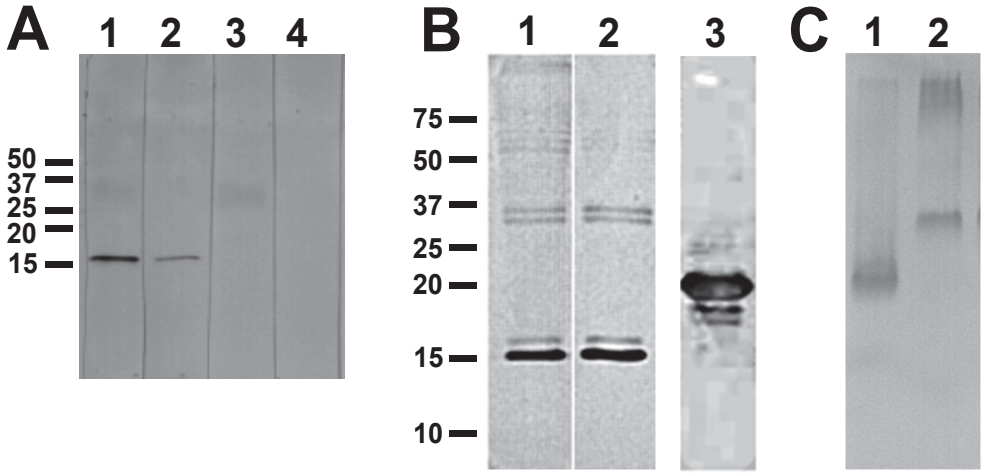

Figure 4. Western blot to discover antigen of V_{HH}s. A) Western blot using V_{HH} A-23 as a probe. 9 µg *M. tb 1* lysate were run on a 15% SDS-PAGE gel in lanes 1–4, and transferred to a nitrocellulose membrane. Lane 1: incubated with V_{HH} A-23 and detected using anti-VSV-HRP; Lane 2: incubated with V_{HH} A-23 and detected using anti-His_6-HRP; Lane 3: incubated with detection antibody anti-VSV-HRP; Lane 4: incubated with detection antibody anti-His_6-HRP. B) Western blot analysis to confirm the specificity of V_{HH} A-23. Lane 1: 9 µg *M. tb 22* lysate detected by monoclonal mouse 16 kDa antibody, using anti-mouse-HRP secondary antibody; Lane 2: 9 µg *M. tb 22* lysate detected by V_{HH} A-23, using anti-VSV-HRP secondary antibody. Lane 3: 3 µg of purified recombinant 16 kDa protein detected by V_{HH} A-23, using anti-VSV-HRP secondary antibody. Due to the tags added for purification and detection purposes the calculated mass of the recombinant 16 kDa protein is 21 kDa. Indicated are the positions of relevant size markers in kDa. C) Western blot analysis of native PAGE analysis. Lane 1: 5 µg *M. tb 27* lysate; Lane 2: 1 µg of purified recombinant 16 kDa protein. Detection was by V_{HH} A-23, using anti-VSV-HRP secondary antibody.

present an immunodominant protein and its gene was cloned.[16-20] To confirm that the band on the western blot corresponded to the 16 kDa hsp reported in the literature, two experiments were performed. Firstly a western blot analysis was performed, testing the V_{HH} A-23 side-by-side to the mouse monoclonal antibody MoAb F24, which specifically recognizes the 16 kDa hsp.[21] Both tested antibodies bound an identical pattern of bands with a major band around 16 kDa (Fig. 4B, lane 1 and 2). Secondly, the gene encoding the 16 kDa hsp of *M. tuberculosis* was cloned and expressed in *E .coli*. Purified 16 kDa heat shock protein of *E. coli* was analyzed by western blotting. V_{HH} A-23 showed reactivity to the recombinant 16 kDa hsp (Fig.

4B, lane 3). Similar results were obtained for the other V_{HH}s tested (A-28, A-89, A-93, B-A1, B-B12, B-D8, B-D10 and B-F9). Both tests confirm that the 16 kDa hsp from *M. tuberculosis* is the antigen recognized by these V_{HH}s. When, prior to western blot, antigen preparations were not subjected to denaturing, the reactivity of the antigen was not altered (Fig. 4C).

The ability of the V_{HH}s to recognize soluble antigen in a biosensor set-up was tested in a surface plasmon resonance analysis. V_{HH} A-23 was immobilized at 3818 RU in Fc4 on a CM5 sensor chip. As a reference, V_{HH} M200, selected for recognition of Foot-and-mouth disease (FMD)[22], was used for immobilization at 3851 RU in channel Fc3. Different concentrations of *Mycobacterium lysates* (*M. tb 1*, *M. tb 27* and *M. smeg*) were run over both flow cells. *M. tb 1* and *M. tb 27* bound to V_{HH} A-23 on the CM5 sensor chip, whereas it did not bind to the reference Fc3 (not shown). Lysate of *M. smeg* showed neither binding to V_{HH} A-23 nor to V_{HH} M200. These results are in agreement with the results obtained by ELISA and demonstrate that V_{HH} A-23 is capable of specifically bind the soluble *M. tuberculosis* antigen (Fig. 5A, shown for *M. tb 1* and *M. smeg*).

The reproducibility of antigen detection by the A-23 biosensor was investigated using whole *M. tuberculosis* lysate *M. tb 1*. The lysate was injected at highest concentration following approximately 8 cycles of antigen binding and regeneration. The maximal RU signals were constant over 31 cycles with a mean of 234 ± 2 suggesting that regeneration conditions (10 mM HCl) do not affect the quality of the immobilized V_{HH} (Fig. 5B). The binding between purified recombinant hsp and a selection of V_{HH} (A-23, A-44, A-50, A-89, B-A1, B-B12, B-D8, B-D10, B-F9 and B-F10) was investigated. Among these, the binding by A-23, A-50, A-44 and B-F10 was found to be the strongest, and binding constants were determined for these V_{HH}. The K_D value of B-F10 was found to be best (4×10^{-10} M), while A-23, A-50 and A-44 had slightly lower affinities (2.4×10^{-9} M, 2.2×10^{-9} M and 3.7×10^{-9} M, respectively).

To quantify the antigen present in *M. tuberculsosis* lysates, different concentrations of recombinant 16 kDa antigen (24 ng/mL to 50 μg/mL) were injected for calibration. By plotting the lower concentrations of 16 kDa antigen against the responses in the biosensor, a linear calibration curve was obtained from a level above the limit of detection of 24 ng/mL (Fig. 5C). The signal in the V_{HH} coated flow cell was almost linear up to the concentration of 780 ng/mL and an RU of 119.5. At higher concentrations the response leveled off. For accuracy, only values below 120 RU were used to calculate the % of antigen in the lysate. From the obtained calibration curve, the amount of antigen in the whole protein content of the lysate was determined to be 6.6 ± 0.6% in *M. tb 1* and 11.7 ± 0.4% in *M. tb 27* whereas *M. smeg* contained 0% of the 16 kDa antigen.

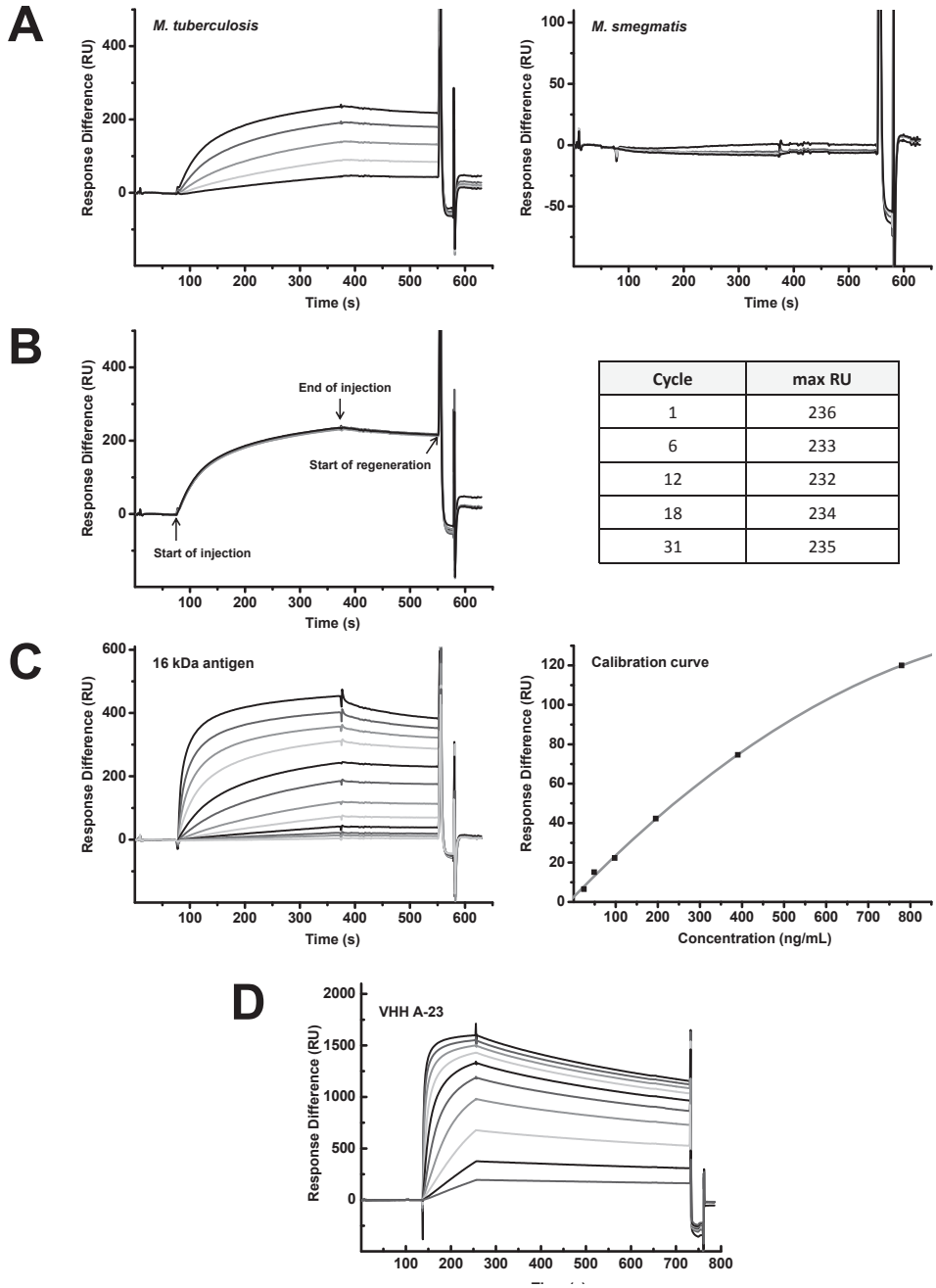

Cycle	max RU
1	236
6	233
12	232
18	234
31	235

Figure 5. Surface plasmon resonance analysis to show specific binding of V_{HH}s to soluble antigen. A–C) V_{HH} A-23 immobilized at 3818 RU on a CM5 sensor chip in Fc4 and V_{HH} M200[22] immobilized at 3851 RU in the reference channel Fc3. Sensorgrams were corrected by subtracting the signal from the reference flow channel Fc3. A) Sensorgrams obtained after injection of *M. tuberculosis* (left) and *M. smegmatis* (right) lysate. 50 µL lysate at concentration of 3.8 (lowest), 7.5, 15, 30 and 60 (highest) µg/mL were injected at a constant flow (10 µL/min.).

B) Sensorgrams obtained after repeated injection of *M. tuberculosis* lysate. 50 µL lysate at concentration of 60 µg/mL were repeatedly injected at a constant flow (10 µL/min.). Sensor was regenerated with 5 µL of a 10 mM HCl solution at 10 µL/min after each run. C) Left: Sensorgrams achieved after injection of purified recombinant 16 kDa antigen. 50 µL lysate at concentration of 24 (lowest), 49, 98, 185, 391, 781, 1.6×10^3, 3.1×10^3, 6.3×10^3, 12.5×10^3, 25×10^3 and 50×10^3 (highest) ng/mL were injected at a constant flow (10 µL/min.). Right: Calibration curve of purified recombinant 16 kDa antigen as obtained by BIAevaluation using the 4 parameter fit. D) Sensorgrams achieved after injection of V_{HH} A-23. Purified recombinant 16 kDa antigen was immobilized at 4100 RU on a CM5 sensor chip in Fc2 and inactivated Fc1 was used as reference. 100 µL V_{HH} at concentration of 0.025 (lowest), 0.05, 0.1, 0.2, 0.4, 0.8, 1.6, 3.2, 6.3 and 12.5 (highest) µg/mL were injected at a constant flow (50 µL/min.). Sensorgrams were corrected by subtracting the signal from the reference flow channel Fc1. To obtain the dissociation equilibrium constant (K_D) the sensorgrams were fitted by a global Langmuir 1:1 model (BIAevaluation software) using the six lowest V_{HH} concentrations.

4.3 DISCUSSION

The present study describes the successful selection of recombinant V_{HH}s specific for *Mycobacterium tuberculosis*. A panel of recombinant antibodies was selected, which distinguish a number of *M. tuberculosis* strains from non-tuberculosis mycobacteria. One of the selected V_{HH} molecules was successfully incorporated into an SPR-biosensor to detect and identify *M. tuberculosis*. To our knowledge this is the first description of recombinant llama antibody fragments specific for infectious *M. tuberculosis*.

Two different phage display selection methods were used, one by depletion of the library from non-tuberculosis lysates, and another by using a partially purified protein preparation. The depletion method aimed to select highly specific *M. tuberculosis* V_{HH} antibody fragments against potentially a very wide range of antigens from the lysate, whereas the direct panning method aimed to select V_{HH} antibody fragments specific for the three dominant proteins in the sample. We expected a large sequence variety, and indeed, a broad spectrum of 68 unique sequences was obtained. Out of which six sequences were found to be the same from both selection methods, suggesting that both procedures overlapped in their selectivity for an epitope. Investigations by ELISA with a range of different mycobacteria revealed that the selected llama antibody fragments allowed specific detection of all tested tuberculosis-causing species, and distinguish them from non-infectious mycobacteria such as *M. kansasii*, *M. avium* and *M. smegmatis* and other respiratory pathogens such as *S. pneumoniae* and *H. influenzae* (Fig. 3B). Apparently, both selection methods lead to antibodies that specifically recognize the *Mycobacterium tuberculosis* complex.

Earlier, selection of several mouse single-chain fragments (scFvs) reactive with *M. tuberculosis* culture proteins by phage display was reported,[23] and very recently

also chicken scFv antibodies for 16 kDa hsp.[24] In the present work, V_{HH} was preferred over scFv, because scFvs are larger, and often suffer from poor stability, unless genetically engineered,[25, 26] while V_{HH}s often display high stability over long periods of exposure to ambient temperature,[10] which allowed for extensive re-use of the SPR chip.

Surprisingly, western blot analysis showed that all 12 tested V_{HH}s from different clusters bind to the species-specific 16 kDa hsp (Fig. 4B), despite the high sequence diversity among the clusters (Fig. 2). Apparently also in alpaca the 16 kDa hsp behaves as an immunodominant antigen, and possibly there are several different epitopes. The specificity for the 16 kDa hsp is consistent with studies into the conservation of this protein among mycobacteria. Southern blot analysis of genomic DNA of several mycobacteria, using the coding sequence of the 16 kDa hsp gene as a probe,[27] showed the absence of a homologue of the 16 kDa hsp in non-tuberculosis species. Only the tuberculosis related *M. bovis* bacillus Calmette-Guérin (BCG) strain showed a specific hybridization, which is in agreement with our observation that 16 kDa hsp specific V_{HH}s (A-23, A-44, A-50 and B-F10) showed binding to *M. tuberculosis* and *M. bovis* BCG but not to any other tested *Mycobacterium* species in ELISA (Fig. 3B). Similar results were observed by Coates et al.[28] for the mouse monoclonal antibody TB68, which binds to the 16 kDa hsp of all tested strains of *M. tuberculosis* and *M. bovis* species.[29]

The 16 kDa hsp is known under several names (Hsp16.3, sHsp16 and Acr)[30] and shares a low sequence homology with the α-crystallin-related small heat shock protein family.[31] It has been suggested that this antigen acts in vitro as an adenosine triphosphate-independent chaperone and may occur as a dodecamer, or as monomers.[17, 32] The form of antigen that is recognized by the V_{HH} is probably the monomeric structure. The hsp was isolated from bacteria by a denaturing treatment, which would cause monomer formation, and reactivity of the antigen is not very different after western blotting from a native gel or a denaturing gel (Fig. 4). Also heat denaturing of antigen hsp did not change its mobility in native gels (not shown). Thus, probably the antigen is recognized in monomeric form, while we have no dodecameric form available for testing its reactivity.

Several murine monoclonal antibodies against the prominent hsp antigen of *M. tuberculosis* have been selected in the past.[21, 29, 33] It has been subcloned, overexpressed and purified.[17, 20] The results of the SPR experiments comparing the *Mycobacterium* lysates to purified recombinant 16 kDa hsp show that 7 to 12% of cellular protein consists of 16 kDa hsp. This would correspond to ± 6 million copies of 16 kDa hsp per cell, taking into account its molecular weight, and an estimated 160 fg total protein per cell.[34] The concentration of hsp in the total protein content of *M. tuberculosis* is comparable with Lipoarabinomannan (LAM), the major glycolipid of the outer cell wall which may represent up to 15% of the total bacterial weight[35] and is used for tuberculosis detection in urine samples.[36] Due to its rich presence in bac-

teria lysate, the highly expressed 16 kDa hsp seems to be a relevant biological target for TB diagnostic assays.[34] Nevertheless it may be worthwhile to develop stable and high affinity V_{HH} antibodies to secreted *M. tuberculosis* proteins such as the 24 kDa protein for diagnosis.[37]

The 16 kDa hsp is a cytosolic protein, as hardly any ELISA signal of the V_{HH}s to whole cells or culture medium of the *M. tuberculosis* cultures could be observed, while a strong signal occurred in the cell lysate (Fig. 3A). These observations are in agreement to reports of others, who report that the 16 kDa hsp is not released into the culture supernatant,[38, 39] but is peripherally associated with the membrane.[40] One consequence of this subcellular localization is that lysis of bacteria will be necessary before detection in sputum. One might argue that a secreted antigen like the 24 kDa protein,[37] would be more convenient for immunological detection. On the other hand, most tuberculosis-detection methods based on nucleic-acid amplification also require vigorous disruption of sputum and mycobacterial cells and a secreted antigen may be too dilute in sputum.[41]

Most serological tests for tuberculosis screen for reactivity in the patient's serum to specific *M. tuberculosis* antigens, such as the 16 kDa hsp.[20, 42, 43] However, such serum-reactivity tests have limited value, as antibodies remain present after BCG vaccination, after successful treatment of the infection and during latent infection, which complicates the diagnosis of active TB disease. Therefore, more efforts have been directed towards direct detection of *M. tuberculosis* antigens in sputum, serum, urine and cerebrospinal fluid of patients, and there V_{HH} antibodies against the 16 kDa hsp may represent a useful tool for the development of diagnostic tests.

An SPR biosensor using one of the selected V_{HH}s allowed detection of recombinantly produced 16 kDa hsp antigen of *M. tuberculosis*. Moreover, the SPR sensor was able to positively identify crude lysates of *M. tuberculosis*, enabling the specific detection of tuberculosis-causing infectious agent. The sensor system proved to provide reproducible results after a significant number of regenerations, which is an important attribute for a sensing device. Importantly, further experiments should prove the value of an SPR sensor in the identification of *M. tuberculosis* in patient's material. At its current sensitivity (24 ng of 16 kDa hsp per mL; Fig. 5C), the limit of detection would be about 10^6 cells per mL, when taking into account that 16 kDa makes up approximately 10% of total *Mycobacterium* protein and a cellular protein content of 150 fg/cell.[34] The current limit of detection using microscopy is around 10,000 cells per mL.

Sensitivity of the SPR system could be greatly enhanced by immobilization of V_{HH}s in an oriented way, leading to increased exposure of antigen-binding sites. Such orientation of antibodies like V_{HH} could be achieved by site-specific biotinylation of the V_{HH}, or other, covalent immobilization methods.[44] SPR results indicated a dissociation constant of 4×10^{-10} M for B-F10. Whereas other V_{HH} with 10-fold higher affinity have also been reported,[45] affinity maturation of the V_{HH} by rounds of mu-

tagenesis and selection could significantly improve the affinity of the antigen, and thereby the sensitivity of the sensor[46] and finally multivalent and multispecific V_{HH}s could be engineered for strongly enhanced affinity for the antigen. V_{HH}s against a broad range of antigen targets could be selected by tuning the phage display selection method and the specificity and sensitivity of *M. tuberculosis* detection could be greatly enhanced by the combination of V_{HH}s for rapid, near patient multiplexing in the near future.

SPR is one of the more established biosensor principles. Other methodologies, such as piezoelectronic immunosensors or fluorescent nanoparticles coupled with flow cytometry, and nanowires are further away from application in practice.[8, 47, 48] Still, SPR equipment is hardly compatible with field settings in countries where tuberculosis diagnosis is needed most. Recent efforts to implement portable SPR devices in tuberculosis diagnostics[49] may contribute to the solution of this problem.

4.4 Materials And Methods

4.4.1 Bacteria Samples

All mycobacteria (Royal Tropical Institute, Amsterdam, The Netherlands) were grown in Middlebrook 7H9 medium (Difco, BD, Sparks, MD, USA) supplemented with 10% OADC (BBL, BD) until mid-log phase and heat-killed at 80°C for 20 min. Other respiratory pathogens (Streptococcus pneumoniae D39 and non-typable Haemophilus influenzae R2866 [Radboud University Nijmegen Medical Center CUKZ, Nijmegen, The Netherlands]) were grown on chocolate agar. Heat-inactivated bacteria were used as 'whole cells` to test binding of antibodies to surface proteins. To obtain the lysate of *Mycobacterium* as antigen source, bacteria were centrifuged at 13,000 g for 5 min after heat killing. After 2 washing steps with phosphate-buffered saline (PBS) to remove all media the bacteria pellet was resuspended in PBS. 500 µL of bacterial suspension was lysed with 0.6 g zirkonia/silica 0.1 mm (BioSpec Products Inc, Bartlesville, OK, USA) in a Retch MM 301 (Retch GmbH, Germany) for 15 min at 30 hertz. To remove soluble particles, the lysate was centrifuged for 5 min at 13,000 g. The obtained supernatant was used as cell lysate. Protein concentration of *Mycobacterium* samples were determined with the Pierce 660 nm Protein assay using Nanodrop and albumin as reference protein for the standard curve.

To obtain enriched lysate 2 mL of centrifuged *M. tuberculosis* lysate was brought into 20 mM ethanolamine (pH 9.0) and loaded on a 1 mL HiTrap MonoQ column (Pharmacia). After washing extensively with 20 mM ethanolamine (pH 9.0), a linear gradient from 0 to 1 M NaCl in 20 mM ethanolamine (pH 9.0) was applied, and 1 mL fractions were collected. Around 0.4 mM NaCl, a fraction eluted in which proteins of 16 kDa, 24 kDa and 63 kDa were overrepresented, and this fraction was used for subsequent selections.

4.4.2 Library Construction

A V_{HH} library was formed from lymphocyte RNA from a 3-year old female alpaca (GDL, Utrecht University, The Netherlands) as previously described.[10] Experiments with alpacas were approved by the Dutch Animal Ethical Commission (Dier Experimenten Commissie, DEC; permit 06/284) of the Utrecht University, following the Dutch Law on animal experiments ('Wet op de Dierproeven` : http://wetten.overheid.nl/BWBR0003081/geldigheidsdatum_05-09-2011). 100 μg of *M. tuberculosis* lysate was used for the immunization. V_{HH}s were amplified from first-strand cDNA with V_{HH} specific primers lam07, lam08 and lam17.[50] Amplified fragments were pooled and ligated into the pHEN2 phagemid vector[51] in frame with the M13 gene 3 for expression of V_{HH}-g3p fusion protein. Electroporation of recombinant plasmid into competent *Escherichia coli* TG1 cells resulted in about 10^7 individual recombinants. Phage particles were produced in *E. coli* as described earlier.[10]

4.4.3 Selection

The library containing approximately 10^7 individual clones was panned separately using two different panning strategies.

4.4.3.1 Direct Panning Method

The first selection was carried out by panning of the V_{HH}-displayed phage library directly against the *M. tuberculosis* lysate, enriched for 16 kDa protein, 24 kDa protein and another high-molecular weight protein around 70 kDa (Fig. 1). Wells of microtiter ELISA plates (GreinerBioOne, The Netherlands) were coated with 100 μL lysate (10 μg/mL in 0.1 M Sodium Carbonate Solution pH 9.6) overnight at 4°C. Plates were emptied the next day and washed 1 time with 200 μL PBS and unspecific binding sites were blocked for 1 h with 250 μL PBS containing 2% (w/v) nonfat powdered milk (2% PBSM). 100 μL phages (1011 cfu/mL) were blocked for 30 min with 50 μL PBS containing 10% nonfat powdered milk (w/v) (10% PBSM) before 100 μL of this mix was applied to the wells and incubated for 1 h on a shaker. Excess phages were washed away with 5 washes of 200 μL 0.05% Tween-20 in PBS (0.05% PBST) and 5 washes of 200 μL PBS. Phages from the *Mycobacterium* selection were eluted with 100 μL of 0.1% trypsin in PBS for 15 min. Eluted phages were then used to infect *E. coli* TG-1 cells. The phage populations were amplified and rescued by VCSM13 helper phage to generate phage displaying V_{HH} to be used for the next round of panning. To raise the selection stringency, the number of washing steps before trypsin elution was increased by 5 after each panning round. After three rounds of panning, the in- and output were titrated to monitor the success of the selection.

4.4.3.2 Depletion Panning Method

Targets were immobilized overnight at 4°C in microtiter ELISA plate wells (GreinerBioOne, The Netherlands) using the following conditions: 6 wells were coated with 100 µL *Mycobacterium* mix (lysate of *M. kansasii, M. avium, M. fortuitum* and *M. chelonae*, 3 µg/mL) in PBS and one well with 100 µL lysate of *M. tuberculosis* (3 µg/mL) in PBS. The next day, plates were emptied and washed one time with 200 µL PBS and blocked for 1 h with 250 µL 2% PBSM. 300 µL phages (1011 cfu/mL) were blocked for 30 min with 100 µL 10% PBSM before 100 µL of this mix were applied to the emptied lysate-containing (*Mycobacterium* mix) well and incubated for 15 min on a microtiter plate shaker. The supernatant was then transferred to the next lysate-containing (*Mycobacterium* mix) well and incubated for 15 min under shaking. This procedure was repeated for the remaining 4 wells coated with the *Mycobacterium* mix lysate. Finally the supernatant was transferred to the well coated with *M. tuberculosis* lysate and incubated for 30 min on the shaker. Excess phages were washed away with 5 washes of 200 µL 0.05% PBST and 5 washes of 200 µL PBS. Phages from the *Mycobacterium* selection were eluted with 100 µL of 0.1% trypsin in PBS for 15 min. Eluted phages were then amplified, rescued and re-used. In additional panning rounds stringency was increased by increasing the number of washing steps by 5 after each panning round.

4.4.4 Recloning of Selected V_{HH}s for Expression

For both panning methods, plasmids from selected phage pools were extracted using QIAprep Spin Miniprep Kit (250) (QIAGEN, The Netherlands). DNA was cut using the unique PstI and NotI restriction sites and then purified using the Jetquick gel extraction kit (Genomed, Germany). V_{HH} sequences were then bulk-ligated into a PstI and NotI digested PRI-VSV expression vector, a strong expression vector for expression in the periplasm, based on the backbone of the pRSET-A vector (Invitrogen, The Netherlands). Expression of the recombinant V_{HH} was under control of the T7 promoter. The C-terminus of the V_{HH} was fused to a VSV-tag (YTDIEMNRLGK) for detection purposes along with a His_6 tag for purification purposes followed by a stop codon. For cloning purposes a NotI restriction site was introduced between the V_{HH} and the VSV-tag.

Constructs were introduced into *E. coli* XL-1 blue. 96 randomly picked colonies were used for colony PCR with the primer T7 (5′- TAATACGACTCACTATAGG -3′) and AS2 (5′- GCTAGTTATTGCTCAGCGG -3′). Sequencing of 96 colonies from the first panning method resulted in 34 unique V_{HH} protein sequences (labeled A-x, with x = 1–96), for the depletion method in 34 unique full length protein sequences (labeled B-yx, with y = A-F and x = 1–12). All duplicate sequences were omitted. The remaining 62 non-redundant V_{HH} sequences were aligned according to ImMunoGe-

neTics system[52] for immunoglobulins and classified into different groups. As V_{HH}s had unusual long CDRs, additional gaps were introduced in the numbering at the end of CDR1 and CDR2 and labeled with letters A and a to e, respectively.

Sequences for 12 representatives which were used for further analysis have been submitted to Genbank under accession numbers JN234011–JN234022.

4.4.5 Expression and Purification of Recombinant V_{HH}s

Representative sequences from each panning method were selected from different groups for expression in *E. coli* BL21-AI, a strain which carries a chromosomal insertion of the T7 RNA polymerase gene in the araB locus of the araBAD operon, allowing the expression of recombinant V_{HH} in the presence of L-arabinose. Bacteria were induced to express the V_{HH} and urea-lysed as described previously[10] using PBS as buffer. V_{HH}s were purified using Ni-NTA Superflow resin (QIAGEN, Germany) as reported before.[10] Eluates were dialyzed against 8 liter of PBS in two steps after Ni-NTA metal-affinity chromatography and samples were stored in 1.5 mL batches containing a final concentration of 15% glycerol at −20°C. Protein concentration was determined using Bradford test[53] while successful expression and purification was verified on a 15% sodium dodecylsulphate polyacrylamide gel electrophoresis (SDS-PAGE) gel. As previously shown by Beekwilder et al.[10] the expressed V_{HH}s were the dominant proteins in the *E. coli* cell pellets (data not shown).

4.4.6 Direct ELISA

Wells of flat-bottom ELISA plates (medium-binding, GreinerBioOne, The Netherlands) were coated with 2 μg/mL lysate of *Mycobacterium* species or other respiratory pathogens (*S. pneumoniae* and *H. influenza*) in PBS and incubated at 4°C overnight. Antigen-coated wells were emptied and washed one time with 200 μL PBS and then blocked with 150 μL PBS containing 4% nonfat powdered milk (w/v) (4% PBSM) for 1 h at room temperature. Wells were emptied and 100 μL V_{HH} (0.5 mg/mL) in 2% PBSM was added and binding was allowed to occur for 1 h. Excess V_{HH}s were removed by washing three times with 200 μL PBST, and anti-VSV-HRP conjugate (Sigma Aldrich, Missouri, USA) was added at a 1:2000 dilution for 1 h in 2% PBSM. Excess conjugate was washed off three times with 200 μL PBST and three times with 200 μL PBS. Subsequently HRP activity was determined by adding 1-StepTM Ultra TMB-ELISA substrate (Pierce, Rockford, IL). The reaction was allowed to proceed in the dark for 10 min and then stopped with 1 M sulphuric acid and the OD was measured at 415 nm in a microtiter plate-reader (TECAN SpectraFluor Microplate Reader).

Similar method was employed for direct ELISA of whole cells and supernatant by using 100 μL for coating.

4.4.7 Western Blot Analysis

Cell lysates containing approximately 9 μg total protein were first boiled and reduced in buffer and electrophoresed on a 15% SDS-PAGE gel and SYPRO ruby (Bio-Rad, Hercules, CA) stained to ensure the full complement of proteins was resolved. For western blotting, proteins were transferred from an unstained gel to nitrocellulose membranes (Trans-Blot, Bio-Rad, Hercules, CA). Membranes were blocked overnight at room temperature in 4% PBSM on a shaker. The membrane was then incubated with purified V_{HH} (0.1 mg/mL in 2% PBSM) for 1 h at room temperature on a shaker. Membranes were washed once in 2% PBSM and three times in 0.1% PBST. Subsequently, membranes were incubated with HRP-conjugated anti-VSV-tag antibodies (1:2000 in 2% (w/v) PBSM, Sigma Aldrich, Missouri, USA) or anti-HIS_6 tag (1:5000 in 2% (w/v) PBSM, Roche, Mannheim, Germany) for 1 h at room temperature on a shaker. Membranes were washed once with 2% PBSM followed by two washing steps with TBS containing 0.1% Tween 20 and two washing steps with TBS. Binding was detected with 3,3′,5,5′-Tetramethylbenzidine (TMB) liquid substrate system for membranes (Sigma-Aldrich, The Netherlands). Molecular weight standard was Precision Plus Kaleidoscope (BioRad, Hercules, CA).

4.4.8 Recombinant 16 kDa Protein

The 16 kDa protein was PCR-amplified from *M. tuberculosis* lysate using the primer HSP16.3-PstI-FW (5′-AAAAAAA<u>CTGCAG</u>AAAATGGCCACCACCCTTCCC-3′) and HSP16.3-NotI-RV (5′- AAAAAAAA<u>GCGGCCGC</u>GTTGGTGGACCGGATCTG-AA-3′) (PstI and NotI restriction sites are underlined). The digested fragment was inserted in a PstI-NotI cut PRI-AVI expression vector. This vector is similar to the earlier described PRI-VSV expression vector, but the C-terminus of the protein is fused to an AVI-tag™ (Avidity, LLC, Denver, Colorado) and a His_6 tag for purification purposes followed by a stop codon. The construct was transformed into *E. coli* XL-1 blue for multiplication. The cloned hsp sequence is identical to GenBank accession number S79751. Isolated plasmid DNA was transformed into *E. coli* strain BL21-AI for expression. Expression and Ni-NTA metal-affinity chromatography purification was performed as described for V_{HH}. The calculated mass of the recombinant 16 kDa protein was determined to be 21 kDa.

4.4.9 Surface Plasmon Resonance (SPR)

The BIAcore 3000, carboxymethyl dextran sensor chips (CM5), HBS-EP buffer (pH 7.4, consisting of 10 mM 4-(2-hydroxyethyl)piperazine-1-ethanesulfonicacid, 150 mM sodium chloride, 3 mM ethylenediaminetetraacetic acid, 0.005% v/v surfactant polysorbate 20), the amine coupling kit (containing 0.1 M N-hydroxysucci-

nimide [NHS], 0.4 M 1-ethyl-3-[3-dimethylaminopropyl]carbodiimide hydrochloride [EDC] and 1 M ethanolamine hydrochloride [pH 8.5]) were purchased from GE Healthcare (Uppsala, Sweden).

Selected V_{HH}s were immobilized onto a CM5 surface by the use of the amine coupling kit and the Surface Preparation Wizard as present in the BIAcore 3000 control software. The biosensor surface was activated by injecting (35 µL at a flow rate of 5 µL/min) a mixture of EDC and NHS (1:1; v/v) into one of the four flow channels (Fcs). Then V_{HH} (50 µg/mL diluted in coupling buffer [10 mM sodium acetate, pH 4.0]) was injected and bound to the activated carboxymethylated dextran surface via its primary amine groups, aiming for an immobilization level of 5000 response units (RU). After coupling, the remaining active groups were blocked with ethanolamine hydrochloride (1 M).

In the experimental set-up, a reference (non-tuberculosis binding, M200)[22] V_{HH} was immobilized in the reference Fc3 and the tuberculosis specific V_{HH} was immobilized in Fc4, both with a final response of approximately 3800 RU. The BIAcore 3000 operated at a constant temperature of 25°C and a constant flow of 10 µL/min. 50 µL *Mycobacterium* lysates in HBS-EP buffer, each of different concentration, were injected over the two serially connected Fcs. Regeneration of sensor surface was done with 5 µL of a 10 mM hydrogen chloride (HCl) solution at 10 µL/min after each run. For quantitative analysis, a calibration graph was prepared by using different concentrations of purified 16 kDa antigen in HBS-EP. All sensorgrams were referenced by subtracting the signal from the reference flow channel (Fc3) from Fc4 and were evaluated using the BIAevaluation software.

To check the affinity of different representative V_{HH}s (A-23, A-44, A-50, A-89, B-A1, B-B12, B-D8, B-D10, B-F9 and B-F10) against the 16 kDa hsp, the antigen was immobilized at 4100 RU on a CM5 sensorchip in Fc2 using the amine coupling method. A second flow cell (Fc1) was treated with the same chemical procedure without antigen and used as a reference. At a constant flow rate of 50 µL/min different concentrations of 100 µL V_{HH} ranging from 12.5 to 0.025 µg/mL in HBS-EP were injected 120 s over the two flow cells and followed by a dissociation step of 400 s. The sensor surface was regenerated with 25 µL of a 20 mM HCl solution. The resulting sensorgrams were referenced by subtracting the signal from the reference flow channel (Fc1) from Fc2. To obtain the dissociation equilibrium constant (K_D) the sensorgrams were fitted by a global Langmuir 1:1 model (BIAevaluation software) using the six lowest V_{HH} concentrations.

4.5 ACKNOWLEDGMENTS

Special thanks to Michiel Harmsen, Cees Waalwijk, Richard Anthony and Alice den Hertog for fruitful discussions and helpful suggestions. Also we would like to express our gratitude to Mohamed El Khattabi for help with lymphocyte purification

procedure. Peter Hermans and Christa van der Gaast-deJongh are acknowledged for kind supply of *S. pneumoniae* and *H. influenzae*.

4.6 REFERENCES

1. WHO (2010) The global plan to stop TB 2011–2015: transforming the fight towards elimination of tuberculosis. World Health Organization Library, Geneva.
2. G Ferrara, M Losi, LM Fabbri, GB Migliori, L Richeldi, L Casali *Archivum Immunologiae et Therapiae Experimentalis*. 2009, 57, 425–433.
3. D Goletti, C Stefania, O Butera, M Amicosante, M Ernst, I Sauzullo, V Vullo, D Cirillo, E Borroni, R Markova, R Drenska, J Dominguez, I Latorre, C Angeletti, A Navarra, N Petrosillo, FN Lauria, G Ippolito, GB Migliori, C Lange, E Girardi *PLoS ONE*. 2008, 3, e3417.
4. D Helb, M Jones, E Story, C Boehme, E Wallace, K Ho, J Kop, MR Owens, R Rodgers, P Banada, H Safi, R Blakemore, NTN Lan, EC Jones-López, M Levi, M Burday, I Ayakaka, RD Mugerwa, B McMillan, E Winn-Deen, L Christel, P Dailey, MD Perkins, DH Persing, D Alland *Journal of Clinical Microbiology*. 2010, 48, 229–237.
5. M Morgan, S Kalantri, L Flores, M Pai *BMC Infectious Diseases*. 2005, 5, 62-71.
6. JC Palomino *FEMS Immunology and Medical Microbiology*. 2009, 56, 103–111.
7. C Wingren, CAK Borrebaeck *Methods in Molecular Biology*. 2009, 509, 57–84.
8. G Zheng, F Patolsky, Y Cui, WU Wang, CM Lieber *Nature Biotechnology*. 2005, 23, 1294–1301.
9. MM Harmsen, HJ De Haard *Applied Microbiology and Biotechnology*. 2007, 77, 13–22.
10. J Beekwilder, A van Houwelingen, J van Beckhoven, A Speksnijder *European Journal of Plant Pathology*. 2008, 121, 477–485.
11. M Dumoulin, K Conrath, A Van Meirhaeghe, F Meersman, K Heremans, LGJ Frenken, S Muyldermans, L Wyns, A Matagne *Protein Science*. 2002, 11, 500–515.
12. JMJ Pérez, JG Renisio, JJ Prompers, CJ van Platerink, C Cambillau, H Darbon, LGJ Frenken *Biochemistry*. 2001, 40, 74–83.
13. S Muyldermans *Biotechnology and Molecular Biology Reviews*. 2001, 74, 277–302.
14. G Knarr, MJ Gething, S Modrow, J Buchner *Journal of Biological Chemistry*. 1995, 270, 27589–27594.
15. S Muyldermans, M Lauwereys *Journal of Molecular Recognition*. 1999, 12, 131–140.
16. AR Coates, J Hewitt, BW Allen, J Ivanyi, DA Mitchison *Lancet*. 1981, 2, 167–169.
17. Z Chang, TP Primm, J Jakana, IH Lee, I Serysheva, W Chiu, HF Gilbert, FA Quiocho *The Journal of Biological Chemistry*. 1996, 271, 7218–7223.
18. KRU Devi, KSS Kumar, B Ramalingam, R Alamelu *Protein Expression and Purification*. 2002, 24, 188–195.
19. A Verbon, RA Hartskeerl, C Moreno, AHJ Kolk *Clinical & Experimental Immunology*. 1992, 89, 395–401.
20. RJ Wilkinson, KA Wilkinson, KAL De Smet, K Haslov, G Pasvol, M Singh, I Svarcova, J Ivanyi *Scandinavian Journal of Immunology*. 1998, 48, 403–409.
21. AHJ Kolk, ML Ho, PR Klatser, TA Eggelte, S Kuijper, S de Jonge, J van Leeuwen *Clinical & Experimental Immunology*. 1984, 58, 511–521.
22. MM Harmsen, CB van Solt, HPD Fijten, L van Keulen, RA Rosalia, K

Weerdmeester, AHM Cornelissen, MGM De Bruin, PL Eblé, A Dekker *Veterinary Microbiology*. 2007, 120, 193–206.
23. PJ Cummings, NE Hooper, SS Rowland *Hybridoma*. 1998, 17, 151–156.
24. J Sixholo, W van Wyngaardt, C Mashau, J Frischmuth, DH Du Plessis, J Fehrsen *Biologicals*. 2011, 39, 110–116.
25. R Mabry, M Snavely *IDrugs*. 2010, 13, 543–549.
26. S Edwardraja, S Sriram, R Govindan, N Budisa, SG Lee *Molecular BioSystems*. 2011, 7, 258–265.
27. Y Yuan, DD Crane, CE Barry III *Journal of Bacteriology*. 1996, 178, 4484–4492.
28. MA Caipa-Campos, JMJ Paulusse, H Zuilhof *Chemical Communications*. 2010, 46, 5512–5514.
29. AR Coates, J Hewitt, BW Allen, J Ivanyi, DA Mitchinson *Lancet*. 1981, 2, 167–169.
30. A Raja, KR Uma Devi, B Ramalingam, PJ Brennan *Clinical and Diagnostic Laboratory Immunology*. 2002, 9, 308–312.
31. A Verbon, RA Hartskeerl, A Schuitema, AH Kolk, DB Young, R Lathigra *Journal of Bacteriology*. 1992, 174, 1352–1359.
32. CK Kennaway, JLP Benesch, U Gohlke, L Wang, CV Robinson, EV Orlova, HR Saibil, NH Keep *Journal of Biological Chemistry*. 2005, 280, 33419–33425.
33. HD Engers, J Bennedsen, TM Buchanan, SD Chaparas, G Kadival, O Closs, JR David, JDA van Embden, T Godal, SA Mustafa, J Ivanyi, DB Young, SHE Katifmann, AG Khomenko, AHJ Kolk, M Kubin, JA Louis, P Minden, TM Shinnick, L Trnka, RA Young *Infection and Immunity*. 1986, 51, 718–720.
34. RA Cox *Microbiology*. 2003, 149, 729–737.
35. SW Hunter, H Gaylord, PJ Brennan *Journal of Biological Chemistry*. 1986, 261, 12345–12351.
36. C Boehme, E Molokova, F Minja, S Geis, T Loscher, L Maboko, V Koulchin, M Hoelscher *Transactions of the Royal Society of Tropical*. 2005, 99, 893–900.
37. AB Andersen, L Ljungqvist, K Hasløv, MW Bentzon *Scandinavian Journal of Immunology*. 2005, 34, 365–372.
38. C Abou-Zeid, I Smith, JM Grange, TL Ratliff, J Steele, GAW Rook *Journal of General Microbiology*. 1988, 134, 531–538.
39. A Verbon, S Kuijper, HM Jansen, P Speelman, AHJ Kolk *Journal of General Microbiology*. 1990, 136, 955–964.
40. BY Lee, SA Hefta, PJ Brennan *Infection and Immunity*. 1992, 60, 2066–2074.
41. Y Guo, Y Zhou, C Wang, L Zhu, S Wang, Q Li, G Jiang, B Zhao, H Huang, H Yu, W Xing, K Mitchelson, J Cheng, Y Zhao *The International Journal of Tuberculosis and Lung Disease*. 2009, 13, 914–920.
42. U Demkow, B Bialas-Chromiec, M Filewska, M Sobiecka, J Kús, M Szturmowicz, T Zielonka, E Augustynowicz-Kopeć, Z Zwolska, M Wasik, E Rowińska-Zakrzewska *Journal of Physiology and Pharmacology*. 2005, 56, 79–84.
43. G Senol, C Ecevit, A Öztürk *Pediatric Pulmonology*. 2009, 44, 839–844.
44. EM Sletten, CR Bertozzi *Angewandte Chemie - International Edition*. 2009, 48, 6974–6998.
45. M Swain, G Anderson, D Zabetakis, R Bernstein, J Liu, LJ Sherwood, A Hayhurst, ER Goldman *Analytical and Bioanalytical Chemistry*. 2010, 398, 339–348.
46. N Kobayashi, H Oyama, Y Kato, J Goto, E Söderlind, CAK Borrebaeck *Analytical Chemistry*. 2010, 82, 1027–1038.

47. F He, L Zhang *Analytical Sciences*. 2002, 18, 397–401.
48. D Qin, X He, K Wang, W Tan *Biosensors & Bioelectronics*. 2008, 24, 626–631.
49. M Duman, E Piskin *Biosensors & Bioelectronics*. 2010, 26, 908–912.
50. LGJ Frenken, RHJ van der Linden, PWJJ Hermans, JW Bos, RC Ruuls, B de Geus, CT Verrips *Journal of Biotechnology*. 2000, l78, 11–21.
51. AD Griffiths, SC Williams, O Hartley, IM Tomlinson, P Waterhouse, WL Crosby, RE Kontermann, PT Jones, NM Low, TJ Allison *EMBO Journal*. 1994, 13, 3245–3260.
52. MP Lefranc,V Giudicelli, C Ginestoux, J Bodmer, W Müller, R Bontrop, M Lemaitre, A Malik, V Barbié, D Chaume *Nucleic Acids Research*. 1999, 27, 209–212.
53. MM Bradford *Analytical Biochemistry*. 1976, 72, 248–254.

CHAPTER 5

The Effect of Uniform Capture Molecule Orientation on Biosensor Sensitivity: Dependence on Analyte Properties

ABSTRACT

Uniform orientation of capture molecules on biosensors has been reported to increase sensitivity. Here it is investigated which analyte properties contribute to sensitivity by orientation. Orientation of capture molecules on biosensors was investigated using variable domains of llama heavy-chain antibodies (V_{HH}s) as capture molecule, and a surface plasmon resonance (SPR) chip as biosensor. Two V_{HH}s were tested in this study: one recognizing foot-and-mouth disease virus (FMDV) and another recognizing the 16 kDa heat-shock protein of *Mycobacterium tuberculosis*. SPR chips with randomly immobilized biotinylated V_{HH}s were compared to streptavidin-coated SPR chips, on which similar quantities of oriented biotinylated V_{HH}s were non-covalently immobilized. Analytes that differ in molecular weight, epitope number and epitope affinity were compared using the FMDV-recognizing V_{HH}. When binding of intact FMDV particles (146S; 8200kDa) or pentameric FMDV coat protein aggregates (12S; 282kDa) was detected, a modest (1–2-fold) increase in sensitivity was observed. When a 26-residue peptide (3 kDa) containing the epitope for V_{HH} recognition was tested, much larger effects of capture molecule orientation (14-fold) on signal were observed. A 20–227-fold improvement was also observed when the epitope peptide was covalently linked to bovine serum albumin (67kDa) or R-phycoerythrin (240kDa). The results indicate that orientation of the capture molecule hardly affects high-affinity interactions, while it leads to strong improvements in sensitivity for lower-affinity interactions.

This chapter was published as:
Anke K. Trilling, Michiel M. Harmsen, Vincent J. B. Ruigrok, Han Zuilhof and Jules Beekwilder. *Biosensors and Bioelectronics.* 2013, 40, 219-226.

5.1 INTRODUCTION

The ongoing need for miniaturization of diagnostic elements such as biosensors implies that space for the actual detection components will be strongly limited. To compensate for this reduction in surface area, the biological detection elements need to be optimized. This optimization may include correct and uniform orientation at high density, in order to enhance analyte binding and to increase sensitivity of the device.[1]

Sensitivity and specificity of biosensors depend on high-affinity and specific capture molecules. Antibodies are generally used as biological capture molecules in immunoassays such as ELISAs, as they form highly specific and high affinity interactions. Nowadays, many biosensors deploy antibodies as capture molecules.[1d, 2] One of the challenges faced in the design of multiplex biosensors is to reach, on a single sensor, a high sensitivity for a large number of targets. One solution may be to achieve a high number of binding units per mm^2, ideally all oriented in the same way. Conventional antibodies, with a typical molecular weight of 150 kDa and a size of 14 nm × 9 nm × 4 nm,[3] are big in size. Due to the presence of many exposed reactive residues, site-specific functionalization of these molecules is challenging. Therefore, the truly oriented printing of antibodies on biosensor surfaces is not straightforward. To deploy antibody-like molecules of smaller size, diverse formats were exploited for use in biosensors.[1d] One such format is the variable domain of heavy-chain antibodies of llamas, which are naturally devoid of light chain (V_{HH}). V_{HH}s offer advantages in terms of size,[4] stability,[5] expression yields[6] and ease in protein engineering.

Various covalent and non-covalent immobilization strategies for proteins have been employed to attach capture molecules to a surface.[7] The extraordinarily high affinity of streptavidin to biotin was frequently used to immobilize biotinylated antibodies on streptavidin-modified surfaces.[8] Site-specific in vivo biotinylation at the C-terminus of V_{HH}s can be achieved by introducing a specific tag sequence, which is biotinylated by the BirA enzyme of *Escherichia coli*.[9] This approach can be used for the orientation of V_{HH} capture molecules onto surfaces. Such orientation provides potential for higher binding capacity of the analyte: whereas in random immobilization, analyte-recognition sites are poorly exposed to the surface, orientation can be tuned for maximal exposure of the capture molecule to the analyte (Fig. 1). Techniques like circular dichroism spectroscopy,[10] total internal reflection ellipsometry,[11] time-of-flight secondary ion mass spectrometry[12] and atomic force microscopy[13] were used to display the antibody orientation in a direct manner. As an alternative, and in fact more directly linked to the application, the signal increase of oriented antibodies can be used as indirect method to determine the successful orientation of antibodies. Increased sensitivity after orientation of antibodies is well documented.[14] However, reported improvements are highly variable, and the impact of analyte properties on the detection limit in uniformly and randomly oriented capture mole-

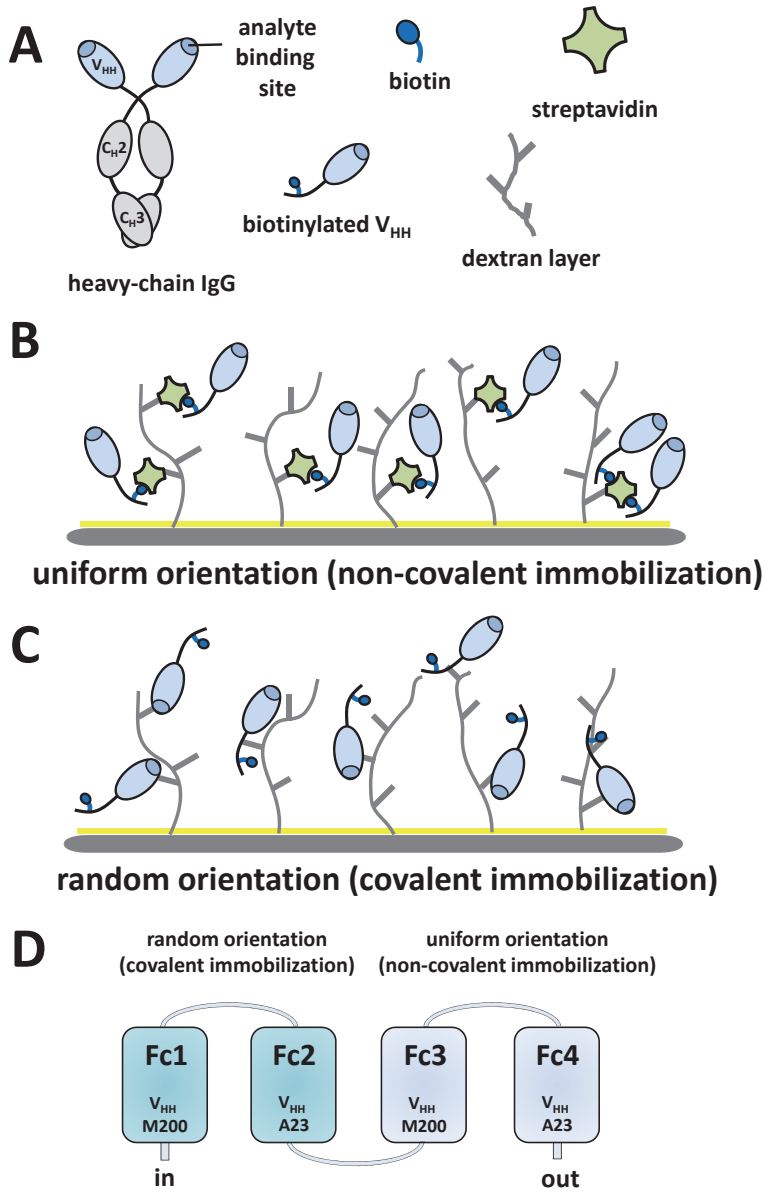

Figure 1. Schematic illustration of immobilized V_{HH}s on a carboxymethyl dextran sensor chip (CM5). A: Heavy-chain antibody IgG. Biotin was introduced at the C-terminus of the V_{HH}, the opposite site of the analyte binding site. B: Biotinylated V_{HH}s non-covalently immobilized in a uniform orientation onto streptavidin-coated CM5 sensor chips. C: Biotinylated V_{HH}s covalently coupled in random orientation via the amine groups onto CM5 sensor chips. V_{HH}s can be immobilized via the ε-amines, present in lysine side chains, or via the α-amine, present at the N-terminus of the protein. D: Set-up of SPR sensor chip with 4 flow channels (Fc). V_{HH} M200 was immobilized randomly oriented in Fc1 and uniformly oriented in Fc3 and V_{HH} A23 was immobilized randomly oriented in Fc2 and uniformly oriented in Fc4. For measurements analyte was injected in series over Fc1, Fc2, Fc3 and Fc4.

cules has not been reported.

In a previous study we showed the use of V_{HH}s as capture molecule using surface plasmon resonance (SPR).[15] In the current study, as a next step, two different V_{HH}s were engineered using a tag sequence to obtain site-specific biotinylation.[9] These two tailor-made V_{HH}s were subsequently immobilized on the sensor surface in two ways: in a randomly oriented, covalent manner (via coupling of amine moieties with the activated surface), and in a uniformly oriented, non-covalent way by the use of streptavidin-coated surfaces and the non-covalent biotin-streptavidin interaction. The sensitivity of the resulting surfaces was studied towards a wide range of analytes. This has led to a high sensitivity enhancement upon uniform orientation (up to factor 227). Finally, we will develop a hypothesis to understand which analyte properties seem to govern the effects of uniform capture molecule orientation on the sensitivity of the sensor, with a specific focus on analyte molecular weight, avidity and specifically affinity.

5.2 Results

5.2.1 Biotinylated V_{HH}s

Two V_{HH}s, M200 and A23 were used. A strategy was used to allow site-specific biotinylation of the V_{HH}s, without affecting their binding properties. The X-ray structure of V_{HH}s reveals that the C-terminus is positioned at the opposite of the analyte-binding site,[16] and biotinylation at the C-terminus is therefore not expected to interfere with analyte binding. Therefore, both V_{HH} genes were fused to a C-terminal AviTag, followed by a His_6 tag for purification. Both V_{HH}s were subsequently produced in *E. coli*, where it was co-expressed with the BirA enzyme. After Ni-NTA purification of the V_{HH}s from the *E. coli* lysate, V_{HH}s were analyzed using western blotting (Fig. 2A). The produced proteins displayed a single band on the western blot, either detected by an anti-His_6-Peroxidase antibody, or by Streptavidin-Peroxidase, indicating that the major biotinylated protein in the capture molecule preparation was the V_{HH}.

5.2.2 Analyte Collection

V_{HH} A23 detects the 16 kDa heat-shock protein in *Mycobacterium tuberculosis*. Two lysates of *M. tuberculosis* (*M. tuberculosis 1* & *M. tuberculosis 27*) were used, which positively react to A23, and compared to a lysate of *M. smegmatis* which is not recognized by A23.[15]

V_{HH} M200 recognizes the foot-and-mouth disease viral particle (FMDV) of the O1 Manisa strain.[17] For an overview of V_{HH} M200 analytes see Table 1. Intact FMDV particles (8200 kDa)[18] are icosahedral and are composed of 60 copies of coat proteins.[19]

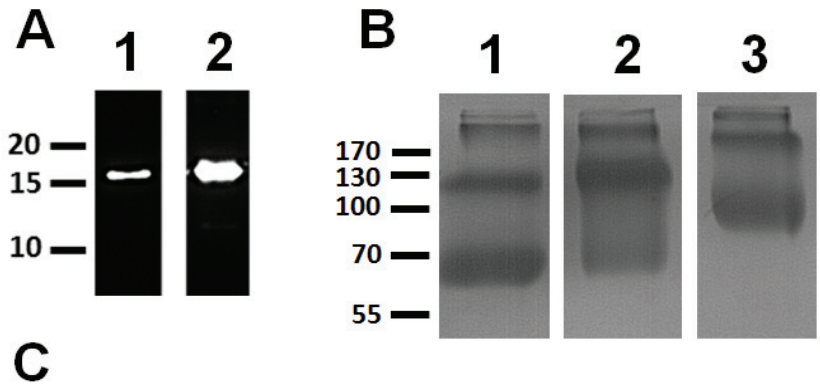

C

```
M200    MQVQLQESGG GLVQPGGSLR LSCVASGTIF SINDISINHL GWYRQAPGKE
A23     MQVQLQESGG GLVQPGGSLR LSCAASGLIF RFSAMS---- -WYRQGPGKE

M200    RELVAAITAD GTSAYEDSV- KGRFIISRDD AKKMVYLQMN SLKPEDTAVY
A23     RELVAGITSN GGTTNYADFA KGRFTISRDN AKNTVDLQMN SLKPEDTAVY

M200    YCNGLRASNA GWEPRFGTWG QGTQVTVSSE PKTPKPQPAA ASSAGGGGSK
A23     YCH---A--- GLRMDSRDWG QGTQVTVSSE PKTPKPQPAA ASSAGGGGSK

M200    LGGGLNDIFE AQKIEWHESH HHHHHG
A23     LGGGLNDIFE AQKIEWHESH HHHHHG
```

Figure 2. Analysis of purified V_{HH}s and BSA-PAT49. A: Western blot analysis of biotinylated V_{HH} M200. 1.5 µg of Ni-resin-purified V_{HH} was used for separation on SDS-PAGE gel. Lane 1: detected with anti-His_6-Peroxidase. Lane 2: detected with Streptavidin-Peroxidase. B: Evaluation of molecular weight shift for BSA upon coupling with PAT49 on SDS-PAGE. Lane1: maleimide-activated BSA starting material. Lane2: BSA-2xPAT49 product after coupling reaction of starting material with 5 molar equivalents peptide PAT49 and blocking of unreacted maleimide-moieties with cysteine, not purified. Lane3: BSA-14xPAT49 product after coupling reaction of starting material with 20 molar equivalents peptide PAT49 and blocking of unreacted maleimide-moieties with cysteine, not purified. Indicated are the positions of relevant size markers in kDa. C: Aligned amino acid sequences of V_{HH} M200 and A23 as produced in *E. coli*. K (green and red) represents amino acid lysine. Underlined sequence at the C-terminus shows AviTag containing one lysine (green) used by enzyme BirA to attach a single biotin molecule. His_6 tag for purification and detection purpose at the C-terminus is shown in blue. Dashes (-) indicate gaps introduced for alignment.

V_{HH} M200 is specific for the GH-loop of coat protein VP1.[17] Intact FMDV are also referred to as 146S particles based on its sedimentation behavior in sucrose density gradients.[20] Mildly acidic conditions were used to breakdown the intact 146S particle into stable 12S particles. 12S particles (265-282 kDa[21]) include 5 copies of VP1,[22] and thus expose 5 epitopic sites for M200.[21] The 3 kDa small peptide PAT49 (YGDGTVANVRGDLQVLAQKAARALPC), corresponding to amino acid residues 136–160 of the GH-loop of structural protein VP1, represents the epitope of FMDV that is recognized by V_{HH} M200.[17] To examine the effect of different analytes on oriented

Table 1. Properties of V_{HH} M200 analytes. For further explanation see text. n.d.: not determined. w/o: without. K_D: affinity constant.

Properties of V_{HH} M200 analytes						
	analyte	**size**	**epitope**	**epitope number per analyte**	**K_D per antigen**	**K_D per epitope**
FMDV (146S)	intact food-and-mouth disease virus particle	8200 kDa[18]	GH-loop	60	0.012 µM	0.72 µM
12S	pentameric subunits of FMDV	265-282 kDa[21]	GH-loop	5	0.19 µM	0.98 µM
peptide PAT49	synthetic peptide representing residues 136–160 of GH-loop of structural protein VP1	3 kDa	synthetic peptide	1	30 µM	30 µM
BSA-14xPAT49 (20 equivalents peptide)	14 peptides PAT49 coupled to BSA	103 kDa	synthetic peptide	ca. 14	n.d.	n.d.
BSA-2xPAT49 (5 equivalents peptide)	2 peptides PAT49 coupled to BSA	72 kDa	synthetic peptide	ca. 2	n.d.	n.d.
R-phycoerythrin-PAT49	peptides PAT49 coupled to R-phycoerythrin	n.d. (240 kDa w/o peptide PAT49)	synthetic peptide	n.d.	n.d.	n.d

capture molecules, proteins exposing multiple copies of peptide PAT49 were prepared. To this end bovine serum albumin (BSA)-PAT49 and R-phycoerythrin-PAT49 were synthesized by coupling the cysteine-containing peptide PAT49 to maleimide-activated proteins. Maleimide-activated proteins possess more than one maleimide-linker, and the coupling reaction with 5 and 20 molar equivalents of peptide PAT49 results in multiple epitope sites exposing analytes. Size shift of BSA-PAT49 on SDS-PAGE (Fig. 2B) indicated that ca. 14 peptides (20 equivalents PAT49) or 2 peptides (5 equivalents PAT49) were bound per BSA molecule, resulting in BSA-14xPAT49 and BSA-2xPAT49, respectively.

5.2.3 A Surface Plasmon Resonance Chip Functionalized with Uniformly Oriented and Randomly Oriented Biotinylated V_{HH}s.

A SPR chip was designed to test the effect of uniform orientation of V_{HH}s on analyte detection. To exclude any influence of the biotinylation of V_{HH} to analyte binding, V_{HH}s were used both in a uniformly oriented and randomly oriented fashion. To this end, two 'uniform orientation` flow channels (Fc3 and Fc4; Fig. 1B and D) of

a CM5 chip were coated with streptavidin, onto which biotinylated V_{HH} was non-covalently immobilized. The other two 'random orientation` flow channels (Fc1 and Fc2; Fig. 1C and D) were functionalized with biotinylated V_{HH}s by covalent carbodiimide chemistry directly onto the CM5 chip, without the use of streptavidin. M200 was immobilized with a uniform orientation in Fc3 and was randomly oriented in Fc1; A23 was immobilized with a uniform orientation in Fc4 and was randomly oriented in Fc2 (Fig. 1D). This set-up allows binding of an analyte sample to uniformly oriented and randomly oriented V_{HH}s in one experiment. To ensure comparability, it was aimed for the same coupling density of V_{HH}s in uniformly oriented and randomly oriented flow channels. Coupling density of antibodies resulted in V_{HH}s immobilized at a level of 3268 ± 391 RU (average of 12 flow channels) over each of the flow channels. To investigate the strength of the different immobilization strategies (covalent versus non-covalent immobilized), repeated cycles of *M.tuberculosis 1* lysate injection and regeneration with 5 µL 10 mM HCl were performed. Non-covalently immobilized V_{HH} (streptavidin-biotin bond) shows a signal loss of 32% after 30 cycles, whereas covalently immobilized V_{HH} (amine group coupled to carboxyl group) shows a signal loss of 10% after 30 cycles (Fig. 3A). In further experiments, binding of analyte was only compared within a cycle rather than between cycles.

5.2.4 Effect of Uniform Orientation of Capture Molecules

5.2.4.1 V_{HH} A23 Binding

To explore the effect of the uniform V_{HH} orientation on analyte binding, different concentrations of analyte were run over all four flow cells of the sensor chip as designed above, using the M200 channels as reference. As expected, *M. tuberculosis 27* lysates showed binding to V_{HH} A23 (Fc2 and Fc4), while negative controls (*M. smegmatis* binding to A23) did not (data not shown). Uniformly oriented V_{HH} A23 showed a signal for *M. tuberculosis 27* lysates that was about five times higher compared to randomly oriented V_{HH} A23 (Fig. 3B).

5.2.4.2 V_{HH} M200 Binding

5.2.4.2.1 Impact of Analyte Size

M200 V_{HH} allows us to test the effect of the molecular weight of the analyte (Table 1), as it binds to both FMDV (8200 kDa) and peptide PAT49 (3 kDa). To this end, these analytes of different size were injected over all four flow channels. As expected, FMDV and peptide PAT49 injections showed binding to V_{HH} M200 (Fc1 and Fc3). When binding was compared between the uniform orientation and the random orientation, orientation yielded a two-fold higher binding of intact FMDV particles

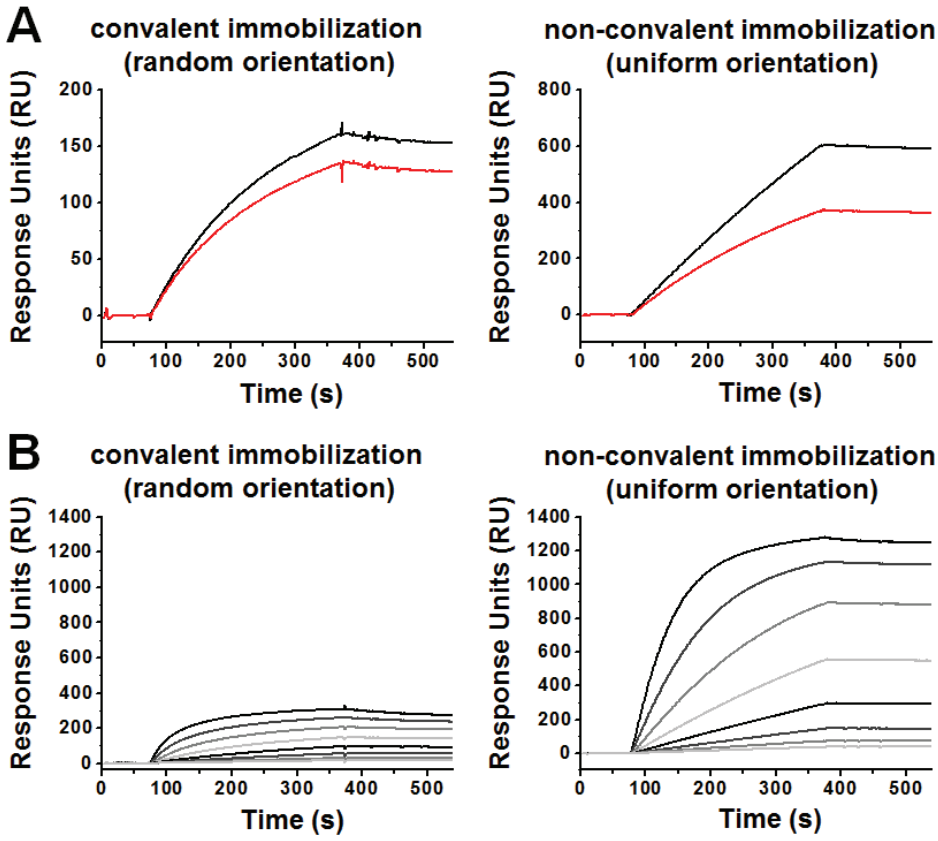

Figure 3. SPR analysis of A23 capture molecule. A: Signal loss of immobilized capture molecules. Samples of *M. tuberculosis 1* lysate (50 µg/mL) were simultaneously analyzed on covalent (left panel) and non-covalent (right panel) immobilized channels, before (black) and after (red) 30 cycles of binding and regeneration by 5 µL 10 mM HCl. B: Signal increase on uniformly oriented capture molecules. Samples of *M. tuberculosis 27* lysate (50 µg/mL) were simultaneously analyzed on randomly oriented (left panel) and uniformly oriented (right panel) channels. Samples contained increasing concentrations of analyte (0.4×10^3, 0.8×10^3, 1.6×10^3, 3.1×10^3, 6.3×10^3, 12.5×10^3, 25×10^3 and 50×10^3 ng protein/mL).

(Fig. 4A). Surprisingly, detection of viral peptide PAT49 benefited much stronger from orientation: a 14 times higher signal was observed when V_{HH}s were uniformly oriented (Fig. 4B).

To investigate the relation between analyte molecular weight and observed signal difference, 12S particle (265-282 kDa) and R-phycoerythrin-PAT49 (240 kDa w/o peptide PAT49) (Table 1) were injected over all four flow channels. Although the molecular weight of both analytes is similar, only detection of R-phycoerythirin-PAT49 benefited from orientation: a 55 times higher signal was observed when V_{HH}s were uniformly oriented (Fig. 4C and D).

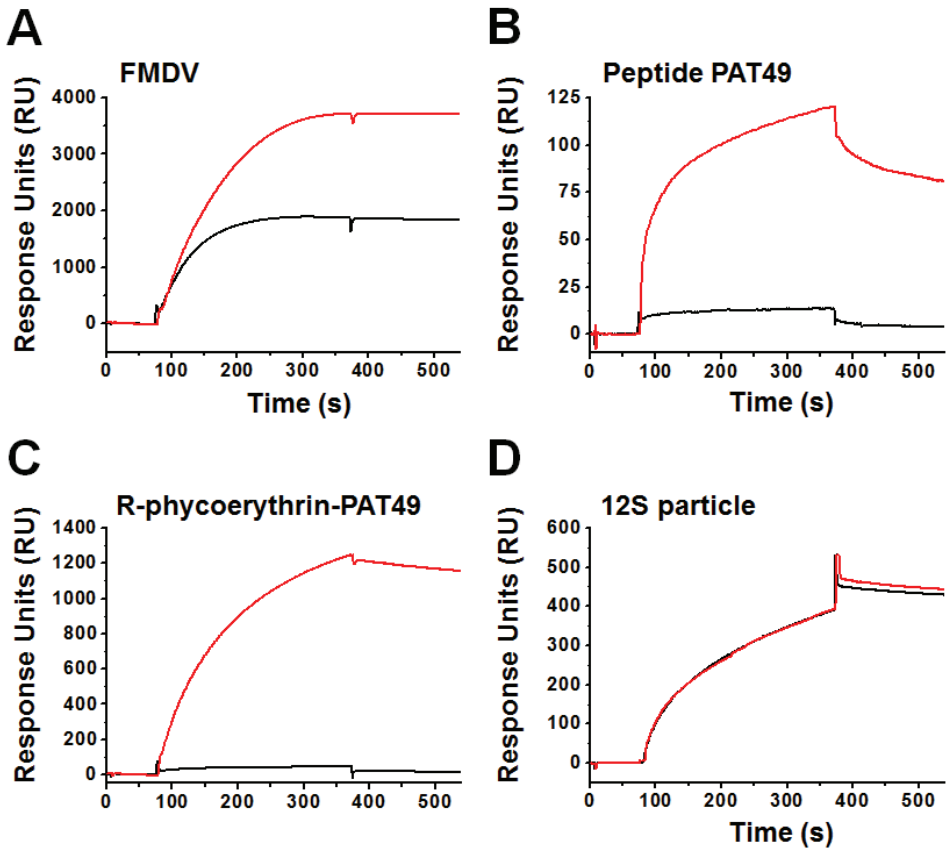

Figure 4. Signal increase by orientation of M200 for analyte with different molecular weight. Sensorgrams obtained after injection of 12.5 µg/mL FMDV (A), 1.25 µg/mL peptide PAT49 (B), 50 µg/mL R-phycoerythrin-PAT49 (C) and 40 µg/mL 12S particle (D). Signal measured by randomly oriented M200 shown in black, measured by uniformly oriented M200 shown in red.

5.2.4.2.2 Impact of Avidity

Comparison of analytes with similar size (R-phycoerythrin and 12S) showed a strong difference in signal increase upon using a uniform orientation of V_{HH}s (Fig. 4C and D), suggesting that other parameters caused the observed signal difference. Another analyte property influencing the binding behavior between analyte and V_{HH} is avidity. Avidity is used to describe the combined binding strength of multiple bond interactions, while affinity is used to define the strength of individual bonds. By the presence of several epitope copies on an analyte, a high apparent affinity will be observed, due to avidity effects. Peptide PAT49 represents a monomeric analyte, whereas FMDV and 12S particles display multiple epitope copies (60 and 5, respectively; Table 1). The influence of avidity on the signal increase was investi-

Table 2. Improvement factor of binding signal obtained by orientation of capture molecule M200. Signal obtained after injection of analyte at indicated concentration. Signal was measured as response unit (RU) 30 seconds after injection was stopped. Improvement factor was calculated by dividing the signal of uniformly oriented V_{HH}M200 by the signal of randomly oriented V_{HH} M200.

FMDV (8200 kDa)			
Concentration analyte (in µg/mL)	SPR signal of randomly oriented M200 (in RU)	SPR signal of uniformly oriented M200 (in RU)	improvement factor
12	1854	3712	2
Peptide PAT49 (3 kDa)			
1	10	138	14
R-phycoerythrin-PAT49 (240 kDa w/o peptide)			
50	22	1208	55
12S particle (265-282 kDa)			
40	446	464	1.0
20	345	345	1.0
5	310	406	1.3
BSA-14xPAT49 (103 kDa)			
50	28	763	27
25	31	695	22
12	29	622	21
6	23	598	26
3	18	521	29
BSA-2xPAT49 (72 kDa)			
50	3	508	170
25	2	454	227
12	2	366	183

gated by injecting various concentrations of BSA-14xPAT49 (ca. 14 peptides PAT49 per binding unit) and 12S particles (5 GH-loops per binding unit) over all four flow channels. Control experiments using BSA-Cys showed no binding onto any of the channels (data not shown), while both 12S particles and BSA-14xPAT49 showed binding to V_{HH} M200 (Fc1 and Fc3), but did not bind to reference V_{HH} A23 (Fc2 and Fc4) (data not shown). For 12S particles only weak increases in signal (1 to 1.3-fold) could be observed for the uniformly oriented channel (Table 2). For BSA-14xPAT49 containing 14 peptides, on the other hand, large increases in signal intensity (21 to 29-fold) were consistently observed in the uniformly oriented channel (Table 2) over a range of analyte concentrations. Decrease of peptide number in BSA-2xPAT49 (2 peptides PAT49 per binding unit) lead to a stronger increase in signal intensity for the uniformly oriented V_{HH} (170 to 227-fold; Table 2).

5.2.4.2.3 Affinity of Analyte

To study the differences of analytes (natural analyte versus peptide PAT49), affinity of M200 was investigated by ELISA.[23] Observed affinity constants (K_D) are shown in Table 1. The K_D of M200 for the viral derived analytes (FMDV and 12S) was 15-fold lower than the K_D value for the peptide PAT49 analyte.

5.3 Discussion

The experiments performed in the current work for the first time highlight the importance of specific analyte properties on the effect of uniform orientation of the capture molecule (Table 2; Fig. 3B and 4). Uniform orientation of the M200 V_{HH} affects the binding efficiency of nearly all analytes, but the range of enhancement is rather large: from a hardly noticeable increase by a factor 1.3 to a large 227-fold increase.

The M200 V_{HH} that were immobilized in randomly and uniformly oriented ways allowed us to investigate binding properties of a collection of analytes, which differ in properties such as molecular weight, number of epitopes and affinity.

Our initial hypothesis was that the size of the analyte is important for the effect of uniform orientation. An experiment comparing peptide PAT49 to FMDV particles suggested this (Fig. 4A and B). Peptide PAT49 binding to randomly oriented M200 resulted in a 14-times lower binding signal compared to uniformly oriented M200, whereas the effect of orientation was modest for analyte FMDV. Peptide PAT49 (3 kDa) is about 6 times smaller than M200 (18 kDa) and therefore diffuses more efficiently through the dextran layer covering the CM5 SPR chip, binding to all accessible V_{HH}s on the surface. This suggests that 14 times less V_{HH}s are available for analyte binding in the random orientation. Larger analytes, however, can affect binding by lateral packing leading to a lower amount of captured analyte. Tested FMDV, with

a mass of 8200 kDa and a diameter of 25 nm,[24] represents such a big analyte. Orientation of capture molecules showed only a modest signal increase for FMDV, which might be caused by molecular weight-related factors, such as steric hindrance, shielding neighboring capture molecules upon analyte binding, and a limitation in the capacity to penetrate the dextran layer. The effect of size should be negligible when 12S particles were compared with R-phycoerythrin-PAT49. Both have similar sizes (Table 1), and would benefit in a similar way from uniform orientation. Surprisingly, however, R-phycoerythrin-PAT49 showed an enormous, 55-fold signal increase upon uniform orientation of the M200 V_{HH}s, while 12S particles did not show any such effect (Fig. 4C and D, Table 2). Therefore other explanations for differences in the effect of uniform orientation were investigated.

A second explanation for differences in the effect of uniform orientation was possibly epitope avidity. Avidity, which reflects the combined binding strength of multiple analyte-antibody interactions, could depend on many factors: e.g. capture molecule density, flexibility of antibody, analyte, dextran layer and the availability of free antibodies. We tried to find consistent effects of the number of epitopes. In SPR, analyte bound to one capture molecule gives the same signal as an analyte bound via several capture molecules. However, binding to multiple capture molecules leads to stabilization of the analyte-antibody complex on the chip and shifts the equilibrium constant.[25] To examine the relation of analyte-avidity and signal increase by uniform orientation, proteins varying in the number of exposed epitopes were compared, but no consistent relationship between epitope number and effect of orientation could be observed.

Comparing intact FMDV (60 GH-loop epitopes) and 12S particles (5 GH-loop epitopes), only a slight effect could be observed, showing that more epitopes would lead to a somewhat stronger effect of orientation (Table 2). On the other hand, the comparison of BSA-PAT49 carrying 14 or 2 peptide epitopes suggests an opposite effect: BSA-14xPAT49 carrying 14 epitopes showed ±25-fold higher binding by orientation, whereas BSA-2xPAT49 carrying only 2 epitopes showed a ±200-fold increase in signal. The monomeric PAT49 peptide by itself, showed again a 14-fold improved signal by orientation. Apparently there is not a straightforward relationship between the number of epitopes and the effect of orientation.

The experiments presented in this work indicate that the effect of uniform orientation is much higher on peptide PAT49 and its protein conjugates (BSA-PAT49 and R-phycoerytrin-PAT49), compared to virus-derived analytes such as FMDV and 12S. In fact, the results in Figure 3 and 4 suggest that the binding of PAT49-containing analytes is hampered on non-oriented M200 V_{HH}. Possibly, the chemistry used for random immobilization could result in a bias towards wrongly-oriented capture molecules. For random orientation, covalent cross-linking between free, accessible primary amines of biotinylated V_{HH} and the carboxyl group on the CM5 surface was used. Primary amines are usually outward-facing in the protein due

to its positive charge under physiological conditions,[26] and therefore are accessible for conjugation. V_{HH}s can be immobilized via the ε-amines, present in lysine side chains, or via the α-amine, present at the N-terminus of the protein. Biotinylated M200 contains eight lysine side chains and A23 contains seven available lysine side chains (Fig. 2C), therefore multiple orientations during immobilization are possible via ε-amines. However, due to its lower pK value, the reactivity of the N-terminal amino group is about 300 times higher than that of amino groups of lysine side-chains.[7] The N-terminus of V_{HH}s is located close to the analyte binding site. Therefore, the use of the standard, non-oriented immobilization method could result in a situation where more V_{HH}s are immobilized 'up-side down` via the N-terminal $\alpha$-amine in the non-orientated immobilization method than by the $\varepsilon$-amines present in lysine side chains. However, a predominant 'up-side down` orientation of V_{HH} would not explain why PAT49-containing analytes would bind more poorly, while this seems not to be the case for the more bulky FMDV and 12S analytes. Possibly, the configuration of the binding site affects binding behavior more strongly than avidity or size. The epitope amino acids as they occur in peptide PAT49 are probably not in their natural analyte environment. Therefore they may adopt a configuration that differs from the native (virus) configuration, which may lower the affinity of V_{HH} M200. Indeed it was previously reported that the peptide conformation plays a crucial role in antibody-analyte interaction.[27] The GH-loop forms a highly flexible, disordered protrusion of structural protein VP1 on the virus surface, but synthetic GH-loop peptides introduced into carrier molecules showed that stabilization of the loop is dependent on contacts of neighboring regions.[28] Therefore the affinity of M200 should differ between investigated analytes. Indeed, the affinity for peptide PAT49 was lower than for the analytes FMDV and 12S, suggesting that affinity of analytes has an effect in the tested set-up. Also Peluso et al.[14c] suggested that affinity might play a major role when low concentrations of analyte were used.

In all cases studied here, the uniform orientation of capture molecules leads to improvements of signal, both for the A23 and the M200 V_{HH}. Although the extent to which orientation results in signal improvement differed. The differential effect of uniform orientation on signal intensity between different capture molecules has been well documented. Many studies have been performed using staphylococcal protein A to orient antibodies, and have demonstrated clear effects of orientation on immunoassay sensitivity (e.g. Tajima et al.)[1b]. Peluso et al. compared randomly biotinylated and site-specifically biotinylated capture molecules (immunoglobulins and Fab fragments), using three different antibodies, and observed 1.6 to 10-fold improvements, depending on the capture molecule.[14c] In their work, the orientation was mediated by either site-specific or random biotinylation. A study carried out on V_{HH}s in a set-up very similar to ours, site-specific biotinylation showed a slightly decreased level of detection compared to V_{HH}s that were randomly immobilized via the primary amines.[8b] Similar to our set-up, Saerens et al. used the C-terminus to

introduce the biotin moiety by BirA enzyme leading to unique probe biotinylation at the antipode of the analyte binding site. One of the explanations for the difference between the two studies could be that the human prostate-specific analyte, which was used in their study, has properties that do not favor recognition by uniformly oriented V_{HH}. Another explanation could be that the rigid human IgA-1 hinge deployed by Saerens et al. between the V_{HH} and the AviTag interfered with correct orientation, while the flexible glycine-rich linker deployed in this study (Fig. 2C) would permit a correct orientation.

5.4 Conclusion

In the current work we show that analyte properties can have a large impact on biosensors signals when uniformly oriented and randomly oriented capture molecules are used. Orientation effects up to a factor 227 have been measured, and the observed range of orientation effects (factor 1.3 to 227) was analyzed with respect to a series of analyte properties. While size and avidity effects do not seem to give a systematic improvement factor, the strength of the interaction dominates the effect of orientation of the antibody: weaker interactions benefit much more from uniform orientation than stronger interactions. Clearly, this steers the further research that is needed into the effect of capture molecule orientation on sensing of target and non-target analytes.

5.5 Material and Methods

5.5.1 Analytes of V_{HH}

V_{HH} A23 (Genbank accession no JN234011) detects the 16 kDa heat-shock protein of *Mycobacterium tuberculosis,* and was characterized before.[15] *Mycobacterium* lysates (*M. tuberculosis 1, M. tuberculosis 27 and M. smegmatis,* Royal Tropical Institute, Amsterdam, the Netherlands) were prepared as described before.[15]

V_{HH} M200 is specific for the GH-loop of structural protein VP1 of foot-and-mouth disease virus (FDMV).[17] FMDV analyte and 12S particles derived thereof by acidification were prepared as described before.[29] Peptide PAT49 (acetyl-YGDGTVAN-VRGDLQVLAQKAARALPC-amide), corresponding to amino acid residues 136-160 of the GH-loop of the FMDV O1 Manisa strain was purchased from Peptide 2.0 (Chantilly, US). Peptide PAT49 was coupled with the additional C-terminal cysteine residue to maleimide-activated bovine serum albumin (BSA) and R-phycoerythrin (Innova Biosciences Ltd., United Kingdom). Maleimide-activated protein was reacted overnight at room temperature in phosphate-buffered saline (PBS) pH 7.2 with peptide PAT49 in a 1:20 and 1:5 molar ratio, resulting in BSA-PAT49 and R-phycoerythrin-PAT49. To subsequently block unreacted maleimide moieties, cysteine was

added in excess. BSA-PAT49 and R-phycoerythrin-PAT49 were purified on Superdex 200 (GE Healthcare, Uppsala, Sweden) and concentrated using filter tubes (Millipore, the Netherlands). Protein concentrations were determined with the Pierce 660 nm Protein assay using NanoDrop 1000 and albumin as reference protein for the standard curve.

5.5.2 Biotinylation of V_{HH}

V_{HH}s are present in a vector for periplasmic V_{HH} expression under control of the T7 promoter, based on the backbone of the pRSET-A vector (Invitrogen, the Netherlands). The C-terminus of the V_{HH} was fused to an AviTag (GLNDIFEAQKIEWHE) (Avidity, LLC, Colorado) for in vivo biotinylation along with a His_6 tag for purification purposes followed by a stop codon. Plasmid pBirAcm, an IPTG inducible plasmid containing the BirA gene engineered into pACYC184 (Avidity), was transformed to *E.coli* BL21-AI and used for in vivo biotinylation. Expression was performed according to Cloutier et al.,[30] purification was performed as reported before.[15]

5.5.3 Western Blot Analysis

Purified biotinylated V_{HH} (1.5 μg) was first boiled and reduced in buffer and electrophoresed on a 15% SDS-PAGE gel. For western blotting, proteins were transferred from gel to a nitrocellulose membrane (Trans-Blot, Bio-Rad, Hercules, CA). These membranes were subsequently blocked overnight at room temperature in 2% milk in PBS pH 9.0 on a shaker, and then incubated with either anti-His_6-Peroxidase (1:4000 in 2% [w/v] milk in PBS pH 9.0, Roche, Mannheim, Germany) or streptavidin-peroxidase (1:5000 in 2% [w/v] milk in PBS pH 9.0, Roche) for 1 h at room temperature on a shaker. Next, the membranes were washed once with 2% milk in PBS pH 9.0, followed by two washing steps with PBS pH 9.0 containing 0.1% Tween 20 and two washing steps with PBS pH 9.0. Specific binding was detected with 3,3',5,5'-tetramethylbenzidine (TMB) liquid substrate system for membranes (Sigma-Aldrich, the Netherlands). The molecular weight standard was Page Ruler Prestained Protein ladder (Thermo Scientific).

5.5.4 Surface Plasmon Resonance (SPR)

Carboxymethyl dextran sensor chips (CM5), HBS-EP buffer (pH 7.4, consisting of 10 mM 4-[2-hydroxyethyl]piperazine-1-ethanesulfonic acid, 150 mM sodium chloride, 3 mM ethylenediaminetetraacetic acid, 0.005% v/v surfactant polysorbate 20), the amine coupling kit (containing 0.1 M N-hydroxysuccinimide [NHS], 0.4 M 1-ethyl-3-[3-dimethylaminopropyl]carbodiimide hydrochloride [EDC] and 1 M ethanolamine hydrochloride [pH 8.5]) were purchased from GE Healthcare (Uppsala, Sweden).

Oriented immobilization: In a BIAcore 3000 streptavidin was immobilized onto a CM5 surface by the use of the amine coupling kit and the ´Aim-for–Immobilization` wizard as present in the BIAcore 3000 control software. To this aim the biosensor surface was activated by injecting (35 µL at a flow rate of 5 µL/min) a mixture of EDC and NHS (1:1; v/v) into flow channels (Fc3 and Fc4). Then streptavidin (50 µg/mL in coupling buffer [10 mM sodium acetate, pH 4.0]) was injected and bound to the activated carboxymethylated dextran surface via its primary amine groups, aiming for an immobilization level of 4000 response units (RU). After coupling, the remaining active groups were blocked with ethanolamine hydrochloride (1 M, 35 µL at a flow rate of 5 µL/min). V_{HH}s with a site-specifically attached biotin label were subsequently captured onto a streptavidin surface in flow channels (Fc3 and Fc4, Fig. 1B) in an oriented manner. To non-covalently immobilize biotinylated V_{HH}s on the streptavidin surface 10 µL biotinylated V_{HH} M200 (50 µg/mL in HBS-EP buffer) was injected at a flow of 5 µL/min over Fc3 resulting in 3183 ± 638 RU. The same procedure was repeated for biotinylated V_{HH} A23 on Fc4 resulting in 3125 ± 423 RU.

Random orientation: Biotinylated V_{HH}s were immobilized onto a CM5 surface by the use of the amine coupling kit and the ´Aim-for–Immobilization` wizard. The biosensor surface was activated by injecting (35 µL at a flow rate of 5 µL/min) a mixture of EDC and NHS (1:1, v/v) into flow channels (Fc1 and Fc2) (Fig. 1C). Then biotinylated V_{HH} (50 µg/mL in coupling buffer) was injected and bound to the activated carboxymethylated dextran surface via its primary amine groups, aiming for an immobilization level of 3500 response units (RU). After coupling, the remaining active groups were blocked with ethanolamine hydrochloride (1 M, 35 µL at a flow rate of 5 µL/min). Immobilization of biotinylated V_{HH} M200 on Fc1 resulted in 3420 ± 317 RU, of biotinylated V_{HH} A23 on Fc2 in 3344 ± 262 RU.

The BIAcore 3000 SPR machine was operated at a constant temperature of 25 °C and a flow of 10 µL/min. 50 µL analyte preparations in HBS-EP buffer, each of different analyte concentration, were injected over the four serially connected flow channels. Regeneration of the sensor surface was achieved with 5 µL of a 10 mM hydrogen chloride solution (HCl), which was passed through at a flow rate of 10 µL/min after each run. Data points were measured 30 seconds after injection end at time point 400.5 sec. All sensorgrams were referenced by subtracting the signal from the reference flow channel and were evaluated using the BIAevaluation software.

5.5.5 Affinity Measurements

Affinity of V_{HH} M200 to peptide PAT49, FMDV and 12S was determined by ELISA, using a competition assay as done before.[30] Shortly, 100 µL of a 50 nM V_{HH} M200 solution was pre-incubated overnight with a dilution series of analyte at room temperature in 2% milk PBS pH 9.0. Pre-incubated V_{HH} M200 was then transferred to a

plate coated with a low density of analyte (FMDV: 1 μg/mL total protein corresponding to 0.2 μg/mL FMDV, 12S particle: 1 μg/mL total protein corresponding to 0.2 μg/mL 12S particle and peptide PAT49: 0.5 μg/mL) in 50 mM carbonate buffer pH 9.6. V_{HH} M200 bound to the plate was detected using anti-His_6-Peroxidase (1:4000 in 2% (w/v) milk in PBS pH 9.0, Roche). Subsequently HRP activity was determined by adding 1-StepTM Ultra TMB-ELISA substrate (Pierce, Rockford, IL). The reaction was allowed to proceed in the dark for 30 min and then stopped with 1 M sulphuric acid and the OD was measured at 415 nm in a microtiter plate-reader (TECAN SpectraFluor Microplate Reader).

5.6 Acknowledgements

This work was funded by the European Union through the Marie Curie Integrated Training Network project Hierarchy (contract: PITN-2007-215851) and the IPOP (Instellings Plan/Ontwikkelings Plan)-Bionanotechnology program, a Wageningen UR strategic research program running from 2008–2011. Sponsors had no influence in study design; collection, analysis, and interpretation of data; in the writing of the report; and in the decision to submit the paper for publication. The help and suggestions made by Dr. Maarten Jongsma and Dr. Willem Haasnoot are kindly acknowledged. The authors also like to thank Saurabh Kumar Srivastava for preparation of V_{HH} constructs.

5.7 References

1 a) MH Seo, J Han, Z Jin, DW Lee, HS Park, HS Kim *Analytical Chemistry*. 2011, 83, 2841-2845.
b) N Tajima, M Takai, K Ishihara *Analytical Chemistry*. 2011, 83, 1969-1976.
c) SK Vashist, CK Dixit, BD MacCraith, R O'Kennedy *Analyst*. 2011, 136, 4431-4436.
d) X Zeng, Z Shen, R Mernaugh *Analytical and Bioanalytical Chemistry*. 2012, 402, 3027-3038.

2 TRJ Holford, F Davis, SPJ Higson *Biosensors & Bioelectronics*. 2012, 34, 12-24.

3 VR Sarma, EW Silverton, DR Davies, WD Terry *Journal of Biological Chemistry*. 1971, 246, 3753-3759.

4 M Dumoulin, K Conrath, A Van Meirhaeghe, F Meersman, K Heremans, LGJ Frenken, S Muyldermans, L Wyns, A Matagne *Protein Science*. 2002, 11, 500-515.

5 D Saerens, L Huang, K Bonroy, S Muyldermans *Sensors*. 2008, 8, 4669-4686.

6 YE Thomassen, W Meijer, L Sierkstra, CT Verrips *Enzyme and Microbial Technology*. 2002, 30, 273-278.

7 K Hernandez, R Fernandez-Lafuente *Enzyme and Microbial Technology*. 2011, 48, 107-122.

8 a) IH Cho, EH Paek, H Lee, JY Kang, TS Kim, SH Paek *Analytical Biochemistry*. 2007, 365, 14-23;
b) D Saerens, F Frederix, G Reekmans, K Conrath, K Jans, L Brys, L Huang,

E Bosmans, G Maes, G Borghs, S Muyldermans *Analytical Chemistry*. 2005, 77, 7547-7555.

9 D Beckett, E Kovaleva, PJ Schatz *Protein Science*. 1999, 8, 921-929.

10 AP Le Brun, SA Holt, DSH Shah, CF Majkrzak, JH Lakey *Biomaterials*. 2011, 32, 3303-3311.

11 Z Balevicius, A Ramanaviciene, I Baleviciute, A Makaraviciute, L Mikoliunaite, A Ramanavicius *Sensors and Actuators B*. 2011, 160, 555-562.

12 a) JE Baio, F Cheng, DM Ratner, PS Stayton, DG Castner *Journal of Biomedical Materials Research Part A*. 2011, 97A, 1-7.
b) IH Cho, JW Park, TG Lee, H Lee, SH Paek *Analyst*. 2011, 136, 1412-1419;
c) JW Park, IH Cho, DW Moon, SH Paek, TG Lee *Surface and Interface Analysis*. 2011, 43, 285-289.

13 L Farris, M McDonald *Analytical Bioanalytical Chemistry*. 2011, 401, 2821-2829.

14 a) IH Cho, SM Seo, JW Jeon, SH Paek *Journal of Biomedicine and Biotechnology*. 2009, 104094, 1110-7243.
b) T Klonisch, G Panayotou, P Edwards, AM Jackson, P Berger, PJ Delves, T Lund, IM Roitt *Immunology*. 1996, 89, 165-171.
c) P Peluso, DS Wilson, D Do, H Tran, M Venkatasubbaiah, D Quincy, B Heidecker, K Poindexter, N Tolani, M Phelan, K Witte, LS Jung, P Wagner, S Nock *Analytical Biochemistry*. 2003, 312, 113-124.
d) G Shen, C Cai, K Wang, J Lu *Analytical Biochemistry*. 2011, 409, 22-27.
e) HY Song, X Zhou, J Hobley, X Su *Langmuir*. 2011, 28, 997-1004.
f) MMLM Vareiro, J Liu, W Knoll, K Zak, D Williams, ATA Jenkins *Analytical Chemistry*. 2005, 77, 2426-2431.

15 AK Trilling, H de Ronde, L Noteboom, A van Houwelingen, M Roelse, SK Srivastava, W Haasnoot, MA Jongsma, A Kolk, H Zuilhof, J Beekwilder *PLoS ONE*. 2011, 6, e26754.

16 a) JG Renisio, J Pérez, M Czisch, M Guenneugues, O Bornet, L Frenken, C Cambillau, H Darbon *Proteins*. 2002, 47, 546-555.
b) S Spinelli, L Frenken, D Bourgeois, L dRon, W Bos, T Verrips, C Anguille, C Cambillau, M Tegoni *Nature Structural Biology*. 1996, 3, 752-757.

17 MM Harmsen, CB van Solt, HPD Fijten, L van Keulen, RA Rosalia, K Weerdmeester, AHM Cornelissen, MGM De Bruin, PL Eble, A Dekker *Veterinary Microbiology*. 2007, 120, 193-206.

18 GF Vande Woude, JB Swaney, HL Bachrach *Biochemical and Biophysical Research Communications*. 1972, 48, 1222-1229.

19 E Fry, D Stuart, D Rowlands *Current Topics in Microbiology and Immunology*. 2005, 288, 71-101.

20 TR Doel, PJ Baccarini *Archives of Virology*. 1981, 70, 21-32.

21 C Vasquez, CD Denoya, JL La Torre, EL Palma *Virology*. 1979, 97, 195-200.

22 DV Sangar, DJ Rowlands, D Cavanagh, F Brown *Journal of General Virology*. 1976, 31, 35-46.

23 SQ Hutsell, DP Siderovski, FS Willard, AJ Kimple in Surface Plasmon Resonance, Vol. 627, Publisher: Humana Press, 2010, 75-90.

24 MJ Grubman, B Baxt *Clinical Microbiology Reviews*. 2004, 17, 465-493.

25 AV Pukin, HM Branderhorst, C Sisu, CAGM Weijers, M Gilbert, RMJ Liskamp, GM Visser, H Zuilhof, RJ Pieters *ChemBioChem*. 2007, 8, 1500-1503.

26 GT Hermanson *Bioconjugate Techniques.* 2008, 2nd edition.
27 P. Gomes, E. Giralt, D. Andreu *Vaccine.* 2001, 19, 3459-3466.
28 a) JX Feliu, A Benito, B Oliva, FX Avilés, A Villaverde *Journal of Molecular Biology*. 1998, 283, 331-338.
b) G de Prat-Gay *Archives of Biochemistry and Biophysics.* 1997, 341, 360-369.
29 a) MM Harmsen, HPD Fijten, A Dekker, PL Eblé in In Proceedings of the First Annual Meeting EPIZONE 'EPIZONE INSIDE OUT', May 30th - June 1st 2007, Lublin, Poland, 2007.
b) MM Harmsen, HPD Fijten, DF Westra, JM Coco-Martin *Vaccine*. 2011, 29, 2682-2690.
30 SM Cloutier, S Couty, A Terskikh, L Marguerat, V Crivelli, M Pugnières, JC Mani, HJ Leisinger, JP Mach, D Deperthes *Molecular Immunology*. 2000, 37, 1067-1077.
31 MM Harmsen, HPD Fijten, A Dekker, PL Eble *Veterinary Microbiology*. 2008, 132, 56-64.

CHAPTER 6

Oriented Llama Antibodies Strongly Increase Sensitivity of Biosensors

ABSTRACT

To reach high sensitivity in biosensors, uniform orientation of capture molecules on sensing surfaces is required. The objective of this study was the organization of capture molecules on surfaces in a way that the analyte binding site is exposed to the analyte solution. For this purpose, V_{HH} proteins recognizing foot-and-mouth disease virus (FMDV) were used. Azides were introduced in the V_{HH} to function as bioorthogonal reactive groups. The importance of oriented organization was addressed by comparing V_{HH} containing multiple exposed azide groups to V_{HH} carrying only a single azide group. A surface plasmon resonance (SPR) chip exposing cyclooctyne was reacted to azide functionalized V_{HH} domains, using click chemistry. Comparison between random and uniform oriented capture molecules showed up to 800-fold increase in biosensor sensitivity. This technique may increase the containment of infectious diseases such as FMDV as its strongly enhanced sensitivity may facilitate early diagnostics.

This chapter was submitted.

6.1 INTRODUCTION

Biosensors combine analytical devices with biological capture components to sense the presence of analytes. Antibodies are proteins that are widely used in biosensors, due to their high specificity. In addition to full-sized antibodies (e.g. IgG), fragments of antibodies, such as Fabs (fragment, antigen binding) have been employed in biosensors.[1] These fragments contain the analyte recognition site, but can be designed and produced as recombinant proteins for applications in biosensors.[2] The smallest natural antibody-based binding unit is the variable domain of llama heavy-chain antibodies (V_{HH}), which has a diameter of a few nm.[3] Such binding fragments are attractive for nanotechnology, since they can be easily tailored by protein engineering and included in biosensors.[4] In the current chapter we show how such tailoring can be used to orient V_{HH}s onto a sensor surface, which can lead to an improvement of the sensor sensitivity of several orders of magnitude (here: up to factor 800).

Immobilization methods have an impact on the analytical performance in biosensors, as they affect the lifetime and orientation of the antibodies. Amine groups located at the surface of the antibody are often used to attach the protein covalently to activated carboxyl groups on sensor materials.[5] This method results in a random orientation, which reduces the efficiency of the sensor, as a large portion of the antibodies will not expose the analyte binding site to the analyte solution. Several techniques to position the antibodies in a uniform orientation on the surface have been explored, such as protein A or G for immunoglobulin or the biotin-streptavidin system.[5a, 6] A common drawback of these methods is that they require an intermediate protein and rely on non-covalent protein-protein interactions. Inevitably this will negatively affect the lifetime of the biosensor and increase the distance between capture component and sensor surface.[5a] To establish stable covalent links to proteins in an aqueous environment, mild, biocompatible and selective click reactions, such as the 1,3-dipolar cycloaddition between an azide and an alkyne, have recently been developed.[7] Such reactions can be catalyzed by copper(I), or may occur in the absence of a catalyst, when the ligand contains a highly strained cyclic alkyne (e.g. cyclooctyne) with a low activation energy (so-called CuAAC and SPAAC reactions, respectively).[8] Azides may be incorporated into proteins as the non-natural amino-acid azidohomoalanine (AHA), an analogue which replaces methionine.[9] In this way, click chemistry has been deployed for the labelling of cells by dye conjugation, or for establishing enzyme complexes.[10] Here we explore both the CuAAC and SPAAC reactions to finally obtain a uniform orientation of V_{HH} antibodies onto a surface plasmon resonance (SPR) biosensor surface (Fig. 1). This biosensor detects epitopes from foot-and-mouth disease virus (FMDV), and the virus itself.

6.2 Results And Discussion

To study oriented antibodies on alkyne-exposing surfaces, a V_{HH} molecule with only a single accessible azide group was designed and compared to a V_{HH} with five accessible azides. V_{HH} M200, which recognizes the virus FMDV,[11] normally contains

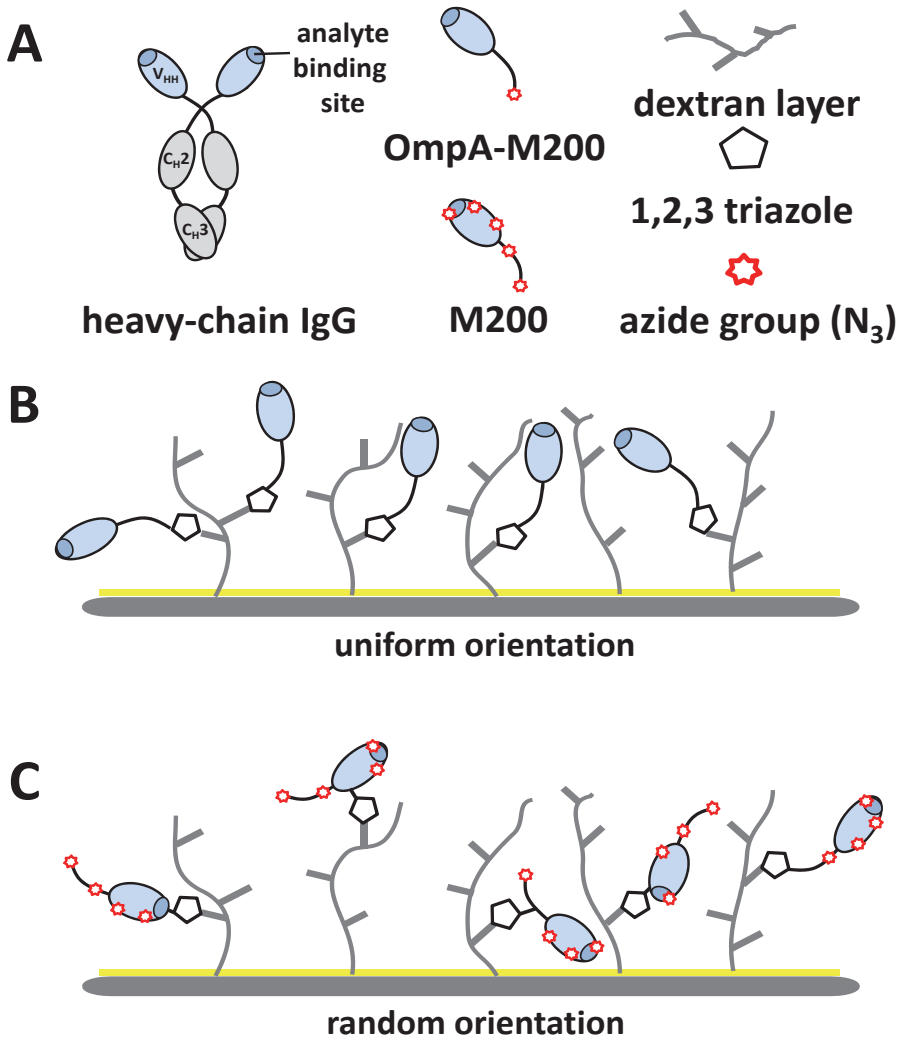

Figure 1. Schematic illustration of the orientation of immobilized V_{HH}s with tailor-made modifications on a sensor chip. A: Azide-functionalized V_{HH} receptors M200 and engineered V_{HH} OmpA-M200 are smaller analogues of full llama heavy-chain IgG. B: Azide-functionalized V_{HH} OmpA-M200 covalently coupled in a uniform orientation onto a cyclooctyne-functionalized CM5 sensor. C: azide-functionalized V_{HH} M200 covalently coupled in a random orientation via one of five available azides onto a cyclooctyne-tailored CM5 sensor.

five methionine positions, and can thus be immobilized in five orientations upon AHA introduction. M200 was mutated to remove those methionines, and to introduce a single, C-terminal methionine group (OmpA-M200, Fig. 2). The C-terminus is one of the exposed parts of the V_{HH} protein, and located opposite of the analyte binding site. Immobilization via this part of the protein would thus orient the V_{HH} to expose its analyte binding region to the solvent (Fig. 1B). To study the influence of replacing the internal methionine residues on binding affinity towards the analyte, V_{HH}s were examined by enzyme linked immunosorbent assay (ELISA). The original V_{HH} M200, containing five methionine residues, showed similar ELISA responses as the engineered M200 (with altered methionines [M83, M88 and M153] and a methionine introduced at the C-terminus, Fig. 2) (Fig. 3). This indicates that in this V_{HH}, replacement of the internal methionine residues does not interfere with analyte binding. To obtain V_{HH}s with only a single methionine, an OmpA singnal sequence

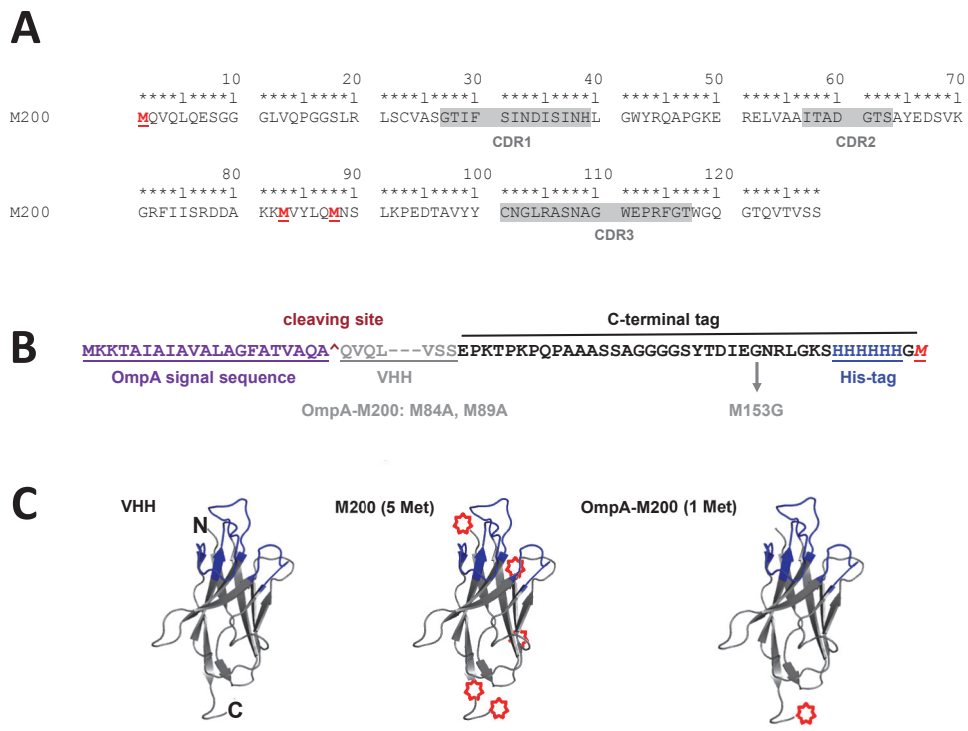

Figure 2. Structure of V_{HH}s. A: Protein sequence of V_{HH} M200. The three complementarity determining regions CDR1, CDR2 and CDR3 are shaded; methionine residues are underlined, cursive and red. B: Protein sequence showing engineered V_{HH} OmpA-M200 construct. C: Crystal structure of llama V_{HH} domain raised against a carbazole hapten (PDB entry 1U0Q) showing N- and C-terminal position in V_{HH}, CDR loops shown in blue (left). Red stars at methionine positions were introduced representative for V_{HH} M200 before (M200, middle) and after engineering (OmpA-M200, right).

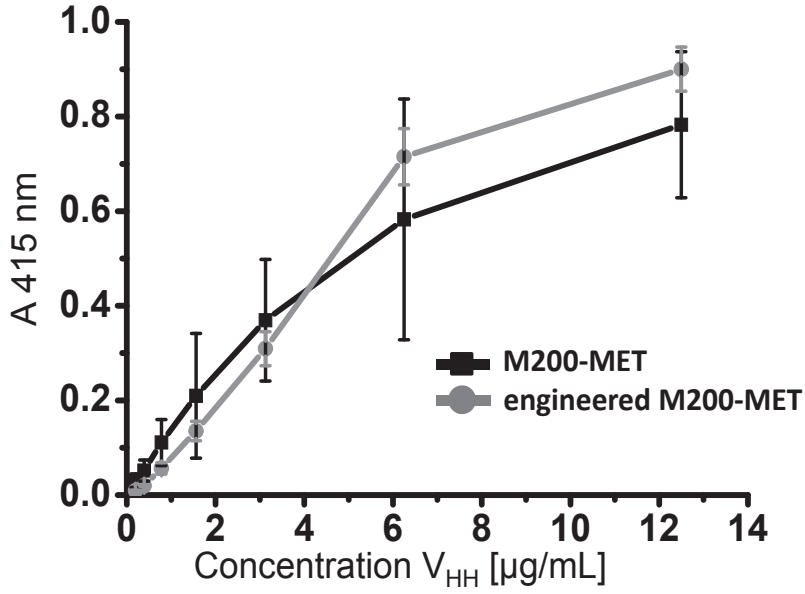

Figure 3. Binding of engineered V_{HH} antibody fragments to analyte investigated by ELISA. Different concentrations of V_{HH} M200-MET and engineered M200-MET (with altered methionines [M83, M88 and M153] and a methionine introduced at the C-terminus) bind to surface coated analyte peptide PAT49 (for more detail see Text). Measurements were performed in duplicates, expressed as means ± SD.

was introduced at the N-terminus of the V_{HH} protein sequence. This signal sequence will be cleaved off during protein expression in bacteria, resulting in the loss of the N-terminal start methionine in the mature protein (OmpA-M200, Fig. 2).

To introduce the azide functionality in the V_{HH}s, proteins were expressed in a methionine auxotrophic *E.coli* strain supplied with AHA in the medium. The efficient incorporation of AHA was confirmed in purified proteins by Electron-spray ionization time-of-flight (ESI-ToF) mass spectroscopy. MET differs by 5 Da in molecular mass to AHA (Fig. 4A). In Figure 4B, mass spectra of the M200-MET protein, the OmpA-M200-MET protein (both produced with MET) and the M200-AHA and OmpA-M200-AHA (both produced with AHA) are shown. The mass of M200-MET (18058.8 Da) corresponds to a full-length M200 protein, including an N-terminal MET (Fig. 4B).The mass of M200-AHA (18034.1 Da) is 24.7 Da lower, indicating replacements of all five MET residues by AHA. For the OmpA-M200-MET protein, the observed mass (17732.0 Da) corresponds to a protein starting from the glutamine immediately after the OmpA cleavage site. The mass of OmpA-M200-AHA protein (17727.1 Da) is 4.9 Da lower than the mass of the OmpA-M200-MET protein, indi-

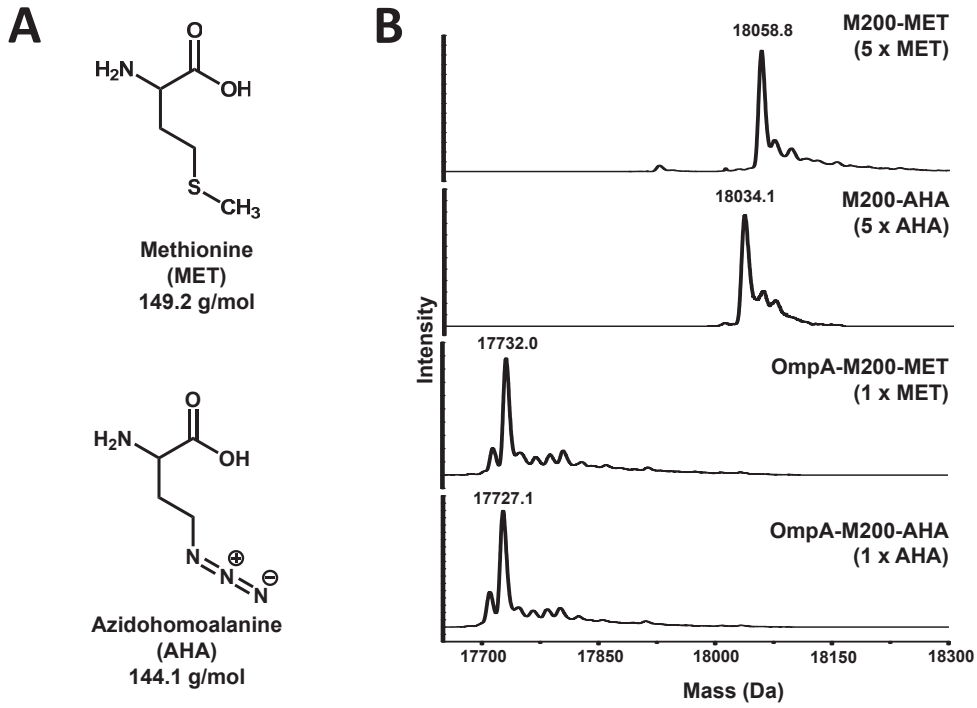

Figure 4. Azidohomoalanine incorporation in V_{HH}. A: Natural amino acid methionine (MET) shows similar structure than its non-natural analog azidohomoalanine (AHA) B: Electron-spray ionization time-of-flight (ESI-TOF) mass spectra of M200 and OmpA-M200. Upon de-convolution, peaks corresponding to the calculated masses (18058.1 Da for M200-MET, 18033.1 Da for M200-AHA, 17732.5 Da for OmpA-M200-MET and 17727.5 Da for OmpA-M200-AHA) were detected.

cating replacement of a single MET residue by AHA. Neither mutation, nor AHA incorporation had an effect on the binding affinity of the V_{HH} towards the analyte as shown by ELISA experiments (Fig. 5).

To investigate the accessibility of incorporated azide groups in the AHA-functionalized proteins, V_{HH} proteins were reacted with alkyne-labelled polyethylene glycol (PEG). Three reactive PEG ligands were tested. The alkyne-PEG_{5000} was reacted to the protein using the CuAAC reaction. PEG_{2000} coupled to dibenzocyclooctyne (DIBO) and PEG_{5000} coupled to bicyclo[6.1.0]non-4-yn-9-ol (BCN) were reacted to the protein by a SPAAC reaction. Increases in molecular weight of the proteins by these click reactions to the PEG moieties were examined by observing mobility shifts of V_{HH} on SDS-PAGE (Fig. 6). Protein M200-AHA, bearing five AHA residues, showed an array of mobility shift bands after reaction to alkyne-PEG_{5000} via CuAAC (Fig. 6A). This indicates that multiple azide groups in M200-AHA are available for the click reaction. For protein OmpA-M200-AHA, all three click reactions showed mobility

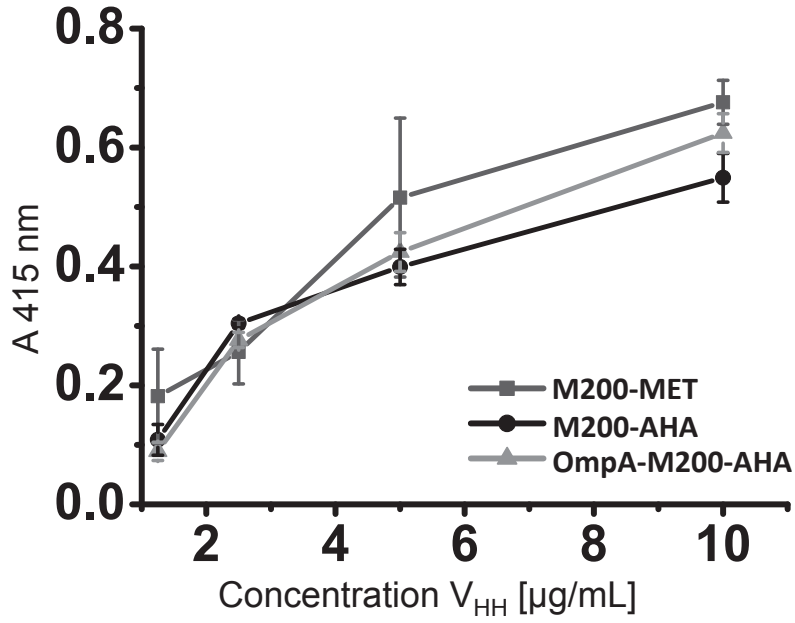

Figure 5. Binding of azidohomoalanine functionalized V_{HH} antibody fragments to analyte investigated by ELISA. Different concentrations of V_{HH} M200 and OmpAM200 bind to surface coated analyte peptide PAT49. Measurements were performed in duplicates, expressed as means ± SD.

shifts corresponding to the coupling of a single PEG unit (Fig. 6A, B, C).

Based on this knowledge, an SPR biosensor surface was functionalized with BCN. Both azide-functionalized V_{HH}s - M200-AHA and OmpA-M200-AHA - were immobilized in separate SPR channels via the SPAAC reaction. M200-AHA will couple to the surface by one of the five exposed azide groups, leaving no control over the orientation (Fig. 1C). In contrast, OmpA-M200-AHA contains only one azide group at the C-terminus and will attach in a uniform direction on the surface (Fig. 1B). For comparison to conventional random immobilization methods, an SPR channel that was functionalized using NHS chemistry was included in the analysis. Two analytes were tested: FMDV viral particles (60 recognition sites), and peptide PAT49, which is the known epitope towards the antibody, with one recognition site. Concentration ranges of both analytes were analyzed to investigate the sensitivity of the sensor surfaces. To our surprise, the uniformly oriented OmpA-M200-AHA showed an 800-fold higher sensitivity for peptide PAT49 than the randomly oriented M200-AHA: the threshold value of 10 RU was reached at 0.07 µg/mL for OmpA-M200-AHA, and at 55.4 µg/mL for M200-AHA (Fig. 7). This orientation effect of almost three orders

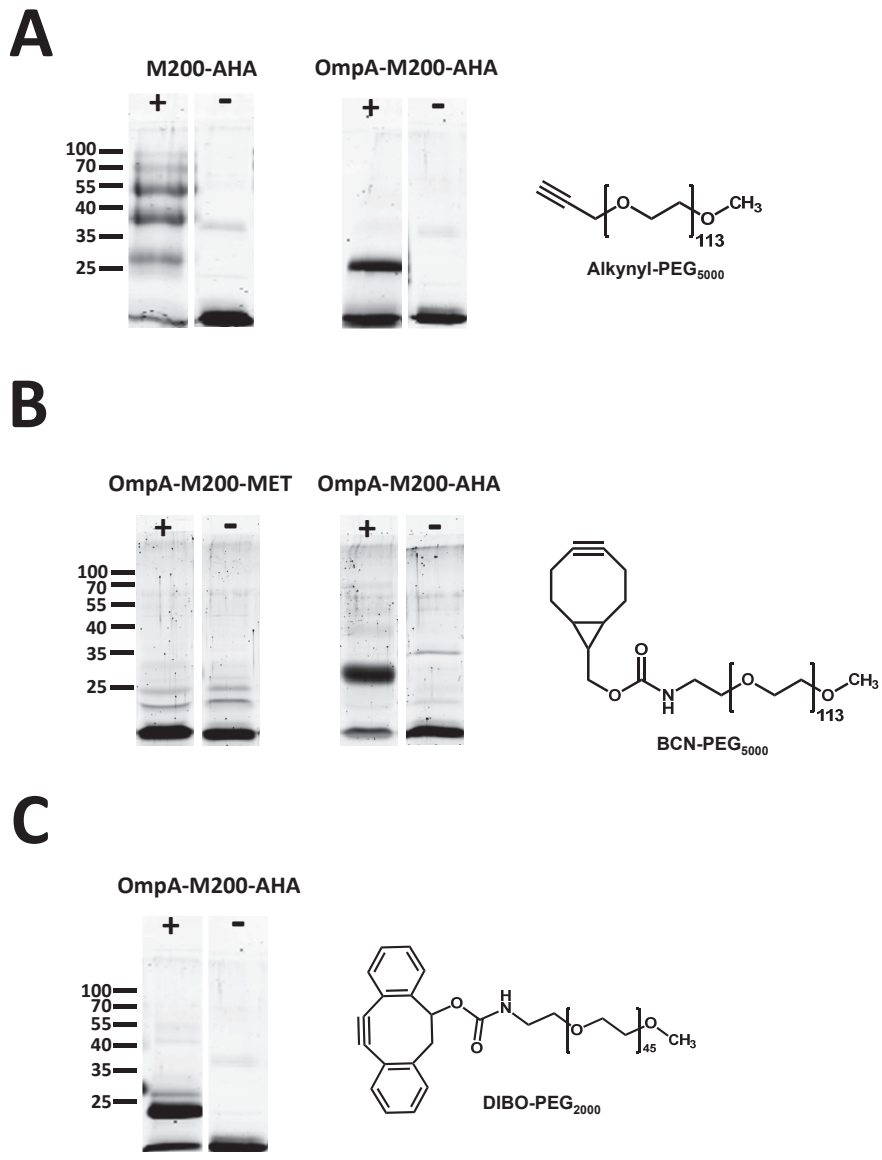

Figure 6. PEG-reacted V_{HH}s size separated by sodium dodecyl sulfate polyacrylamide gel electrophoresis. A: M200-AHA and OmpA-M200-AHA reacted with alkynl-PEG_{5000} via Cu-AAC B: OmpA-M200-MET and OmpA-M200-AHA reacted with BCN-PEG_{5000} via SPAAC. In contrast to OmpA-M200-AHA, control reactions with OmpA-M200-MET, which was produced in the absence of AHA, did not show a mobility shift, indicating that the reaction was specific for the azide group. C: OmpA-M200-AHA reacted with DIBO-PEG_{2000} via SPAAC. Plus (+) indicates presence of PEG-compound, minus (-) absence. Indicated are the positions of relevant size markers in kDa.

of magnitude is, as far as we know, by far the largest orientation effect observed up to now for any antibody-mediated biosensing event. Orientation effects typically range from 1 – 10.[5b, 6a, 12] with only a handful reports that indicate significantly larger ones.[13]

For FMDV, the signals were much stronger, and the orientation effect was less pronounced. Still ~10-fold higher sensitivity was observed in the oriented channel (Fig. 6). Previously we studied the effect of analyte properties, such as the number of recognition sites, the molecular weight and the affinity, on the biosensor response, using streptavidin-biotin and NHS chemistry.[5a] In that study it was already observed that the signal response of peptide PAT49 benefits (14-fold) from orientation, while detection of FMDV only marginally (2-fold) improved. These differences appeared to depend on the higher affinity of FMDV for the M200 antibody: with a lower affinity, the orientation effects increased. It is not fully clear why the current orientation enhancement is even bigger, and more experimentation is required for a further development of the hypothesis, but the sheer magnitude of this effect holds great promise for diagnostics.

To investigate the stability of V_{HH}s attached to the surface via the various immobilization strategies, repeated cycles of peptide PAT49 and FMDV injection and regeneration with 5 µL 10 mM HCl were performed. V_{HH} immobilized by click chemistry show an average signal loss of 0.23% after each cycle, whereas V_{HH}s immobilized by NHS chemistry show an average signal loss of 0.26% after each cycle (Appendix 2: Table S2). In other words: the azide-alkyne click reaction provides a covalent link that is at least as good as NHS-induced amide bond formation.

In summary, previously the effect of orientation of antibodies has been studied using different immobilization strategies, which may complicate comparisons.[5b, 6a] The current study was performed using identical (SPAAC) chemistry for uniform and random immobilization, before comparing their sensing properties. Under these circumstances, orienting antibodies on sensor surfaces by click chemistry leads to strongly improved sensitivity of biosensors, up to a factor 800. Such orientation effects thus greatly enhance the potential of diagnostics, which is crucial for the early detection of diseases that is needed to contain spreading of aggressive viruses such as FMDV. Finally, further improvements may be anticipated by combining orienting proteins with tuning surfaces at the nanoscale, such as via polymer brushes or monolayers, as this will allow to create more intelligent materials.[14]

6.3 Materials and Methods

6.3.1 Variable domain of llama heavy-chain antibodies (V_{HH})

V_{HH} M200 (GenBank accession no: AJ811563.1) is specific for peptide PAT49 (ace-

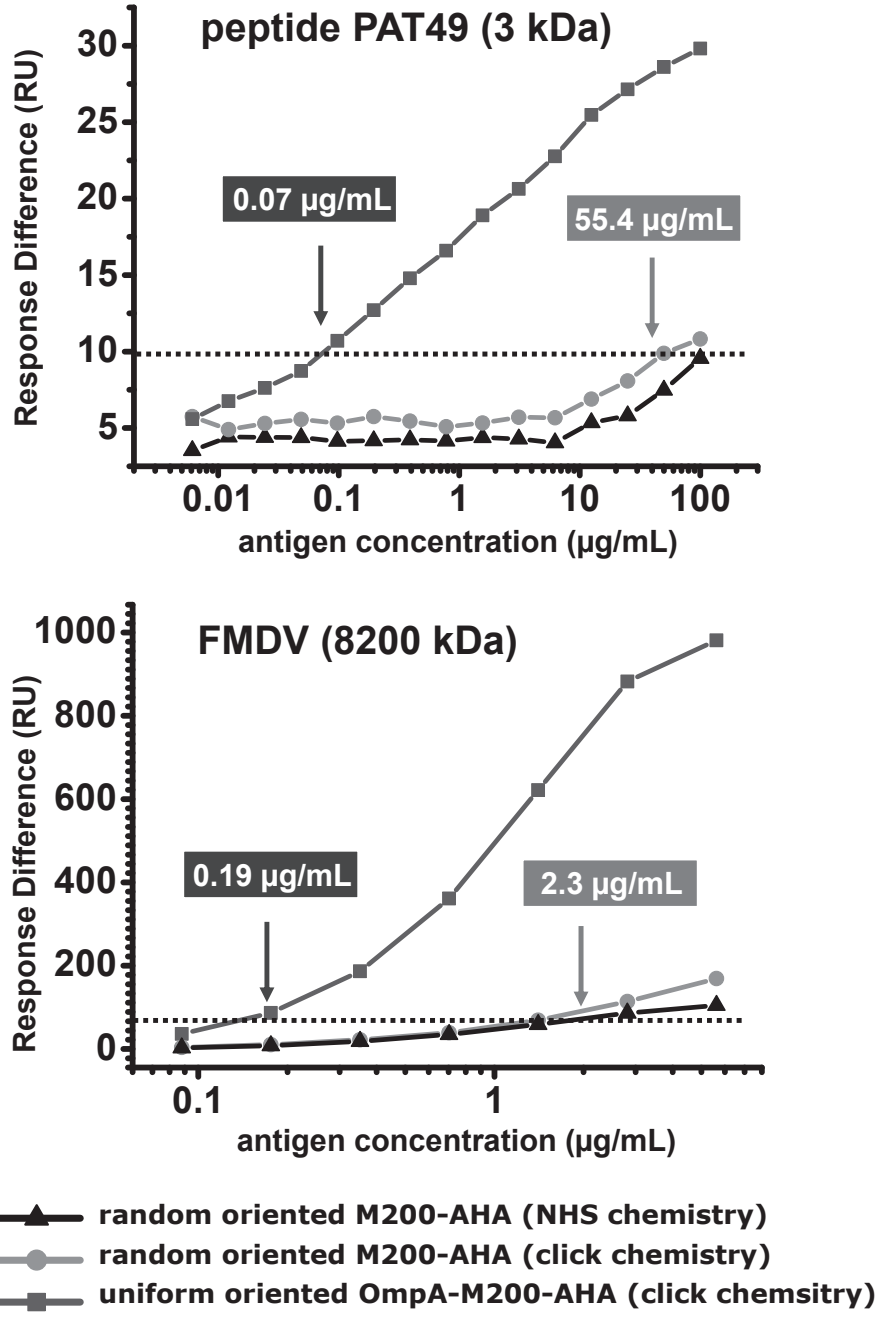

Figure 7. Surface plasmon resonance analysis of M200-AHA and OmpA-M200-AHA capture molecules. A dilution series of peptide PAT49 (100 µg mL^{-1} - 0.006 µg mL^{-1}) and FMDV (5.6 µg mL^{-1} – 0.08 µg mL^{-1}) was simultaneously analyzed on randomly oriented (M200-AHA click chemistry [circles] and M200-AHA NHS chemistry [triangles]) and uniformly oriented (OmpA-M200-AHA click chemistry [squares]) channels.

tyl-YGDGTVANVRGDLQVLAQKAARALPC-amide), corresponding to amino acid residues 136-160 of the GH-loop of the foot-and-mouth disease virus (FDMV) of the O1 Mansia strain.[11] Native V_{HH} M200-encoding DNA is present in the PRI-VSV expression vector.[5a] A variant (OmpA-M200) of this plasmid was made which expresses a protein with only a single methionine. Two internal methionine codons (coding for M83 and M88: Fig. 2) were altered to alanines by overlap extension PCR using oligonucleotides M200-M83A-M88A-F and M200-M83A-M88A-R (Appendix 2, Table S1). Subsequently, the methionine residue (M153) in the C-terminal part of the protein, just before the His_6 tag was altered to glycine using the same strategy and oligonucleotides M200-M153G-F and M200-M153G-R. A methionine was introduced at the C-terminus by introducing six additional nucleotides (GGGATG) before the stop codon, encoding glycine and methionine, by amplifying the engineered M200 fragment using oligonucleotides M200-F and M200-R, and recloning the engineered fragment in the PstI/NotI restriction sites of the PRI-VSV expression vector. Lastly, an OmpA signal sequence was introduce at the N-terminus of engineered M200 using oligonucleotides OmpA-F and OmpA-R. Oligonucleotides were hybridized and ligated into PstI/NdeI digested PRI-VSV expression vector. Introduction of OmpA signal sequence results in loss of N-terminal start methionine in the mature protein. The entire V_{HH} fragment of the resulting plasmid PRI-V_{HH}-OmpA-M200 (Fig. 2) was analyzed by DNA sequencing using oligonucleotides M200-F and M200-R.

6.3.2 Expression and purification of recombinant V_{HH}s

Plasmids PRI-V_{HH}-M200 and PRI-V_{HH}-OmpA-M200 were introduced into *E. coli* B834 (DE3) pLysS bacteria (Novagen). Bacteria were used for protein expression as previous described.[4b] Azidohomoalanine (AHA) synthesis and expression of AHA containing V_{HH}s (V_{HH}-AHA) were performed as described before.[15] To obtain recombinant protein, bacteria were lysed by sonication. In short, pellets were dissolved in 1/10 volume lysis buffer (50 mM NaH_2PO_4, 300 mM NaCl, adjusted to pH 6.0), complemented with 1/100 volume protease inhibitor cocktail (Sigma, St Louis) and 1 mg/mL lysozyme. Lysozyme digestion was allowed for 30 min at 4°C before cells were sonicated with a Soniprep150 (MSE, London, United Kingdom) in 5 mL batches for 10 cycles á 10 seconds with a break of 10 seconds. Cell lysate was then centrifuged for 30 min at 13.000 rpm and 4°C. Supernatant was used for V_{HH} purification using Ni-NTA Superflow resin (QIAGEN, Germany) as reported before.[16] Eluates were concentrated to 200 µL using Amicon ultra-15 centrifugal filter units (cut-off 10K, Millipore, The Netherlands). Further purification was performed by size exclusion chromatography using a Superdex 200 GL 10/300 column on an ÄKTA FPLCTM. V_{HH}s were stored with a final concentration of 15% glycerol at −20°C. Protein concentration was determined using Bradford test[17] while successful expression and

purification was verified by 15% sodium dodecylsulphate polyacrylamide gel electrophoresis (SDS-PAGE) stained with SYPRO ruby (BioRad, The Netherlands).

6.3.3 Investigation of engineered V_{HH} by enzyme linked immunosorbent assay (ELISA)

Wells of ELISA plates (Maxisorb, NUNC, The Netherlands) were coated with 5 μg/mL peptide PAT49 in 50 mM carbonate buffer pH 9.6 and incubated at 4°C overnight. Antigen-coated wells were emptied and washed three times with 200 μL 10 mM phosphate-buffered saline pH 7.4 (PBS) with 0.05% Tween 20 (PBST) and then blocked with 200 μL PBS containing 3% nonfat powdered milk (w/v) and 0.05% Tween 20 (3% PBSMT) for 8 h at room temperature. Wells were emptied and washed three times with 200 μL PBST. 100 μL V_{HH} at indicated concentration in PBS was added and binding was allowed to occur at 4°C overnight. Excess V_{HH}s were removed by washing three times with 200 μL PBST and 100 μL anti-His_6-PO conjugate (Sigma Aldrich, Missouri, USA) was added at a 1:2000 dilution for 1 h in 3% PBSMT. Excess conjugate was washed off one time with 200 μL PBST and two times with 200 μL demi water. Subsequently peroxidase activity was determined by adding 1-Step™ Ultra 3,3`,5,5`-tetramentylbenzidine (TMB) ELISA substrate (Pierce, Rockford, IL). The reaction was allowed to proceed in the dark for 30 min and then stopped with 50 μL 1 M sulphuric acid. The absorbance was measured at 415 nm in a microtiter plate-reader (TECAN SpectraFluor Microplate Reader). All samples were measured in duplicates.

6.3.4 Click reaction with V_{HH}

Bicyclo[6.1.0]non-4-yn-9-ol-polyethylene-glycol 5000 (BCN-PEG_{5000}) conjugate was purchased from Synnaffix (Nijmegen, The Netherlands). DIBO-PEG_{2000} was supplied by Marjoke Debets (Nijmegen University, The Netherlands). Alkyne-PEG_{5000} was synthesized as described before.[18] Bathophenanthroline sulfonated sodium salt was purchased from GFS Chemicals (Powell, US).

Click reactions were carried out overnight at ambient temperature. The Copper-catalyzed azide–alkyne cycloaddition (CuAAC) was performed in Click solution (1 vol. of 0.1 M CuBr with 2 vol. of 0.1 M ligand [bathophenanthroline sulfonated sodium salt] in DMSO/t-BuOH 3:1). 20 μL phosphate buffer containing 2 μL click solution and 2 μg V_{HH} were reacted with 1 mM alkyne-PEG_{5000}. Strain-promoted azide–alkyne cycloaddition (SPAAC) was performed in 20 μL phosphate buffer containing 2 μg V_{HH} and 1 mM alkyne-reagent (BCN-PEG_{5000} or DIBO-PEG_{2000}). Reactions were quenched by addition of 5 mM benzyl azide in DMSO. Quenching was allowed for 3 h at ambient temperature before the efficiency of the click reaction was verified by SDS-PAGE protein chromatography.

6.3.5 Surface plasmon resonance (SPR)

The BIAacore 3000, carboxymethyl dextran sensor chips (CM5), HBS-EP buffer (pH 7.4, consisting of 10 mM 4-(2-hydroxyethyl)piperazine-1-ethanesulfonicacid, 150 mM sodium chloride, 3 mM ethylenediaminetetraacetic acid, 0.005% v/v surfactant polysorbate 20), the amine coupling kit (containing 0.1 M N-hydroxysuccinimide [NHS], 0.4 M 1-ethyl-3-[3- dimethylaminopropyl]carbodiimide hydrochloride [EDC] and 1 M ethanolamine hydrochloride [pH 8.5]) were purchased from GE Healthcare (Uppsala, Sweden). N-(1R,8S,9s)-bicyclo[6.1.0]non-4-yn-9-ylmethyloxycarbonyl 1,8-diamino-3,6-dioxaoctane (BCN-POE_3-NH_2) was purchased from Synnaffix (Nijmegen, The Netherlands). The experiment was replicated with two chips, which produced comparable results.

BCN functionalized surface: In a BIAcore 3000 alkyne-functionalized surfaces were prepared using standard EDC/NHS coupling chemistry. To this end the CM5 biosensor surface was activated by injecting a mixture of EDC and NHS (1:1; v/v, 35 µL at a flow rate of 5 µL/min) into flow channels (Fc1, Fc3 and Fc4). Then 50 µL BCN-POE_3-NH_2 (0.1 mg/mL in 10 mM maleic acid pH 6.0) was injected and bound to the activated carboxymethylated dextran surface via its primary amine groups. After coupling, the remaining active groups were blocked with ethanolamine hydrochloride (35 µL at a flow rate of 5 µL/min).

Reference channel (Fc1): All active free cyclooctynes were blocked with 35 µL 2-azidoethanol (0.1 mg/mL in HBS-EP buffer at a flow rate of 5 µL/min).

Random orientation by NHS chemistry (Fc2): The biosensor surface was activated by injecting (35 µL at a flow rate of 5 µL/min) a mixture of EDC and NHS (1:1, v/v) into flow channel Fc2. Then M200-AHA V_{HH} (50 µg/mL diluted in coupling buffer [10 mM sodium acetate, pH 4.0]) was injected and bound to the activated carboxymethylated dextran surface via its primary amine groups, aiming for a similar immobilization level as Fc3. After coupling, the remaining active groups were blocked with ethanolamine hydrochloride (1 M, 35 µL at a flow rate of 5 µL/min). Immobilization of M200-AHA on Fc2 resulted in 4809 RU for chip1 and 3103 RU for chip 2.

Random orientation by click chemistry (Fc3): 50 µg/mL M200-AHA in 10 mM sodium acetate, pH 4.0 was immobilized (120 µL at a flow rate of 5 µL/min) on the BCN functionalized surface. After V_{HH} coupling, the remaining active free cyclooctynes were blocked with 35 µL 2-azidoethanol (0.1 mg/mL in HBS-EP buffer at a flow rate of 5 µL/min). Immobilization of M200-AHA on Fc3 resulted in 6717 RU for chip1 and 4349 RU for chip 2.

Uniform orientation by click chemistry (Fc4): 50 µg/mL OmpA-M200-AHA in 10 mM sodium acetate, pH 4.0 was immobilized (120 µL at a flow rate of 5 µL/min) on the BCN functionalized surface. After V_{HH} coupling, the remaining active free cyclooctynes were blocked with 35 µL 2-azidoethanol (0.1 mg/mL in HBS-EP buffer

at a flow rate of 5 μL/min). Immobilization of OmpA-M200-AHA on Fc4 resulted in 4378 RU for chip 1 and 3419 RU for chip 2.

The BIAcore 3000 SPR machine was operated at a constant temperature of 25°C and a flow of 10 μL/min. 50 μL analyte preparations in HBS-EP buffer, each of different analyte concentration, were injected over the four serially connected flow channels. Regeneration of the sensor surface was achieved with 5 μL of a 10 mM hydrogen chloride solution (HCl). Data points were measured 30 s after injection end. All sensorgrams were referenced by subtracting the signal from the reference flow channel (Fc1) and were evaluated using the BIAevaluation software.

6.3.6 Electron-spray ionization time-of-flight (ESI-TOF) measurements

V_{HH} constructs were analyzed by ESI-TOF on a JEOL AccuTOF. V_{HH} (~ 1 mg/mL) in 100 mM ammonium acetate was injected through an Agilent system run on MilliQ/0.1% formic acid. Deconvoluted spectra could be obtained using Mag Tran software. Calculated masses included the loss of two protons due to disulphide bond formation.

6.4 Acknowledgments

This work was funded by the European Union through the Marie Curie Integrated Training Network project Hierarchy (contract: PITN-2007-215851). Sponsors had no influence in study design; collection, analysis, and interpretation of data; in the writing of the report; and in the decision to submit the paper for publication. The help and suggestions made by Angelique Wammes, Michiel Harmsen, Vincent Ruigrok and Willem Haasnoot are kindly acknowledged. The authors also like to thank Marjoke Debets for supply of DIBO-PEG_{2000}.

6.5 References

1 a) H Chen, J Huang, J Lee, S Hwang, K Koh *Sensors and Actuators B.* 2010, B147, 548-553.
b) K Yoshimoto, M Nishio, H Sugasawa, Y Nagasaki J*ournal of the American Chemical Society.* 2010, 132, 7982-7989.

2 a) PJ Conroy, S Hearty, P Leonard, RJ O'Kennedy *Seminars in Cell & Developmental Biology.* 2009, 20, 10-26.
b) X Zeng, Z Shen, R Mernaugh *Analytical and Bioanalytical Chemistry.* 2012, 402, 3027-3038.

3 a) TAC Hamers-Casterman, S Muyldermans, G Robinson, C Hammers, E Bajyana, Songa, N Bendahman, R Hammers *Nature.* 1993, 363, 446-448.
b) K Deffar, H Shi, L Li, X Wang, X Zhu *African Journal of Biotechnology.* 2009, 8, 2645-2652.

4 a) D Saerens, F Frederix, G Reekmans, K Conrath, K Jans, L Brys, L Huang, E Bosmans, G Maes, G Borghs, S Muyldermans *Analytical Chemistry*. 2005, 77, 7547-7555.
b) AK Trilling, H de Ronde, L Noteboom, A van Houwelingen, M Roelse, SK Srivastava, W Haasnoot, MA Jongsma, A Kolk, H Zuilhof, J Beekwilder *PLoS ONE*. 2011, 6, e26754.

5 a) AK Trilling, MM Harmsen, VJB Ruigrok, H Zuilhof, J Beekwilder *Biosensors & Bioelectronics*. 2013, 40, 219-226.
b) SK Vashist, CK Dixit, BD MacCraith, R O'Kennedy *Analyst*. 2011, 136, 4431-4436.

6 a) TQ Huy, NTH Hanh, P Van Chung, DD Anh, PT Nga, MA Tuan *Applied Surface Science*. 2011, 257, 7090-7095.
b) JW Park, IH Cho, DW Moon, SH Paek, TG Lee *Surface and Interface Analysis*. 2011, 43, 285-289.
c) HY Song, X Zhou, J Hobley, X Su *Langmuir*. 2011, 28, 997-1004.

7 HC Kolb, MG Finn, KB Sharpless *Angewandte Chemie - International Edition*. 2001, 40, 2004-2021.

8 a) MF Debets, SS van Berkel, J Dommerholt, AJ Dirks, FPJT Rutjes, FL van Delft *Accounts of Chemical Research*. 2011, 44, 805-815.
b) JC Jewett, CR Bertozzi *Chemical Society Reviews*. 2010, 39, 1272-1279.

9 KL Kiick, E Saxon, DA Tirrell, CR Bertozzi *Proceedings of the National Academy of Sciences*. 2002, 99, 19-24.

10 a) V Hong, NF Steinmetz, M Manchester, MG Finn *Bioconjugate Chemistry*. 2010, 21, 1912-1916.
b) S Schoffelen, L Schobers, H Venselaar, G Vriend, JCM v Hest, *Green Polymer Chemistry: Biocatalysis and Biomaterials, American Chemical Society*. 2010, 1043, 125-139.

11 MM Harmsen, CB van Solt, HPD Fijten, L van Keulen, RA Rosalia, K Weerdmeester, AHM Cornelissen, MGM De Bruin, PL Eblé, A Dekker *Veterinary Microbiology*. 2007, 120, 193-206.

12 a) Z Balevicius, A Ramanaviciene, I Baleviciute, A Makaraviciute, L Mikoliunaite, A Ramanavicius *Sensors and Actuators B: Chemical*. 2011, 160, 555-562.
b) N Bereli, G Şener, H Yavuz, A Denizli *Materials Science and Engineering C*. 2011, 31, 1078-1083.
c) Y Yuan, M Yin, J Qian, C Liu *Soft Matters*. 2011, 7, 7207-7216.

13 a) M Park, J Jose, JC Pyun *Sensors and Actuators B: Chemical*. 2011, 154, 82–88.
b) G Yoo, M Park, EH Lee, J Jose, JC Pyun, *Analytica Chimica Acta*. 2011, 707, 142–147.

14 AT Nguyen, J Baggerman, JMJ Paulusse, H Zuilhof, CJM van Rijn *Langmuir*. 2011, 28, 604-610.

15 S Schoffelen, MHL Lambermon, MB van Eldijk JCM van Hest *Bioconjugate Chemistry*. 2008, 19, 1127-1131.

16 A van Houwelingen, T de Saeger, T Rusanova, C Waalwijk, MJ Beekwilder *World Mycotoxin Journal*. 2008, 1, 407 - 417.

17 MM Bradford *Analytical Biochemistry*. 1976, 72, 248–254.

18 A Deiters, TA Cropp, M Mukherji, JW Chin, JC Anderson, PG Schultz J*ournal of the American Chemical Society*. 2003, 125, 11782-11783.

CHAPTER 7

General Discussion

Abstract

This chapter gives an overview on the work done in this thesis and discusses some remaining questions and additional ideas.

7.1 General Discussion

The previous chapters explored the formation of tailor-made monolayers on copper substrates, as well as several strategies to immobilize llama antibodies on surfaces. Combined, the achievements of both research topics described in this thesis are highly valuable for the further development of biosensors. Yet not all problems are solved and there is some room for improvement. This chapter reflects on the work done, poses some remaining questions, and presents additional ideas and recommendations to place this work into a broader context.

In chapter 2, the generation of well-defined organic monolayers on oxide-free copper was described. Using a wet-chemical route, decanethiol self-assembled monolayers (SAMs) were created while the copper remained oxide-free. Using this route, extreme care has to be taken at any time to prevent the appearance of copper-oxide during monolayer formation. The wet-chemical route explored by us is a promising technique for oxide-free monolayer fabrication on copper, yet there is some room for improvements in regard of handling. Hutt and Liu used acetic acid as *in situ* etching agent during octadecanethiol monolayer formation to prevent copper-oxide formation.[1] Such an addition, for instance, could simplify the preparation of SAMs on copper. However, oxidation of copper substrates is fast, and even after formation of well-ordered monolayers oxidation remains an issue. In view of future applications a prolonged stability of oxide-free copper would be essential. Longer alkyl chains are known to self-assemble in a denser monolayer and provide a better protection barrier against oxygen and aqueous ions.[2] Further research should therefore investigate longer molecule chains than octadecanethiol on copper substrates, as well as focus on the effects of introduced functional groups, so as to make SAMs more stable against oxygen penetration.

SAM formation is a flexible route to generate thin and ordered bio-active monomolecular films on a variety of substrates by organic molecules (both aliphatic and aromatic) containing free anchor groups such as thiols, disulphides, amines, silanes, or acids.[3] Using such tailor-made surfaces detection elements like antibodies can be immobilized onto sensor surfaces. In chapter 2 it was shown that N-succinimidyl mercaptoundecanoate (NHS-MUA) monolayers allowed for the successful attachment of biomolecules via the amine group. Biotin-modified copper surfaces were generated and successfully employed for streptavidin binding. It is expected that in a similar manner antibody immobilization can be achieved on NHS-terminated SAMs on copper in a one-step reaction via surface-accessible amine groups on the antibody. Nonspecific adsorption tailor-made surfaces due to a high surface energy is a further issue to be overcome. Nonspecific protein adsorption can be reduced by using functional end groups with specific properties.[4] Also polymeric films, such as dextran layers used on surface plasmon resonance (SPR) chips or the generic used polyethylene glycols (PEGs), and protein-repellent zwitterionic polymer brushes

have been shown to reduce unspecific protein binding.[5] Future research should therefore focus on the fine-tuning of the surfaces of interest in order to minimize nonspecific protein binding and maximize specific binding of the analyte to the surface-immobilized detection element.

The development of a rapid, sensitive and specific method for analyte detection is of great importance in many sectors, such as food safety, disease control and health care. The ongoing miniaturization of sensor devices will stress the need of more efficient detector elements in the future. This can be achieved by (1) altering the biological detection element, or by (2) improving the immobilization method thereof.

7.1.1 Biological Detection Elements in Biosensors

Chapter 3 outlined some of the commonly used detection elements in biosensors. Antibodies have long been the most popular bio-recognition elements in biosensors as they display high sensitivity and selectivity. By reducing the size of the antibody (in order to increase the immobilized quantity) and/or by increasing the binding efficiency of the biological detection element, biosensor performance can be improved. Detection elements should ideally be small in size, specific, available for engineering and should have a high stability leading to a long shelf-life. The variable domain of llama antibodies (V_{HH}) fulfills all of these requirements, and was thus explored as detection element in a SPR-based biosensor. In chapter 4 the successful selection of tuberculosis specific V_{HH}s was described in detail. A broad set of V_{HH}s against the species-specific cytosolic 16 kDa heat-shock protein was obtained using two different phage display selection strategies. Surprisingly, all selected V_{HH}s bound to the same protein of *M. tuberculosis*. This was unexpected, as the alpacas were immunized with a lysate of *M. tuberculosis* and therefore exposed to a large range of bacterial proteins. Each of these proteins is capable to trigger the immune response by stimulating a number of relevant cells. As a result, antibodies towards the ´foreign` proteins are generated, resulting in a batch of detection elements specific towards several bacterial proteins. In our study, however, selection resulted in a batch of different V_{HH}s all specific for the 16 kDa heat-shock protein of *M. tuberculosis.* Recently it was shown that the selected V_{HH}s bind to different recognition sites (epitopes) of the 16 kDa heat-shock protein, making them a useful tool for *M. tuberculosis* detection.[6] It remains unclear for which reason all selected V_{HH}s bind to only one bacterial protein of *M. tuberculosis.* It might be due to its rich presence in bacteria lysate, since it is a highly expressed protein, or due to its immunodominant behavior. A new immunization of alpacas would be necessary to unravel the phenomena. Obviously it would be also interesting to have V_{HH}s specific for other proteins of *M. tuberculosis*, for example for a secreted protein. Secreted antigens would be freely available in the sputum/blood and would not require the lysis of the bacteria to sense its presence. However, also here the generation of a new V_{HH} library would

be necessary and one could argue that a secreted antigen may be too dilute for direct antigen detection in e.g. a sputum sample, making time consuming concentration steps necessary.

Beside that, antibodies with a higher affinity would be advantageous. The highest dissociation constant found for the tuberculosis specific V_{HH}s was 4×10^{-10} M. However, other V_{HH}s with a 10-fold higher affinity have also been reported.[7] *In vivo* or *in vitro* affinity maturation based on mutation and selection can raise antibodies displaying a higher affinity towards the antigen. First results indicated that in vitro affinity-maturated tuberculosis specific V_{HH}s showed better antigen binding behavior.[8] Selection can also be used to yield antibodies with other beneficial properties, such as a longer shelf-life due to higher stability or an increased pH tolerance. Future research should therefore explore possibilities to optimize properties of detection elements in order to increase the overall biosensor performance.

7.1.2 Immobilization Method of Detection Elements in Biosensors

As summarized in chapter 3, many methods have been explored in the past to orient antibodies on sensor surfaces in order to increase the antigen-binding capacity. In chapter 5 and 6, oriented immobilization of V_{HH}s was put into practice using non-covalent and covalent strategies, respectively. The investigated methods disclosed that orientation of detection elements is beneficial for antigen binding.

In chapter 5, oriented non-covalent immobilization via the biotin-streptavidin system was compared to random covalent immobilization via the amine group. A broad set of antigens with different properties was studied with this sensor set-up. Results showed that such antigen properties influence the antigen-binding behavior and therefore also the outcome of the experiment. It remains unclear to which extent the introduced streptavidin layer influences the antigen binding behavior in the oriented non-covalent set-up (chapter 5). To clarify this issue, random biotinylated V_{HH}s (via the amine groups) should be compared to site-specifically biotinylated V_{HH}s (via Avi-tag at the C-terminus) on streptavidin-coated surfaces.

In chapter 5, a set of antigens with different properties (molecular size, epitope number and affinity) was studied on the same pair of sensor chips (oriented vs non-oriented V_{HH}s). Orientation of V_{HH}s yielded in an insignificant low binding improvement for some antigens, but yielded in up to two orders of magnitude more sensitivity for other antigens. In our study, low affinity antigens profited most from V_{HH} orientation. Still it remains to be explored which features determine the relative affinity of an antibody/analyte pair and which role is played by other factors (such as steric hindrance, epitope number and molecular size) in the whole sensor set-up. This outcome also suggests that it is complex to compare different immobilization strategies when another set of antibody/analyte was used. Since every antibody/analyte pair differs in its properties, the same immobilization method might lead to

different outcomes. Gaining more knowledge about this issue will greatly help to improve the design of biosensors. Investigating different antibody/analyte pairs on the same sensor using the same immobilization strategy should shed light on this issue.

To yield covalently bound V_{HH}s, a click immobilization method was explored in chapter 6. This work is essential for a better fundamental understanding of the antibody orientation since both V_{HH}s were immobilized in a direct manner using the same chemistry without the interference of intermediate proteins. As observed before (chapter 5), resulted V_{HH} orientation in a more sensitive antigen detection. The stunning observation that this orientation effect could be as large as 800 was, in fact, way beyond our own hopes and expectations. This proved that for specific cases the (molecular biology) work required to obtain appropriately modified antibodies and the surface improvements to get an optimal surface architecture can be worth every minute of it! It should be pointed out that antigen binding was in the covalent immobilization set-up dependent on the antigen properties, even when the same immobilization chemistry was used for random and oriented V_{HH} attachment (chapter 6). These pioneering observations are probably the most remarkable achievements of this thesis. It was shown for the first time that sensor sensitivity is not only influenced by the detection element orientation, but much stronger influenced by the analyte properties.

The in chapter 6 chosen method to introduce azide in the protein requires time consuming protein engineering, but allowed the comparison of random and uniformly oriented V_{HH}s. In future applications, azide groups can be incorporated at the V_{HH} C-terminus in a more direct approach. The group of Schultz showed that functionally unique unnatural amino acids such as p-azido-L-phenylalanine can be incorporated in proteins by expressing orthogonal tRNAs and aminoacyl-tRNA synthetase.[9] Introduction of the unnatural azide containing amino acid can be achieved in response to an amber nonsense codon. Another method was shown by the group of Ploegh.[10] Anti-GFP V_{HH} with azide or cyclooctyne moieties at the C-terminus was prepared using a sortase A-catalyzed ligation followed by click chemistry to prepare V_{HH} dimers. Such azide functionalized V_{HH}s could also be covalently immobilized onto cyclooctyne-functionalized surfaces using the strain-promoted alkyne-azide cycloaddition (SPAAC). Clearly, such approaches steer the further research that is needed into the effect of capture molecule orientation on sensing of target and non-target analytes.

It should be also noted that the V_{HH} orientations investigated in chapter 5 and 6 (oriented vs random immobilization) were studied in an indirect method by comparing the antigen-binding capacity using SPR as a model sensor. Where possible, future research should pay closer attention to the real orientation of the V_{HH}s. However, methods to visualize antibody orientation in a direct manner are still challenging, as was reviewed in chapter 3.

Further expansion of the work could include studying V_{HH} orientation on a two-dimensional layer. The three-dimensional hydrogel matrix investigated in chapter 4, 5 and 6 is flexible and could influence orientation effects. To have better control over orientation, oriented and random V_{HH} immobilization should be studied on two-dimensional SAMs. Further on, the influence of the linker used to couple the V_{HH} to the surface should be investigated. Linker properties (rigid, flexible, short or long) will significantly influence V_{HH} orientation and knowledge in this field would be valuable for future research in the biosensor sector.

Another topic to investigate in the future concerns the newly produced OmpA-V_{HH} (chapter 6). In this constructs, the N-terminal start codon methionine was cut-off during posttranslational processing at the OmpA signal sequence. This results in V_{HH}s starting with glutamine as N-terminal amino acid (Fig. 1). In such materials, cyclization of the N-terminal amine and the subsequent loss of NH_3 was observed as post-translational modification in other monoclonal antibodies.[11] This leads to a molecular weight loss of 17 Da, and was not observed as main product for our V_{HH}s, but was to observe as side product (Fig. 4, chapter 6). Nevertheless, since this cyclization reaction is spontaneous and highly dependent on temperature and buffer composition, adjusting this condition could favor the formation of pyro-glutamine. This would ensure that the amine group at the N-terminus situated close to the antigen binding site is no longer available for NHS-chemistry immobilization, as was used for random immobilization in chapter 4 and 5. Since immobilization via the N-terminus amine group leads to a V_{HH} immobilization not able to bind target analyte, using an N-terminally blocked V_{HH}s could be interesting, as it may bias the distribution of random immobilized antibodies towards a more favored orientation and therefore maybe improve biosensor sensitivity.

To summarize, many new insights have been obtained within the research project showing that orienting antibodies on surfaces can yield an increase in the sensi-

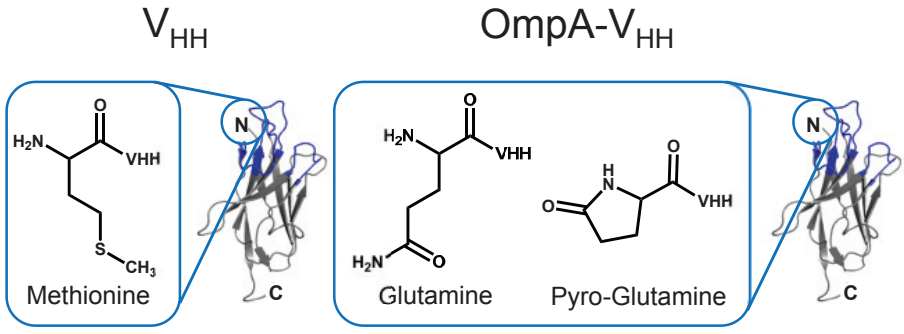

Figure 1. Ribbon diagram of V_{HH} and OmpA-V_{HH}. The N-terminus of the protein situated close to the analyte binding site (shown in blue). V_{HH} starts with methionine at the N-terminus, OmpA-V_{HH} with glutamine. Spontaneous formed pyro-glutamine displays no free amine group at the N-terminus for immobilization via NHS chemistry.

tivity up to two orders of magnitude! Therefore, next to other routes, the biosensor sector should further follow this research path to improve sensitivity. Improving the detection element opens up several new possibilities, such as the development of smaller detection elements for the same limit of detection, or of detection elements that have a significantly lower limit of detection. More sensitive biosensors will lead to an earlier detection of compounds present in small amounts, and will therefore be able to contribute to a further improvement of the overall quality of life. The achievements obtained here will thus hopefully help to optimize techniques to immobilize detection elements onto biosensing surfaces, and as such be highly relevant to improve the performance of biosensors.

7.2 References

1 DA Hutt, C Liu *Applied Surface Science*. 2005, 252, 400-411.

2 a) P Srivastava, WG Chapman, PE Laibinis *Journal of Physical Chemistry B.* 2009, 113, 456-464.
b) P Srivastava, WG Chapman, PE Laibinis *Langmuir*. 2009, 25, 2689-2695.

3 a) LJ Yang, YB Li *Biosensors & Bioelectronics.* 2005, 20, 1407-1416.
b) SK Arya, PR Solanki, M Datta, BD Malhotra *Biosensors & Bioelectronics.* 2009, 24, 2810-2817.

4 E Ostuni, RG Chapman, RE Holmlin, S Takayama, GM Whitesides *Langmuir*. 2001, 17, 5605-5620.

5 a) AT Nguyen, J Baggerman, JMJ Paulusse, H Zuilhof, CJM van Rijn *Langmuir*. 2012, 28, 604-610.
b) RG Chapman, E Ostuni, MN Liang, G Meluleni, E Kim, L Yan, G Pier, HS Warren, GM Whitesides *Langmuir*. 2001, 17, 1225-1233.

6 SK Srivastava, VJB Ruigrok, NJ Thompson, AK Trilling, AJR Heck, C van Rijn, J Beekwilder, MA Jongsma *PloSONE.* accepted.

7 M Swain, G Anderson, D Zabetakis, R Bernstein, J Liu *Analytical and Bioanalytical Chemistry*. 2010, 398, 339–348.

8 K Suster, Graduate Thesis University Ljubljana, 2012.

9 a) DR Liu, TJ Magliery, M Pastrnak, PG Schultz *Proceedings of the National Academy of Sciences.* 1997, 94, 10092–10097.
b) L Wang, PG Schultz *Chemistry & Biology*. 2001, 8, 883-890.

10 MD Witte, JJ Cragnolini, SK Dougan, NC Yoder, MW Popp, HL Ploegh *Proceedings of the National Academy of Sciences.* 2012, 109, 11993.

11 LWD Jr Dick, C Kim, D Qiu, KC Cheng *Biotechnology and Bioengineering*. 2007, 97, 544-553.

Appendices

Appendix 1 (Chapter 2)

Appendix 2 (Chapter 6)

1.1 Monolayers of *n*-alkanethiols on copper

1.1.1 Freshly-etched copper substrate:

Employing glycolic acid in EtOH (EKC 570, copper compatible post-etch residue remover from DuPont).

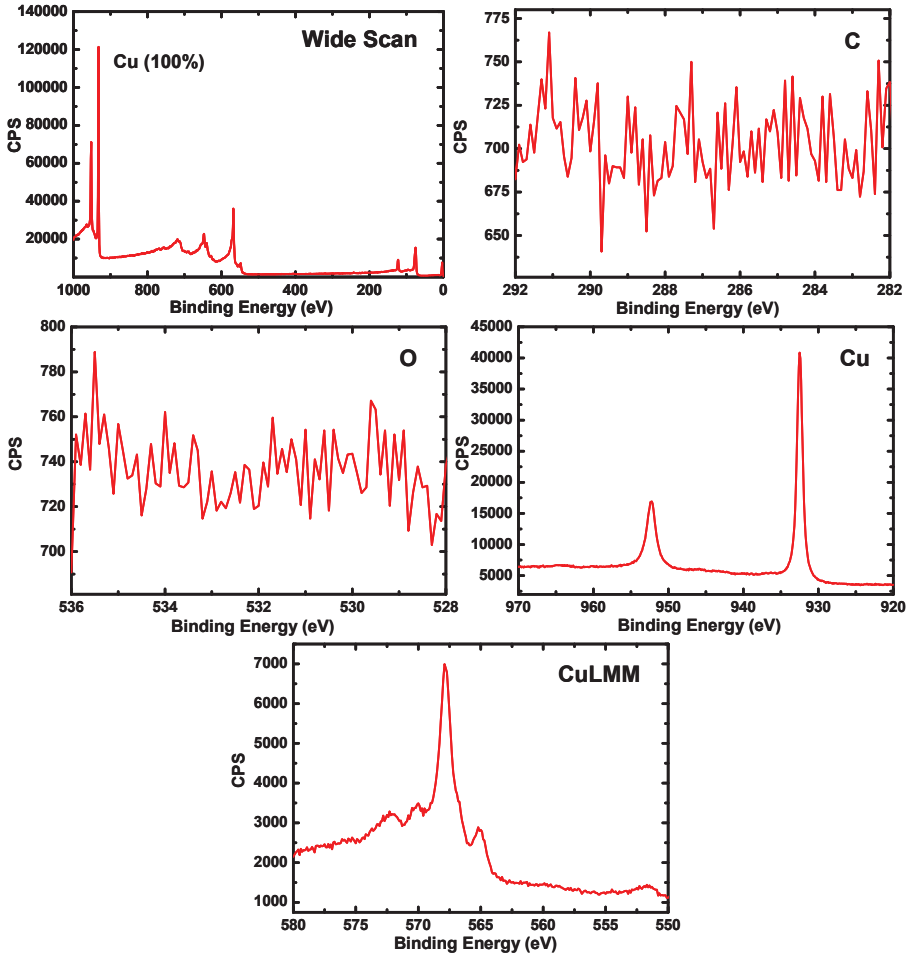

Figure S1. XPS spectra of copper substrate after etching step.

1.1.2 *n*-Decanethiol:

Copper substrates were etched with EKC-570 solution in EtOH and the monolayers were prepared under argon atmosphere at 20 °C. Static water contact angle of resulting monolayers: 109°.

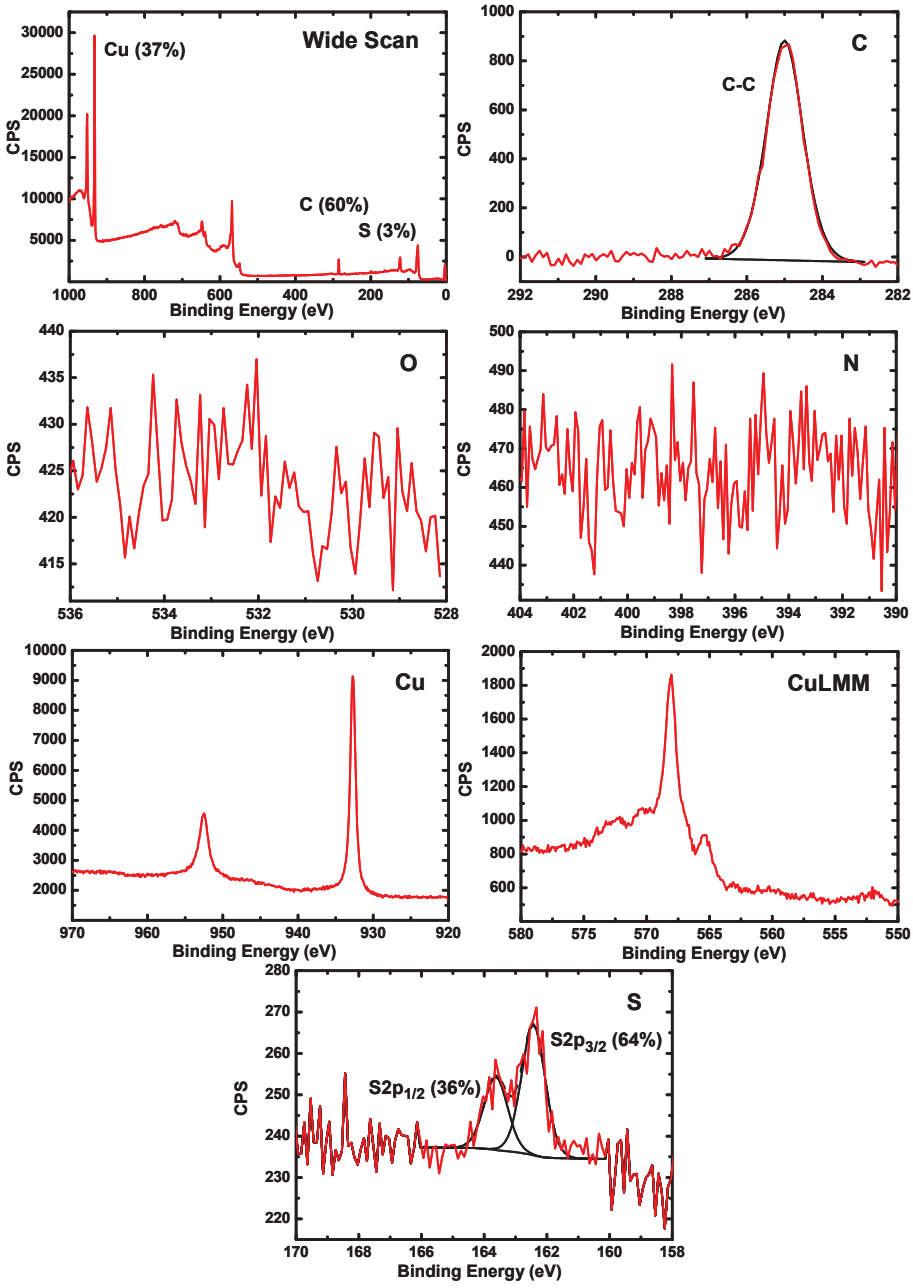

Figure S2. XPS spectra of neat *n*-decanethiol monolayer on copper, 2 h.

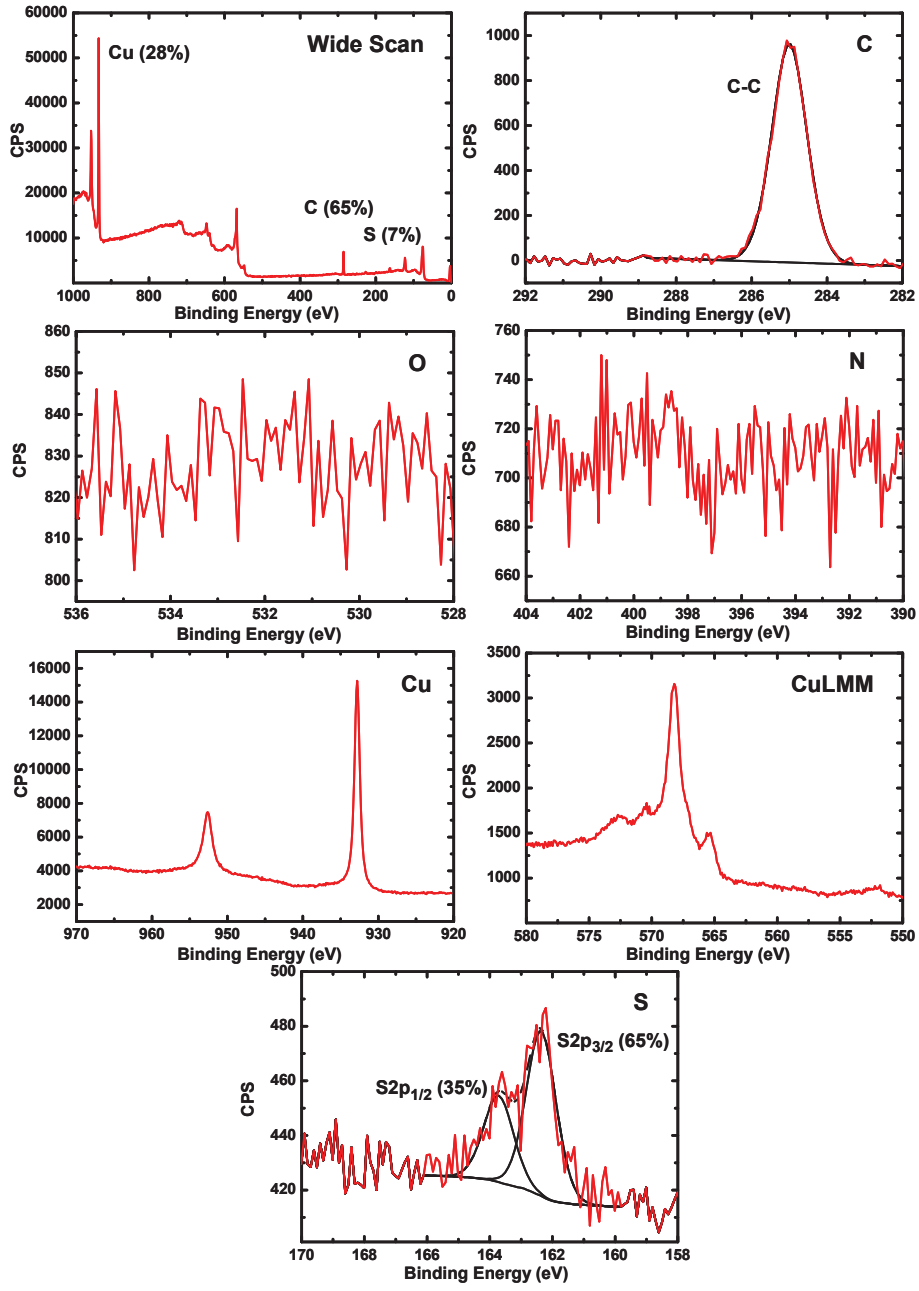

Figure S3. XPS spectra of neat *n*-decanethiol monolayer on copper, 16 h.

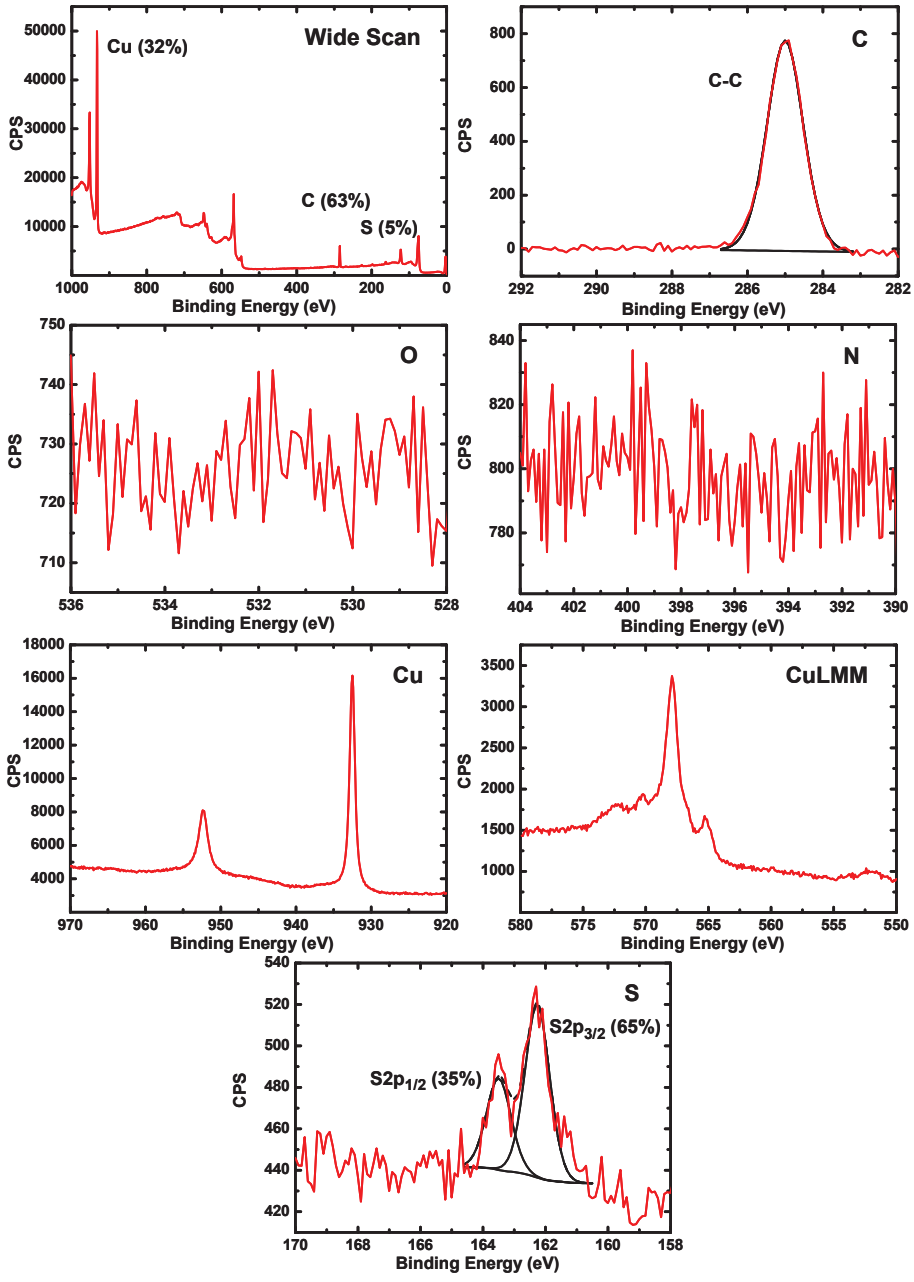

Figure S4. XPS spectra of 500 mM (174 mg in 2.0 mL EtOH) *n*-decanethiol monolayer on copper, 2 h.

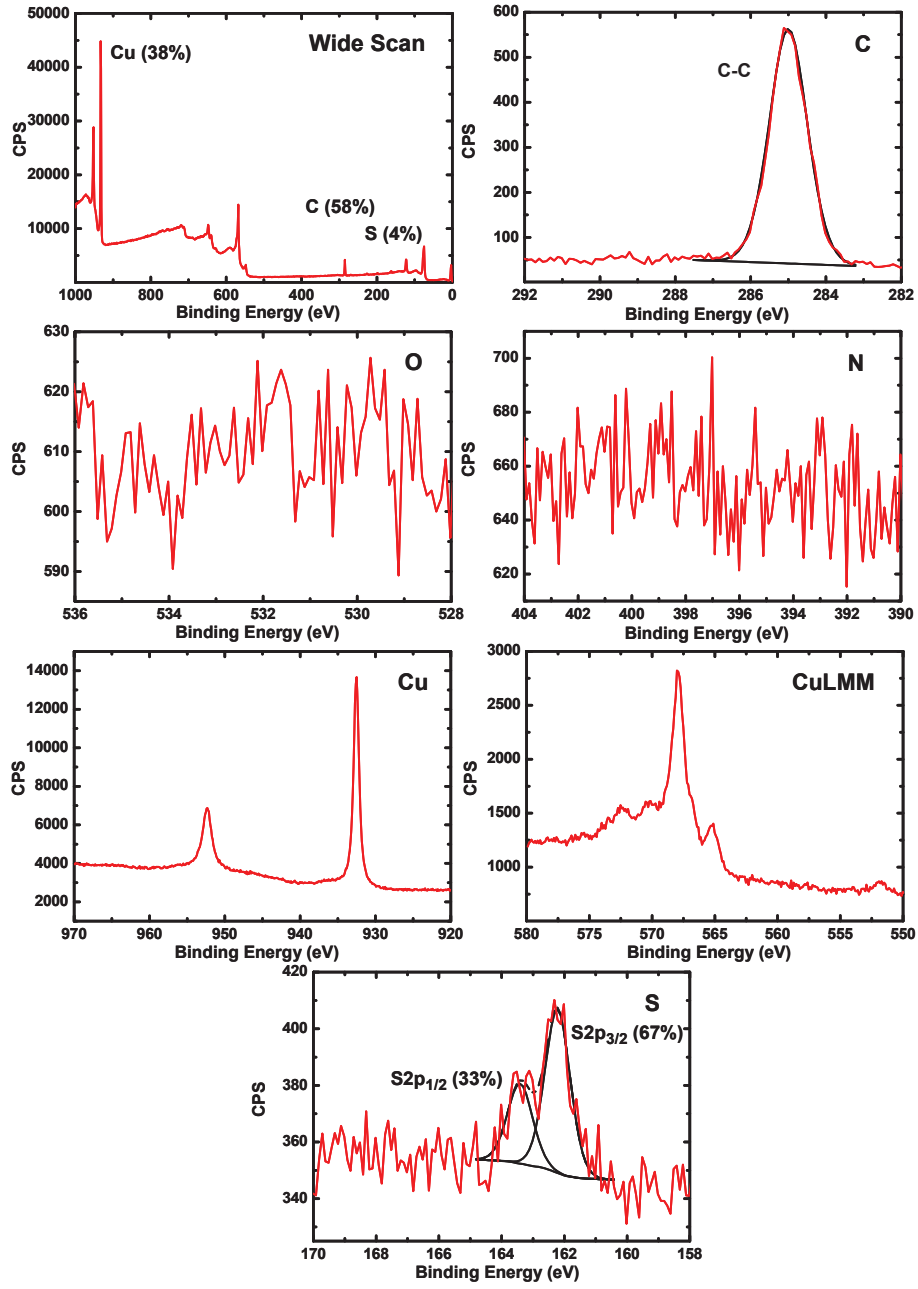

Figure S5. XPS spectra of 400 mM (140 mg in 2.0 mL EtOH) *n*-decanethiol monolayer on copper, 2 h.

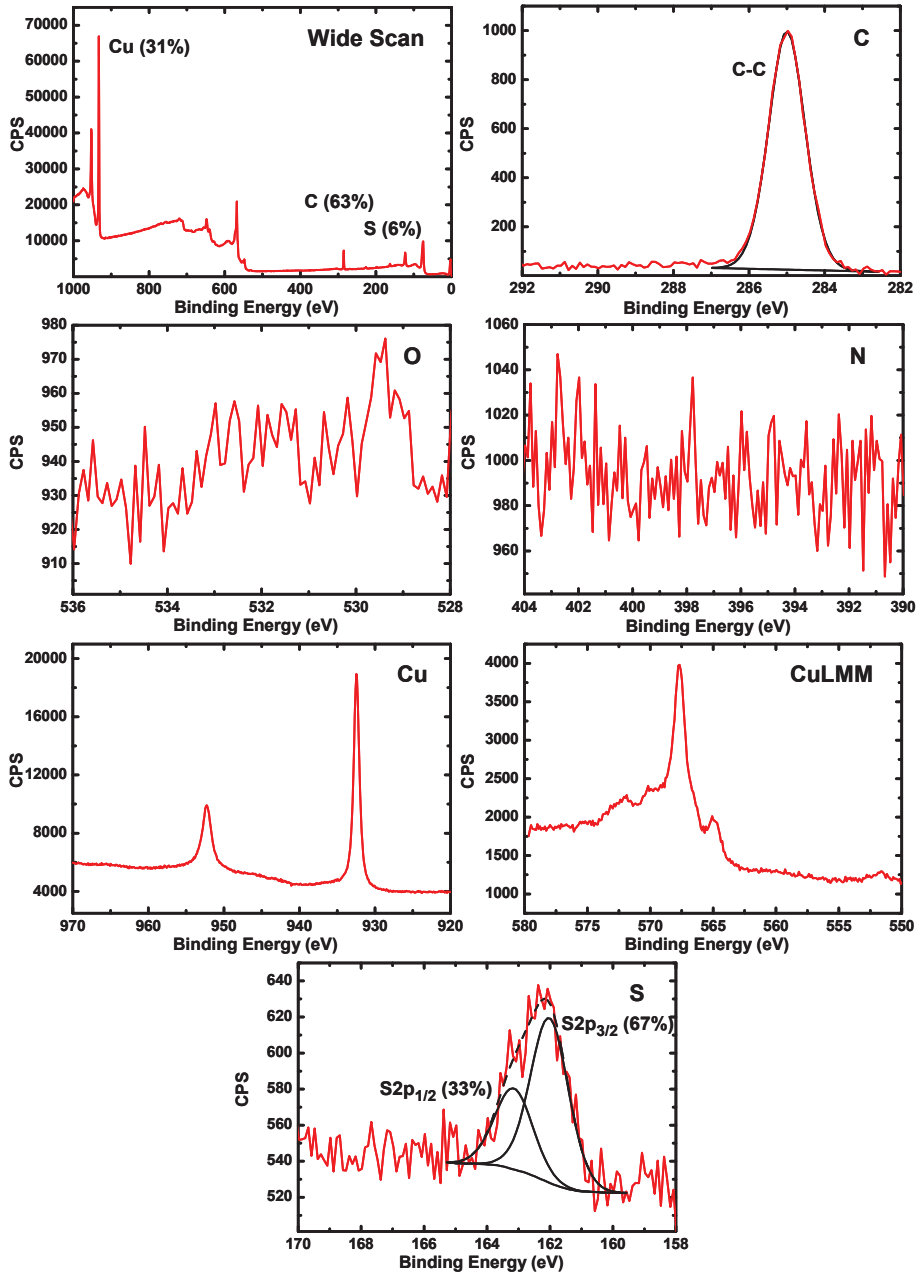

Figure S6. XPS spectra of 200 mM (70 mg in 2.0 mL EtOH) *n*-decanethiol monolayer on copper, 8 h.

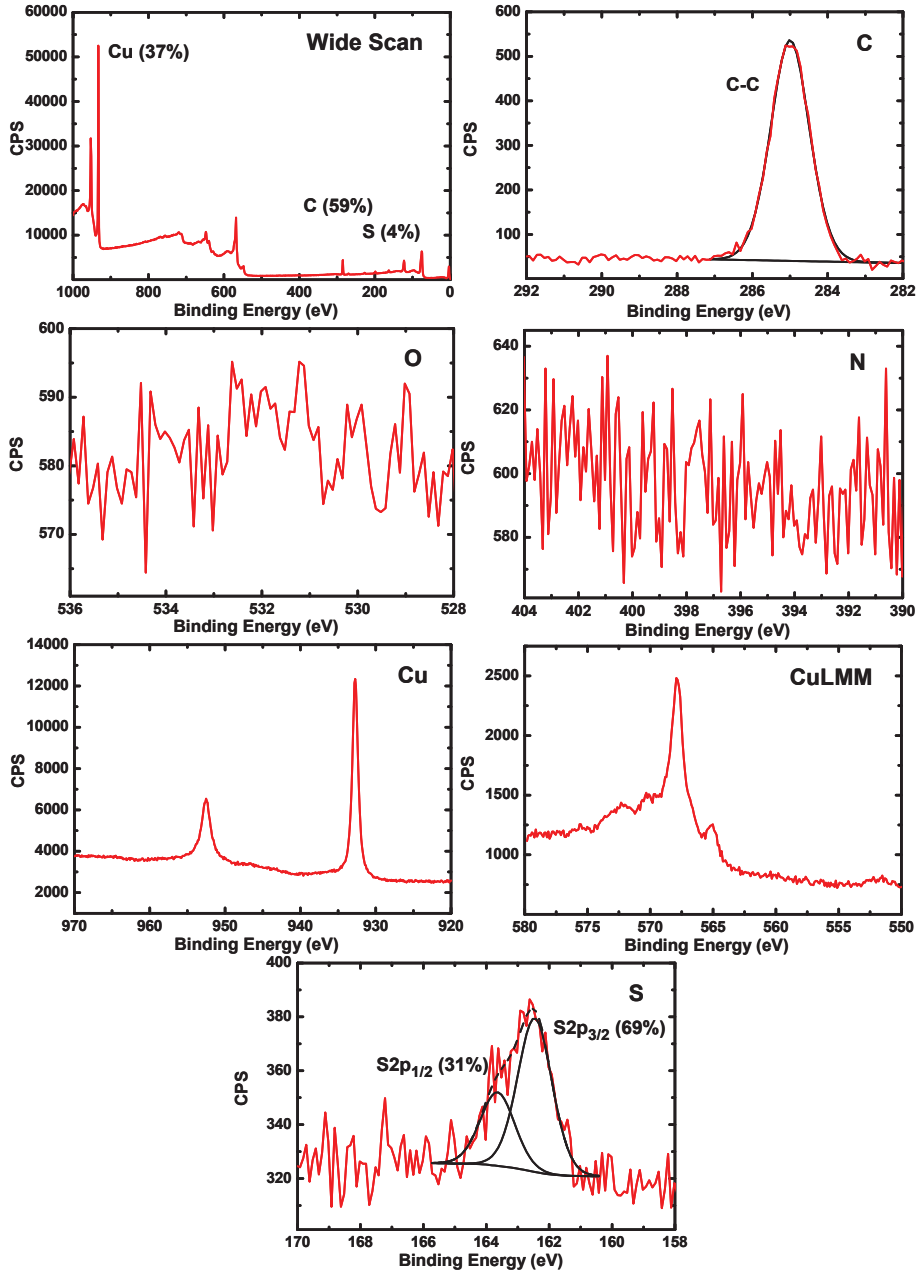

Figure S7. XPS spectra of 50 mM (17 mg in 2.0 mL EtOH) *n*-decanethiol monolayer on copper, 2 h.

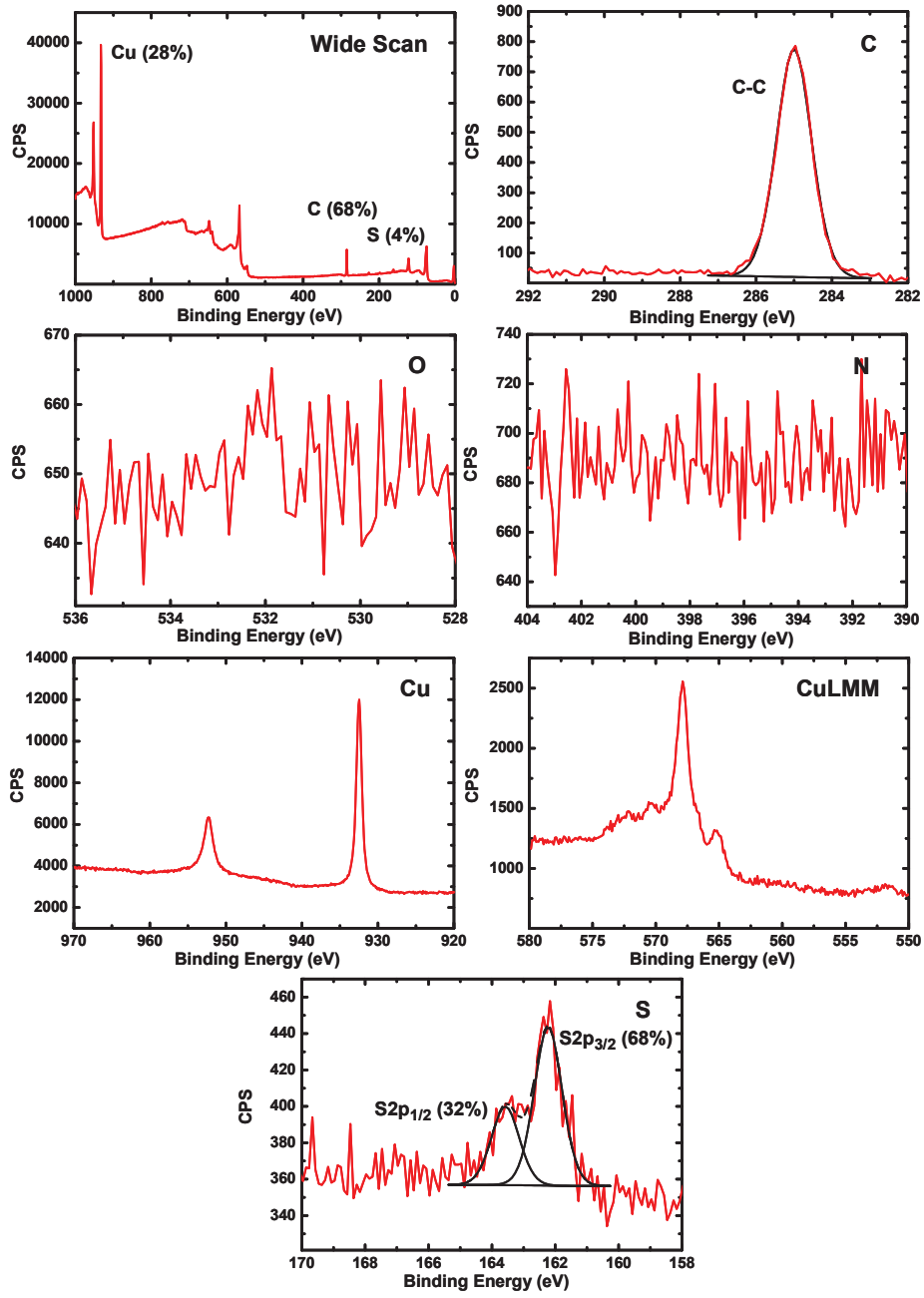

Figure S8. XPS spectra of 50 mM (17 mg in 2.0 mL EtOH) *n*-decanethiol monolayer on copper, 16 h.

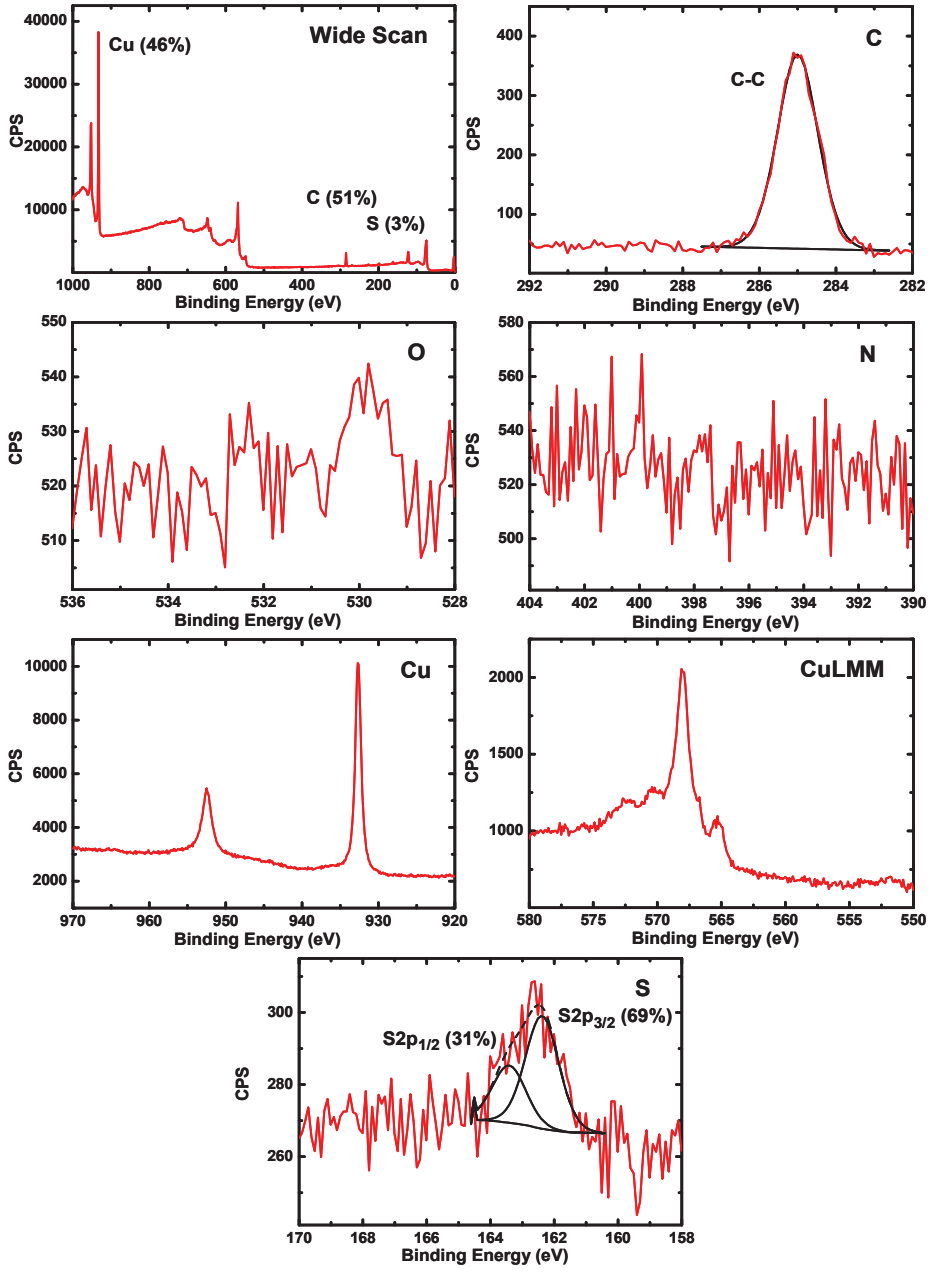

Figure S9. XPS spectra of 10 mM (3.5 mg in 2.0 mL EtOH) *n*-decanethiol monolayer on copper, 16 h.

1.1.3 *n*-Decanethiol - etching with HCl:

Copper substrates were etched with HCl in EtOH (3.3 %) and the monolayers were prepared under argon atmosphere at 20 °C.

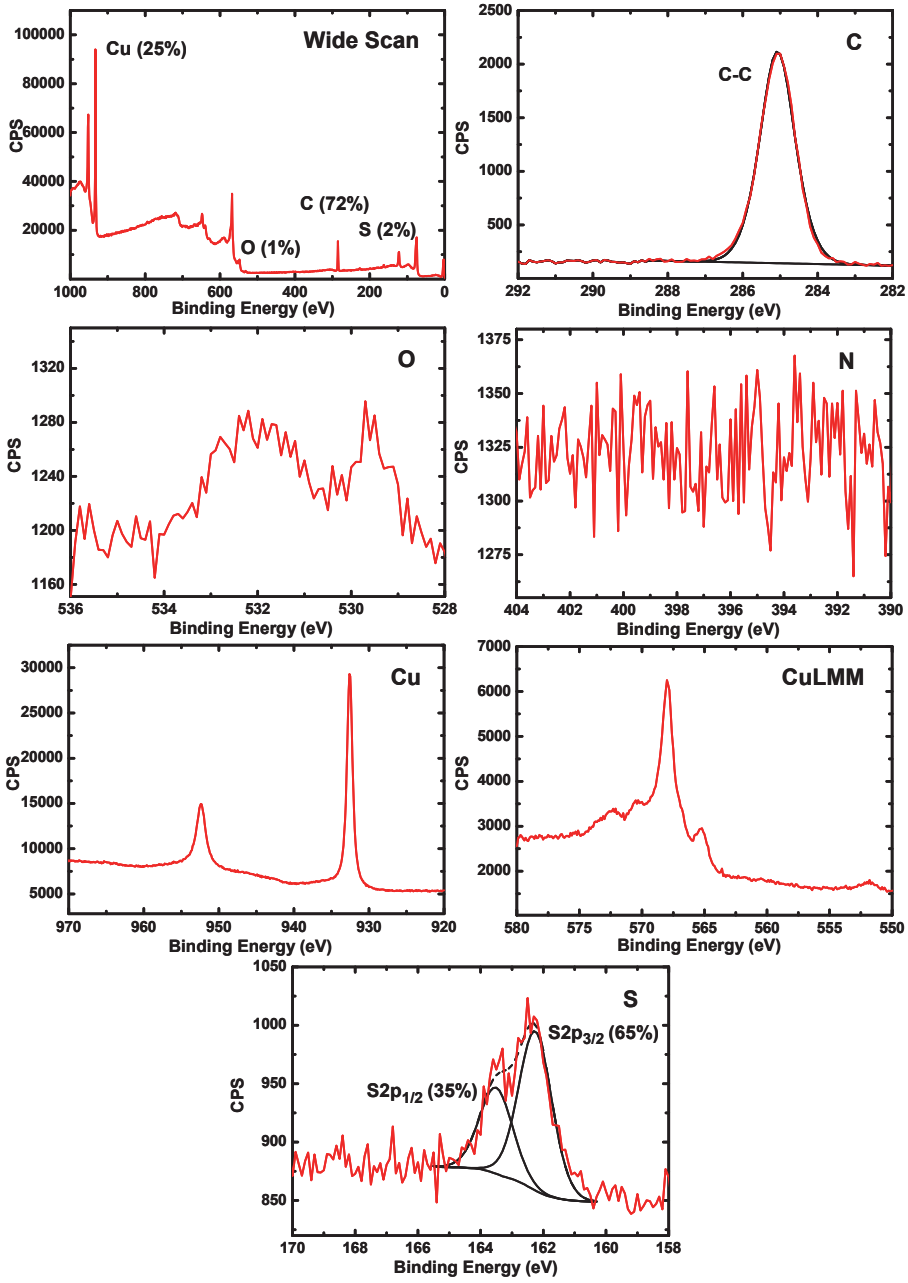

Figure S10. XPS spectra of neat *n*-decanethiol monolayer on copper, etching with HCl, 16 h.

1.1.4 *n*-Octadecanethiol:

Copper substrate was etched with EKC-570 solution in EtOH and the monolayer was prepared in toluene under argon atmosphere at 20 °C. Static water contact angle of resulting monolayer: 110°.

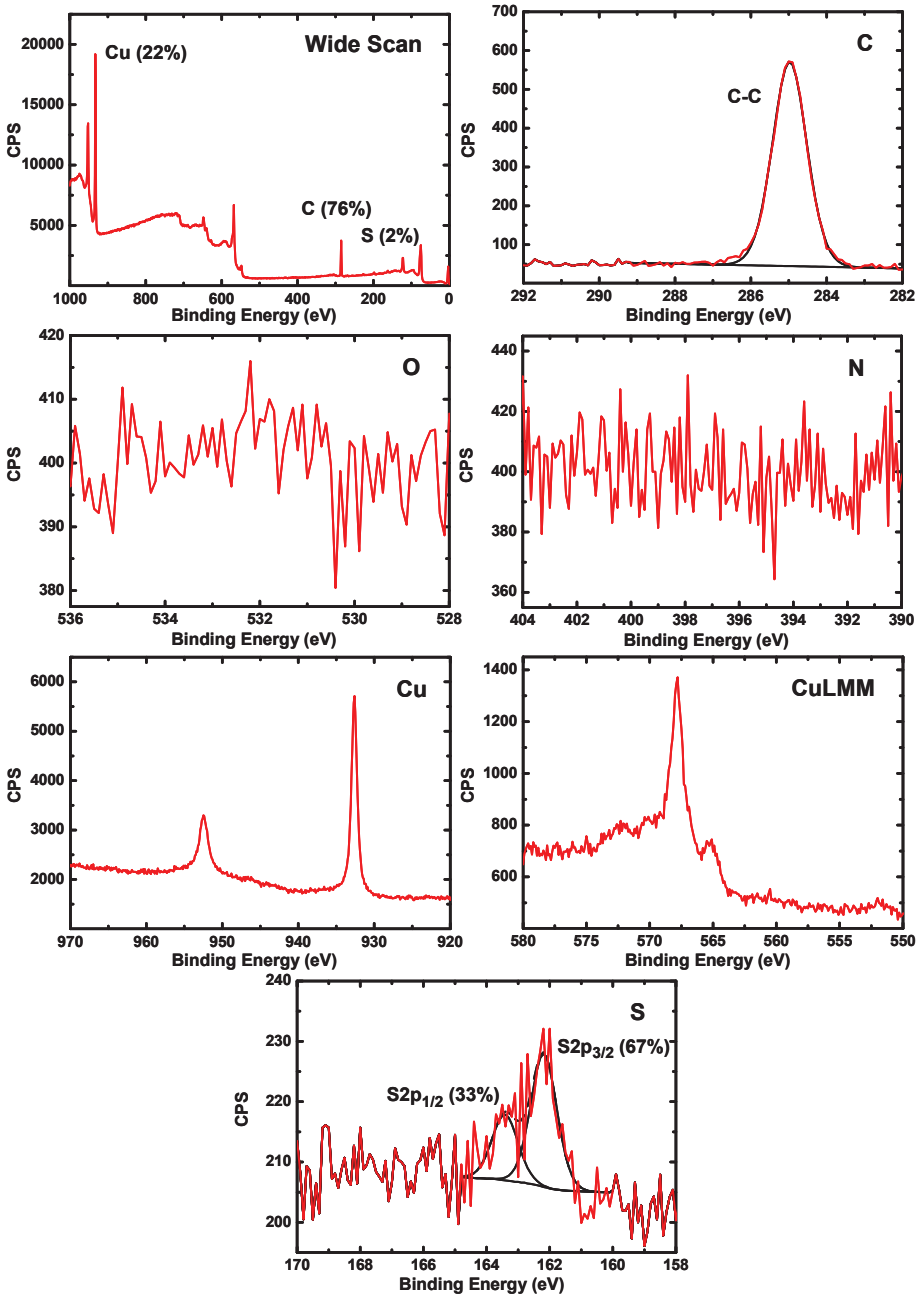

Figure S11. XPS spectra of 500 mM (287 mg in 2.0 mL toluene) *n*-octadecanethiol monolayer on copper, 16 h.

1.2 Functional organic monolayers on copper:
Copper substrates were etched with EKC-570 solution in EtOH and the monolayers were prepared in toluene under argon atmosphere at 20°C, for 16 h.

1.2.1 11-Mercaptoundecanoic acid (MUA):
200 mM (87 mg, 0.40 mmol) MUA in 2.0 mL dry toluene. Static water contact angle of resulting monolayer: 50°.

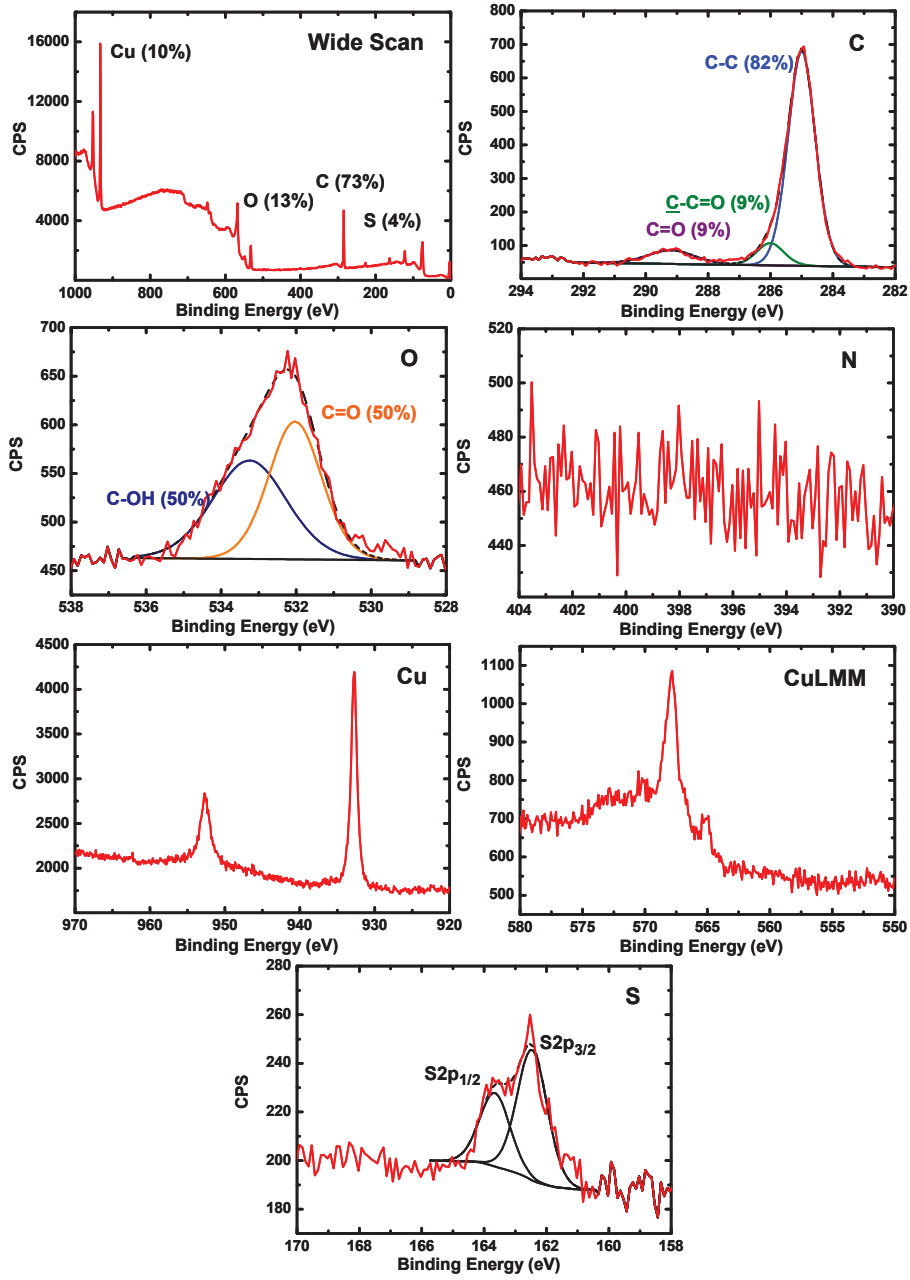

Figure S12. XPS spectra of the acid-terminated copper monolayer.

1.2.2 10-Mercaptodecanol (MD):
200 mM (82 mg, 0.40 mmol) MD in 2.0 mL dry toluene. Static water contact angle of resulting monolayer: 40°.

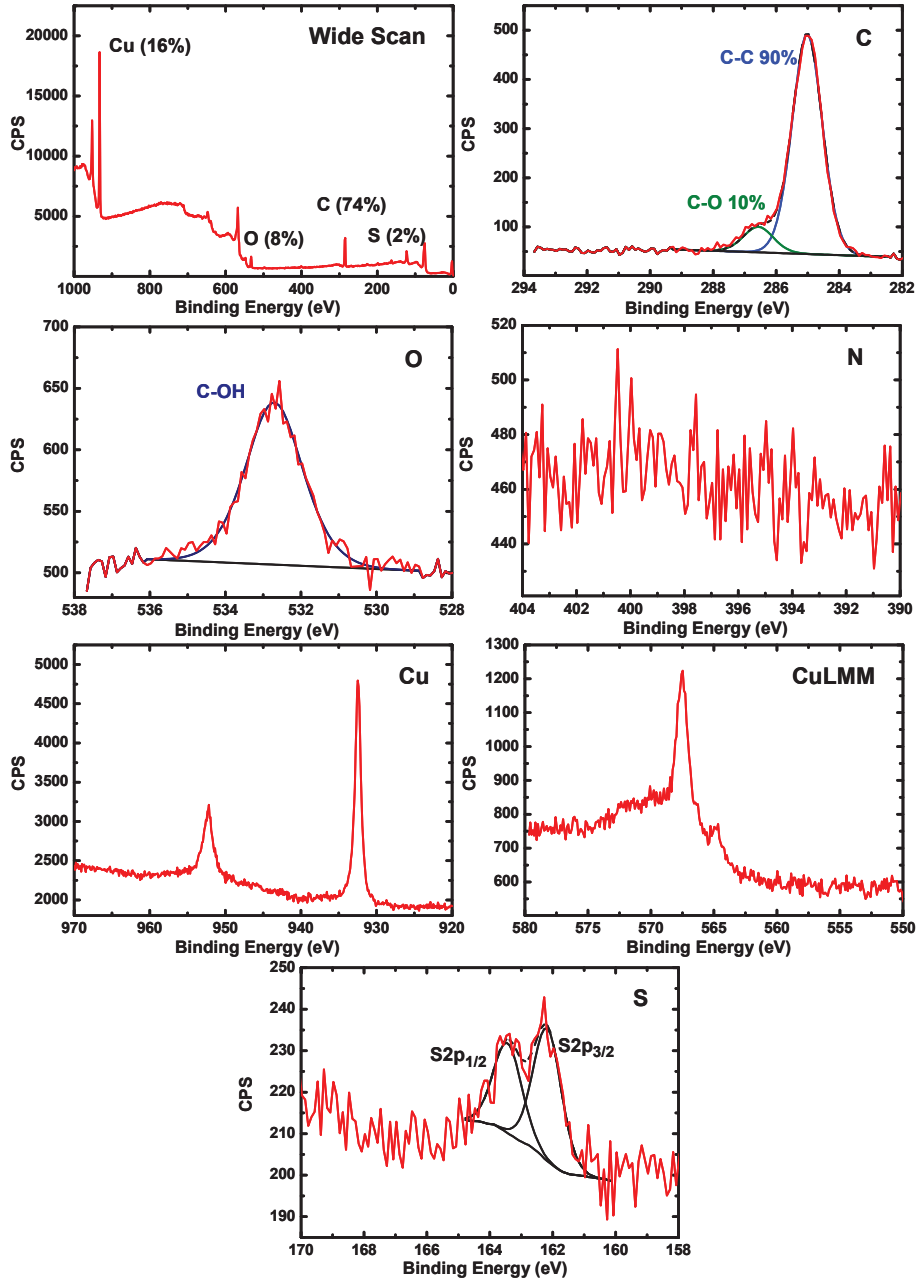

Figure S13. XPS spectra of the alcohol-terminated copper monolayer.

1.2.3 N-Succinimidyl mercaptoundecylenate (NHS-MUA):

200 mM (126 mg, 0.40 mmol) NHS-MUA in 2.0 mL dry toluene. Static water contact angle of resulting monolayer: 55°.

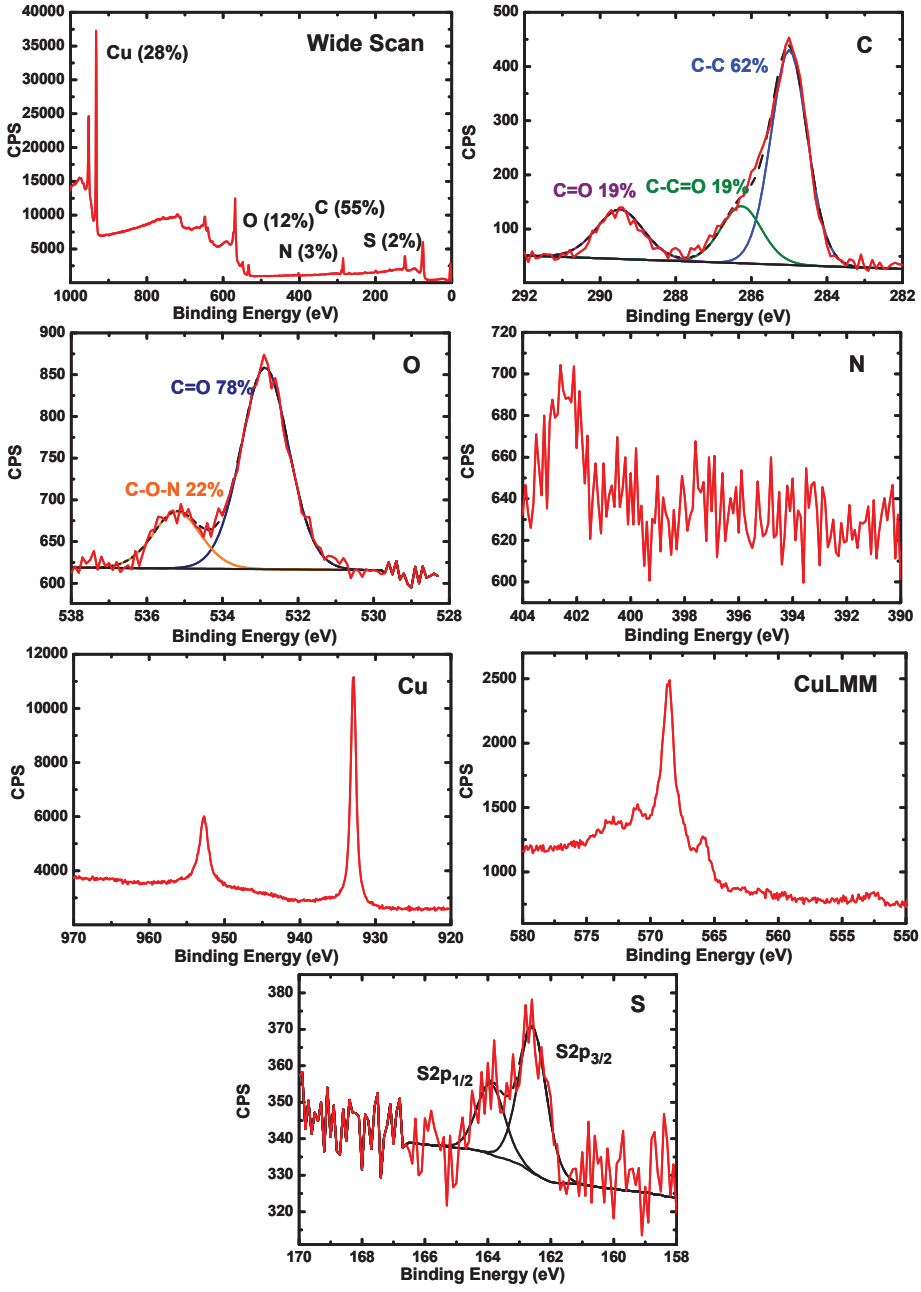

Figure S14. XPS spectra of the NHS-ester-terminated copper monolayer.

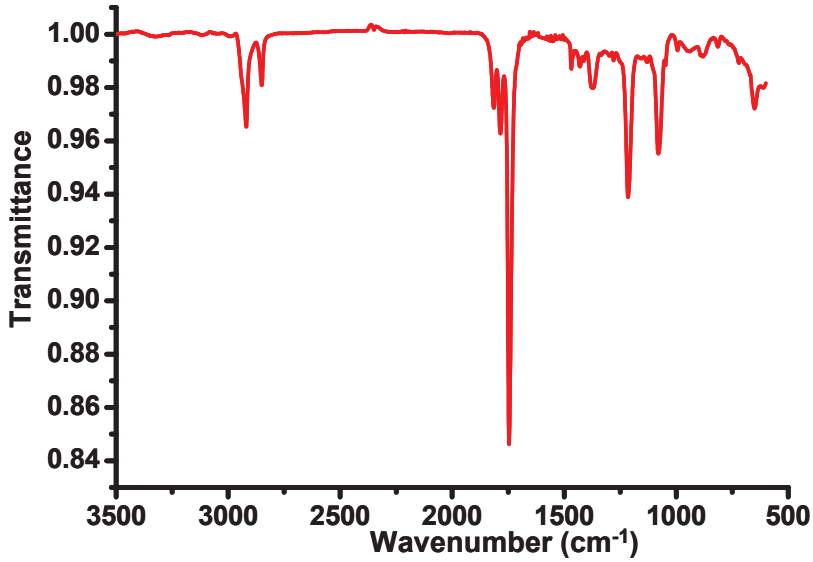

Figure S15. IRRA spectrum of the NHS-ester-terminated copper monolayer.

Table S1. Selected IR data for the NHS-ester-terminated copper monolayer.

Frequency (cm^{-1})	Assignment
2919	$\nu_a(CH_2)$, antisymmetric stretch
2851	$\nu_s(CH_2)$, symmetric stretch
1817	ν(C=O), carbonyl stretch of the ester
1788	ν_s(C=O), symmetric stretch of the NHS
1745	ν_a(C=O), antisymmetric stretch of the NHS
1375	ν_s(C-N-C), symmetric C-N-C stretch of the NHS
1214	Amide III, N-C=O vibration in the NHS
1078	(N-C-O), N-C=O stretch of the NHS

1.3 Conjugation reactions:

These reactions were carried out under argon atmosphere at 20 °C for 16 h.

1.3.1 β-D-Glucosamine:

0.1 M (43 mg, 0.20 mmol) β-D-glucosamine, 0.1 mL NEt_3 in 1.9 mL dry methanol. Static water contact angle of resulting monolayer: 76°.

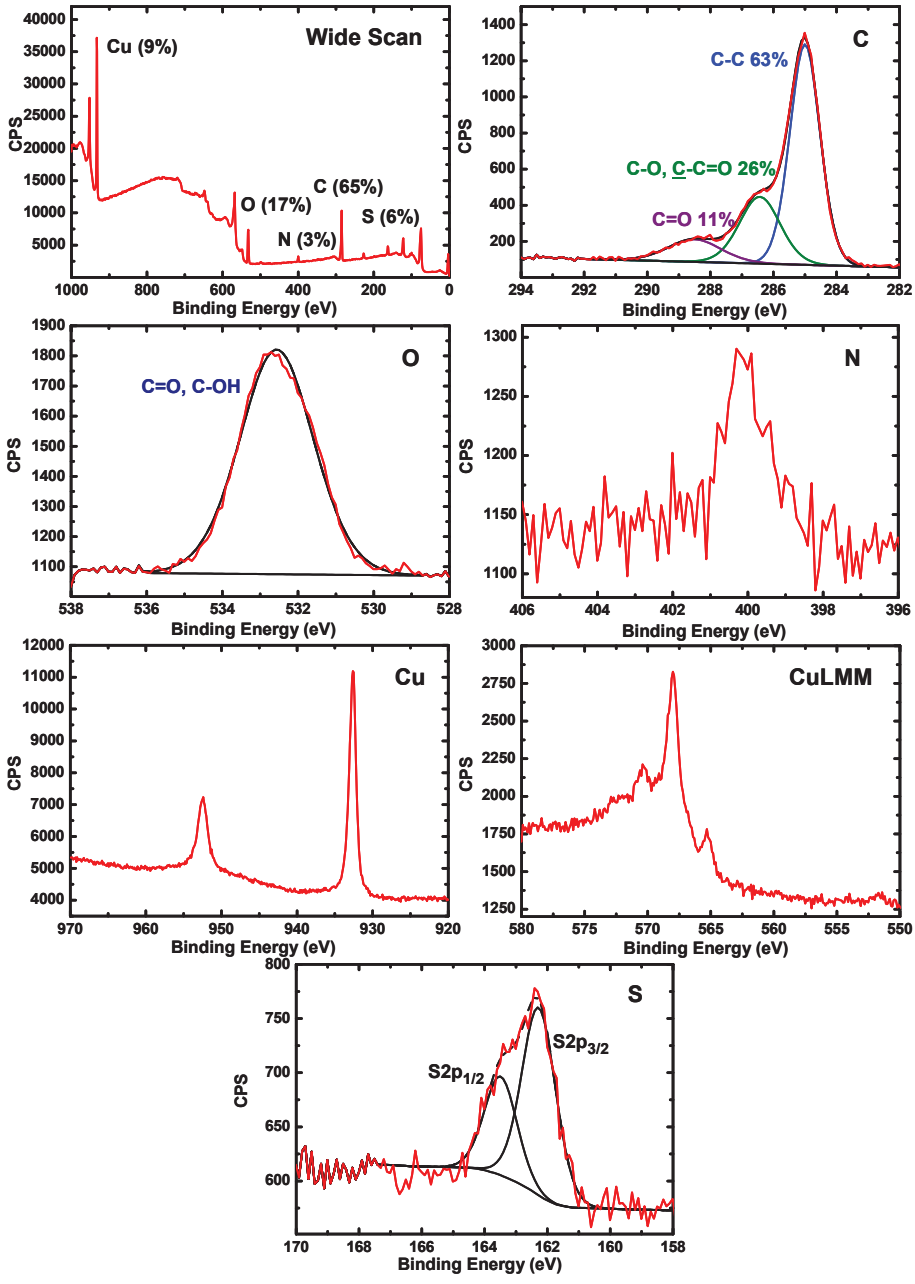

Figure S16. XPS spectra obtained after reaction of NHS-ester-terminated copper monolayer with β-D-glucosamine.

1.3.2 Glutathione:

0.1 M (61 mg, 0.20 mmol) glutathione, 0.1 mL NEt_3 in 1.9 mL dry methanol. Static water contact angle of resulting monolayer: 24°.

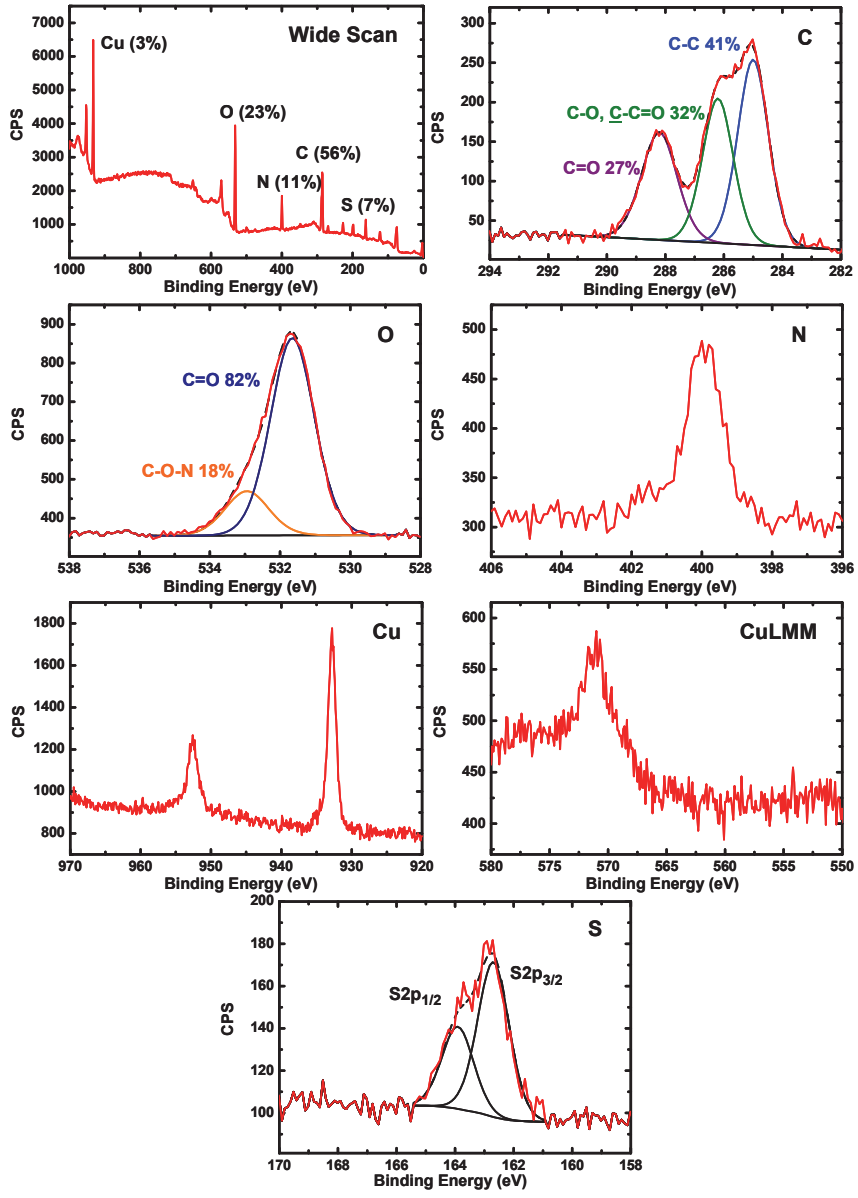

Figure S17. XPS spectra obtained after reaction of NHS-ester-terminated copper monolayer with glutathione.

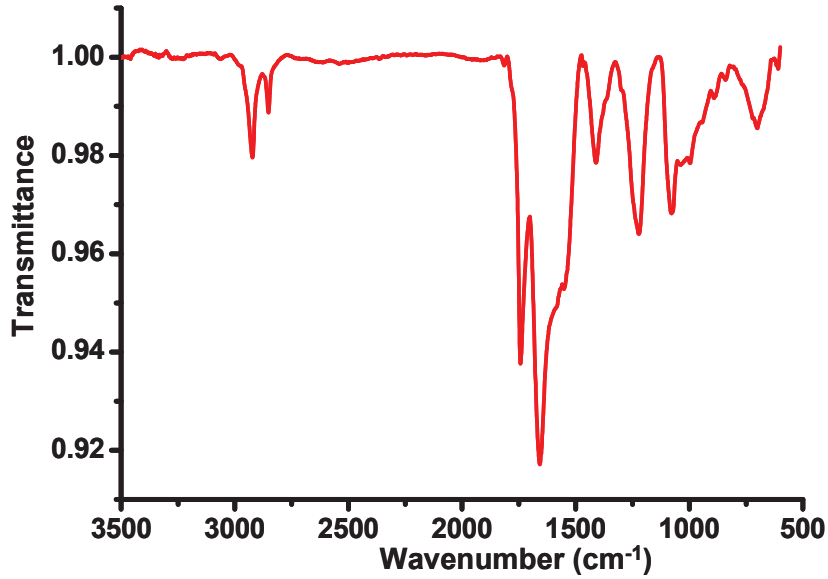

Figure S18. IRRA spectrum obtained after reaction of NHS-ester-terminated copper monolayer with glutathione.

Table S2. Selected IR data for the glutathione monolayer on copper.

Frequency (cm^{-1})	Assignment
2921	$\nu_a(CH_2)$, antisymmetric stretch
2851	$\nu_s(CH_2)$, symmetric stretch
1742	ν(C=O), free carboxylic acid stretch
1659	Amide I, C=O (stretch) amide
1552	Amide II, C-N (stretch); C-N-H (deformation)
1410	$\delta_s(CH_2)$, scissoring
1222	δ(C-OH), bending

1.3.3 5-(Biotinamido)pentylamine:

0.01 M (6.6 mg, 0.02 mmol) 5-(biotinamido)-pentylamine, 0.1 mL NEt_3 in 1.9 mL dry methanol. Static water contact angle of resulting monolayer: 57°.

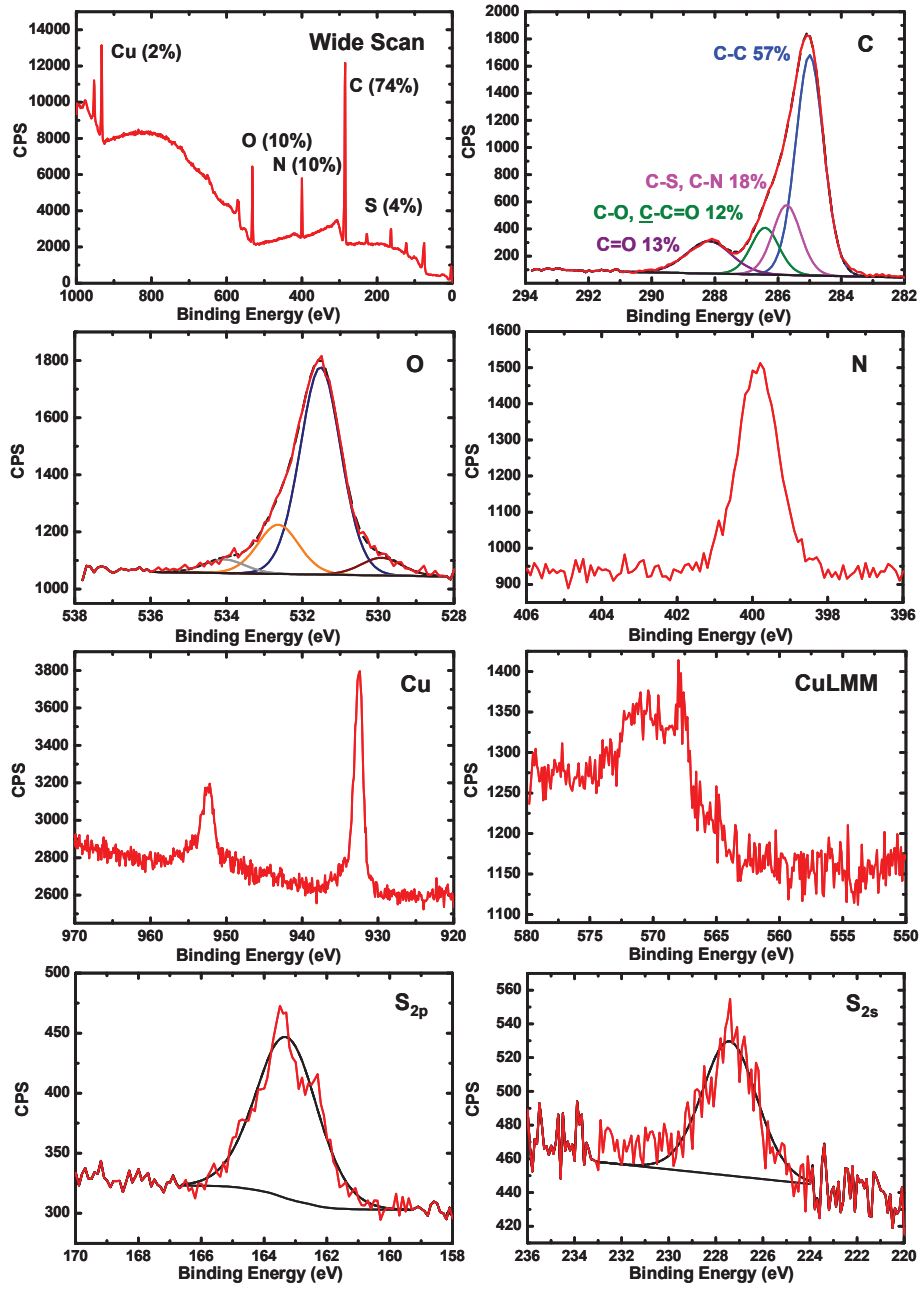

Figure S19. XPS spectra obtained after reaction of NHS-ester-terminated copper monolayer with 5-(biotinamido)pentylamine.

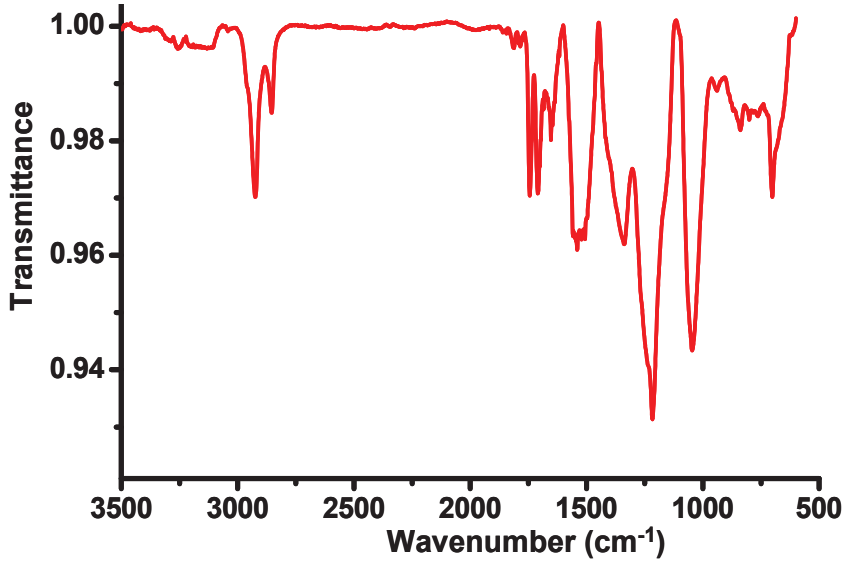

Figure S20. IRRA spectrum obtained after reaction of NHS-ester-terminated copper monolayer with 5-(biotinamido)pentylamine.

Table S3. Selected IR data for the biotin monolayer on copper.

Frequency (cm^{-1})	Assignment
3252	N-H stretch vibration
2924	$\nu_a(CH_2)$, antisymmetric stretch
2853	$\nu_s(CH_2)$, symmetric stretch
1819	ν(C=O), carbonyl stretch of the ester
1786	ν_s(C=O), symmetric stretch of the NHS
1747	ν_a(C=O), antisymmetric stretch of the NHS
1711	Amide I, C=O stretch vibration of cyclic urea
1653	Amide I, C=O stretching vibration of the amide groups
1539	Amide II, C-N (stretch), C-N-H (deformation) of the amide moiety
1341	ν_s(C-N-C), symmetric C-N-C stretch of the NHS
1217	Amide III, N-C=O vibration in the NHS and biotin moiety
1045	ν(N-C-O), N-C=O stretch of the NHS and biotin moiety

2.1 Oligonucleotides used for OmpA-M200

Table S4. Oligonucleotides.

Name	Primer (5'→ 3')
M200-F	CACTATAGGGAGACCACAACGG
M200-R	CACCATCACCACGGT***ATG***TAAG
M200-M83A_M88A-F	CGCCAAAAAG***GCG***GTGTATCTGCAA***GCG***AACAGCCTG
M200-M83A_M88A-R	CAGGCTGTT***CGC***TTGCAGATACAC***CGC***CTTTTTGGCG
M200-M153G-F	CCGATATAGAA***GGG***AACCGCCTGGGC
M200-M153G-R	CCGATATAGAA***GGG***AACCGCCTGGGC
OmpA-F	*TATG*AAAAAGACAGCTATCGCGATTGCAGTGGCACTGGCTGGTTTCGCTACCGTGGCCCAGGCGCAGGTGCAG*CTGCA*
OmpA-R	*G*CTGCACCTGCGCCTGGGCCACGGTAGCGAAACCAGCCAGTGCCACTGCAATCGCGATAGCTGTCTTTTT*CA*

Changed amino acids in oligonucleotides shown in red and cursive. PstI/NdeI sticky ends are shown in cursive and underlined.

2.2 Average signal loss after peptide PAT49 binding

Table S5. Average signal loss after peptide PAT49 binding followed by regeneration

	NHS chemistry M200-AHA	click chemistry OmpA-M200-AHA
Cycle 20	22.28 RU	12.19 RU
Cycle 47	20.70 RU	11.42 RU
loss RU after 27 cycles:	7.07%	6.32%
loss per cycle:	0.26%	0.23%

The average signal loss per cycle (measured in response difference [RU]) was determined after repeated cycles of peptide PAT49 (50 µg mL^{-1}) injection followed by regeneration with 5 µL 10 mM HCl. Data points were measured 30 sec after injection end.

SUMMARY

SUMMARY

In this thesis we set out to increase the knowledge of oriented detection elements on biosensor surfaces. In natural sensing systems, such as the eye, oriented proteins on surfaces are a common principle, which mediates highly sensitive detection systems. By following similar principles, namely the orientation of detection elements, biosensors can be up-graded to ´natural` standards with regard to sensitivity and potential for miniaturization.

Chapter 1 is the introduction of this thesis, and describes several aspects that are important for the field of biosensors. The research reported in this thesis is taking place at the interface of several scientific research disciplines: surface chemistry, protein engineering and coupling chemistry. Each of these aspects itself has the power to improve biosensor performance. Therefore, research and optimization in each area is of value for the biosensor community.

Chapter 2 describes the formation of self-assembled monolayers (SAMs) on oxide-free copper. The preparation and characterization of well-ordered alkyl-thiol monolayers were described in detail. Monolayers of N-succinimidyl mercaptoundecanoate (NHS-MUA) were prepared and served as a platform for further functionalization with amine exposing biomolecules, such as β-d-glucosamine, the tripeptide glutathione, and biotin. Finally, the biotinylated copper surface was used to selectively immobilize streptavidin.

Chapter 3 reviews the state-of-the-art of various antibody immobilization methods. The presented methods differ in control over orientation (oriented vs random immobilization) as well as in the resulting stability of immobilization (covalent vs non-covalent attachment). The chapter also describes several methods that are currently used to elucidate antibody orientation in a more direct manner.

We next selected llama antibody domains (V_{HH}s) to obtain detection elements against tuberculosis (chapter 4). Two different selection strategies based on phage display were employed and resulted in a selection of V_{HH}s. It was demonstrated that the selected V_{HH}s were specific for tuberculosis causing mycobacteria and could be used as detection element in enzyme-linked immunosorbent assay (ELISA) as well as in a surface plasmon resonance (SPR)-based biosensor.

In order to be able to orient llama antibody domains on surfaces, a strategy introducing biotin at the C-terminus of V_{HH}s was used in chapter 5. Two different llama antibody domains were used, one V_{HH} specific for tuberculosis and one for the foot-and-mouth-disease virus (FMDV). By immobilization on a streptavidin coated-biosensor surface, biotinylated V_{HH}s were oriented. In this set-up, the analyte binding site of the V_{HH} was exposed to the analyte solution. The influence on analyte binding of the oriented set-up was compared to a random set-up. Random immobilization was achieved using the amine groups in the V_{HH}, via NHS-EDC coupling. By using

a batch of different analytes, all specific for V_{HH}, the influence of analyte properties on binding was studied. It was shown that epitope number, molecular size and binding affinity greatly influence the analyte binding. Importantly, it was shown that orientation of detection elements may strongly improve the intensity of the analyte binding signal, and that this effect is much stronger for lower-affinity analytes.

In chapter 6 we investigated a novel strategy to immobilize V_{HH}s specific for FMDV, and we deployed this strategy to couple V_{HH} either in an oriented or in a random manner on the surface. An introduced azide group was used as functional handle for immobilization of the V_{HH}. Azide groups were introduced in V_{HH} with azidohomoalanine, a non-natural amino acid that replaces methionine in proteins expressed in methionine-depleted bacterial cultures. It was demonstrated that residue-specific incorporation of azidohomoalanine enabled modification of V_{HH} (M200) at several positions of the five introduced azide groups. Using molecular techniques, V_{HH}s containing only a single azide were prepared (OmpA-M200). The two distinct azide-functionalized V_{HH}s, M200 and OmpA-M200, containing five or one azide group, respectively, were immobilized on cyclooctyne-functionalized surfaces. The oriented and non-oriented surfaces were investigated for detection sensitivity with SPR as model-biosensor. It was shown that oriented immobilization resulted in a much higher sensitivity of the biosensor.

In the general discussion, the most important achievements of this thesis are presented. Recommendations as well as additional thoughts on how to incorporate results of this research into the biosensor field are discussed.

SAMENVATTING

Dit proefschrift is geschreven met als doel de kennis van georiënteerde detectie-elementen op biosensoren te vergroten. In natuurlijke sensing systemen, zoals het oog, zijn zelfgeordende eiwitten aan het oppervlak een algemeen begrip. Door het volgen van hetzelfde principe, de oriëntatie van eiwitten zoals in dit proefschrift, kunnen synthetische biosensoren met recombinant eiwitten opgewaardeerd naar ´natuurlijke` normen inzake gevoeligheid en miniaturisatie.

Hoofdstuk 1 is de inleiding van dit proefschrift en beschrijft diverse aspecten die belangrijk zijn op het gebied van biosensoren. Het onderzoek beschreven in dit proefschrift valt onder verschillende wetenschappelijke onderzoeksdisciplines: oppervlakte chemie, eiwit engineering en koppelingschemie. Elk van deze aspecten is van belang voor een verbeterde werking van biosensoren. Daarom is onderzoek en optimalisatie in elk facet van waarde voor de biosensor-wereld.

Hoofdstuk 2 beschrijft de vorming van zelf-geassembleerde monolagen (in Engels: self-assembled monolayers [SAM]) op oxide-vrij koper. Ook de bereiding en karakterisatie van welgeordende alkynthiol monolagen zijn beschreven. Monolagen van N-succinimidyl mercaptoundecanoaat (NHS-MUA) zijn gemaakt. Deze dienden als een platform voor verdere functionalisering met amine-biomoleculen zoals β-D-glucosamine, het tripeptide glutathion en biotine. Ten slotte wordt het gebiotinyleerde koperoppervlak worden gebruikt om streptavidine selectief te immobiliseren.

In hoofdstuk 3 wordt de stand van zaken op het gebied van methodes voor antilichaam immobilisatie beschreven. De gepresenteerde methoden verschillen in controleerbaarheid van oriëntatie (georiënteerde vs willekeurige immobilisatie) en in de resulterende stabiliteit van immobilisatie (covalent vs non-covalent gebonden). Ook worden verschillende actuele karakterisatiemethoden beschreven die worden toegepast om de oriëntatie van antilichamen op een directe manier te analyseren.

Vervolgens zijn lama antilichaam domeinen (V_{HH}s) geïsoleerd om detectie-elementen tegen tuberculose (hoofdstuk 4) te verkrijgen. Twee verschillende selectiestrategieën gebaseerd op faagdisplay zijn toegepast en resulteerden in een selectie van een aantal verschillende V_{HH}s. De gekozen V_{HH}s zijn specifiek voor tuberculose veroorzaakt mycobacteriën en kunnen worden gebruikt als detectie-element in enzyme-linked immunosorbent assay (ELISA) en in oppervlakte plasmon resonantie (Engels: surface plasmon resonance [SPR]) gebaseerde biosensoren.

Om lama antilichaam domeinen op oppervlakken te kunnen oriënteren is een biotine aan de C-terminus van V_{HH}s gekoppeld (hoofdstuk 5). Er zijn twee verschillende lama antilichaamdomeinen gebruikt, een V_{HH} specifiek voor tuberculose en een voor het mond- en klauwzeer (MKZ) virus. Door immobilisatie op streptavidine gecoate biosensoren, kunnen de gebiotinyleerde V_{HH}s georiënteerd worden gebonden. Op deze manier is de analyt bindingsplaats van het V_{HH} vrij toegankelijk en kan

direct worden blootgesteld aan de analytoplossing. De invloed op de bindingseffectiviteit van de analyt gerichte set-up werd vergeleken met een willekeurige opstelling. Met een standaard (niet-georiënteerd) NHS-EDC koppeling werd willekeurige immobilisatie bereikt middels de aminegroepen in het V_{HH}. Door het gebruik van een batch van verschillende analyten, specifiek voor V_{HH}, is de invloed van analyt binding met het detectie element orientatie onderzocht. Er is aangetoond dat o.a. epitoop aantal, molecuulgrootte en bindingsaffiniteit de analyt binding sterk beïnvloeden. Aangetoond is dat oriëntatie van detectie-elementen de intensiteit van het analyt bindende signaal sterk verbetert en dat dit effect veel sterker is voor analyten met een lagere affiniteit.

In hoofdstuk 6 werd een nieuwe strategie introduceerd om V_{HH}s specifiek voor de mond-en-klauwzeer virus (MKZ virus, Engels: FMDV van ´foot-and-mouth-disease` virus) te immobiliseren. Deze strategie wordt ingezet om V_{HH}s hetzij in een georiënteerd, of op willekeurige wijze aan een oppervlak te koppelen. Voor immobilisatie van de V_{HH} M200, die MKZ virus herkend, werd een azidegroep geïntroduceerd als functionele handgreep. Deze azide groepen worden ingebouwd in V_{HH} M200 via het aminozuur azidohomoalanine, een niet-natuurlijk aminozuur dat in plaats van methionine kan worden ingebouwd. Met behulp van moleculaire technieken is het mogelijk om V_{HH}s met slechts een azide (OmpA-M200) te bereiden. De twee verschillende azide-gefunctionaliseerde V_{HH}s, M200 en M200-OmpA, met vijf of slechts één azidegroep respectievelijk, worden geïmmobiliseerd op cyclooctyn-gefunctionaliseerde oppervlakken. De georiënteerde en niet-georiënteerde oppervlakken worden onderzocht en vergeleken op gevoeligheid in een SPR biosensor. Er wordt aangetoond dat georiënteerde immobilisatie resulteert in een significant hogere gevoeligheid van de biosensor.

In de algemene discussie worden de belangrijkste resultaten van dit proefschrift gepresenteerd. Tenslotte worden er aanbevelingen en alsmede aanvullende gedachten gegeven over de wijze waarop de resultaten van dit onderzoek toegepast kunnen worden in de biosensor-wereld.

Zusammenfassung

Diese Doktorarbeit gibt Einblicke in die Auswirkungen von orientierten Detektionselementen auf Biosensoroberflächen. In natürlichen Messsystemen, wie dem Auge, sind orientierte Proteine an Oberflächen ein gängiges Prinzip und tragen maßgeblich zur Sensitivität der empfindlichen Detektionssysteme bei. In dieser Doktorarbeit werden diverse Strategien zur Orientierung von Proteinen dargestellt, um leistungsfähigere Biosensoren zu entwickeln. Durch die orientierte Immobilisierung von Detektionselementen (hier: rekombinante Proteine) sollen Model-Biosensoren in Bezug auf Sensitivität und Potential zur Miniaturisierung verbessert werden.

Kapitel 1 dieser Doktorarbeit dient als Einführung und erläutert relevante Forschungsbereiche auf dem Gebiet der Biosensoren. Aufgrund des Schwerpunktes der Doktorarbeit betreffen die Forschungstätigkeiten verschiedene Disziplinen: Oberflächenchemie, Protein-Engineering (von englisch: engineering; hier etwa Konstruktion oder Manipulation) und Kopplungschemie. Jeder dieser Aspekte trägt dazu bei, die Leistung von Biosensoren zu verbessern. Die Forschung und Optimierung in diesen Bereichen ist daher wertvoll für den Biosensorensektor.

In Kapitel 2 wird die Bildung von selbstorganisierten Monoschichten (von englisch: Self-assembled monolayers [SAMs]) auf oxid-freiem Kupfer beschrieben. Die Herstellung und Charakterisierung von wohlgeordneten Alkanethiol Monoschichten werden im Detail dargestellt. Monoschichten von N-Succinimidyl mercaptoundecanoate (NHS-MUA) wurden hergestellt und dienten als Plattform für weitere Funktionalisierungen mit aminehaltigen Biomolekülen wie β-D-Glucosamine, dem Tripeptid Glutathion und Biotin. Ferner konnten biotinylierte Kupferoberflächen zur selektiven Immobilisierung von Streptavidin genutzt werden.

Das dritte Kapitel beschäftigt sich mit diversen Antikörper-Immobilisierungs-Methoden, die aktuell in der Forschung Verwendung finden. Die vorgestellten Methoden unterscheiden sich in ihrer Kontrolle über die Orientierung (orientierte vs zufällige Immobilisierung) sowie in der Stabilität der entstehenden Immobilisierung (kovalente vs nicht-kovalente Bindung). Zudem werden verschiedene Methoden beschrieben, um Antikörper-Orientierung in direkter Weise nachzuweisen.

Daran anschließend wird aufgezeigt, wie Antikörperdomänen (V_{HH}s) von Lamas selektiert und als Detektionselemente gegen Tuberkulose verwendet wurden (Kapitel 4). Zwei verschiedene Auswahl-Strategien, basierend auf Phagen-Display, wurden angewendet und mündeten in einer Auswahl von V_{HH}s. Die ausgewählten V_{HH}s waren spezifisch für Tuberkulose verursachende Mykobakterien und konnten als Detektionselement in einem antikörperbasierenden Nachweisverfahren (Enzym-Linked Immunosorbent Assay, ELISA) sowie in einem Model-Biosensor verwendet werden.

Um die Lama Antikörperdomänen auf Oberflächen zu orientieren, wurde - wie in Kapitel 5 dargestellt - eine Strategie verwendet, die ein Biotin Molekül an dem

C-Terminus der V_{HH}s anhängt. Dazu wurden zwei verschiedenartige Lama Antikörperdomänen verwendet: ein V_{HH} spezifisch für Tuberkulose und ein V_{HH} spezifisch für das Maul-und-Klauen-Seuche-Virus (MKSV, im Englischen: FMDV von ´foot-and-mouth-disease` virus). Durch die Immobilisierung auf einer mit Streptavidin beschichteten Biosensoroberfläche konnten die biotinylierten V_{HH}s eine orientierte Anordnung auf der Oberfläche einnehmen. In diesem Versuchsaufbau ist die Analyten-Bindestelle des V_{HH}s der Analyten-Lösung zugewandt. Die orientierte Anordnung der Antikörperdomänen wurde mit einer zweiten, zufälligen Anordnung verglichen. Die Immobilisierung in einer zufälligen Anordnung wurde unter Verwendung der Aminogruppen in den V_{HH}s über NHS-EDC Kupplung erzielt. Durch die Verwendung einer Auswahl verschiedener Analyten, alle spezifisch für die Antikörperdomäne, konnte der Einfluss von Analyteigenschaften auf das Binden an die Antikörperdomäne untersucht werden. Es stellte sich heraus, dass Epitopnummer, Molekülgröße und Bindungsaffinität großen Einfluss auf das Bindeverhalten des Analyten haben. Durch die Orientierung von Detektionselementen konnte das Analyt-Bindesignal stark verbessert werden und es zeigte sich, dass der Effekt für Analyten mit niedrigerer Affinität viel dominanter ist.

In Kapitel 6 wurde eine neue Strategie untersucht, um die MKSV spezifischen V_{HH}s zu immobilisieren. Mit der verwendeten Methode wurden die V_{HH} gezielt in einer orientierten oder in einer zufälligen Anordnung auf der Oberfläche gekoppelt. Eine eingeführte Azidgruppe diente hierbei als funktioneller Griff, an dem die V_{HH} immobilisiert werden konnten. Die Azidgruppe wurde unter Verwendung der nicht in der Natur vorkommenden Aminosäure Azidohomoalanine in die Proteine eingebaut. Es zeigte sich, dass einige der fünf spezifisch eingebauten Azidgruppen in V_{HH} M200 für eine chemische Reaktion mit einem Alkine zur Verfügung stehen. Durch die Verwendung molekularbiologischer Techniken konnten V_{HH}s mit nur einem einzigen Azid hergestellt werden (OmpA-M200). Die zwei verschiedenen Azid-funktionalisierten V_{HH}s, M200 und OmpA-M200, mit fünf oder nur einer Azidgruppe, wurden jeweils auf Cyclooctin-funktionalisierten Oberflächen immobilisiert. Die orientierten (OmpA-M200) oder zufällig (M200) immobilisierten V_{HH}s wurden auf Nachweisempfindlichkeit mit Hilfe eines Model-Biosensors untersucht. Es stellte sich heraus, dass orientierte Immobilisierung zu einer viel höheren Sensitivität des Biosensors führt.

In der allgemeinen Diskussion werden die wichtigsten Erkenntnisse dieser Doktorarbeit zusammenfassend dargestellt. Empfehlungen, sowie weitere Gedanken darüber, wie die Ergebnisse dieser Forschung Anwendung im Biosensorsektor finden könnten, werden aufgezeigt.

About the Author

Curriculum Vitae

Anke Kristin Trilling was born on 27th October 1982 in Freiburg im Breisgau, Germany. She studied Biology at the Albert-Ludwigs-Universität in Freiburg, Germany to obtain her Vordiplom (pre-diploma). She then continued her studies at the Ecole Supérieure de Biotechnologie de Strasbourg in France. During this trinational course of studies she gained additional experimental experience during two internships. She executed her first internship at the Institute of Biological Sciences of the University of Wales in Aberystwyth under supervision of Dr. Luis Mur and Dr. Aileen Smith. In this project the role of the plant hormone ethylene in the response of *Arabidopsis thaliana* ethylene mutants to the necrotroph *Botrytis cinerea* was investigated. In her second internship she generated suppressors and enhancers of the *Arabidopsis thaliana* gs1 mutant by activation tagging under supervision of Prof. Mike Bevan at the John Innes Centre, Norwich, England. To obtain her Diplôme d'Ingénieur en Biotechnologie she carried out a research project at Planet Biotechnology Inc., Hayward, California under supervision of Dr. Keith Wycoff and Dr. Archana Belle. Her diploma thesis described the production of an ELP fusion tag for purification purposes in tobacco plants. In November 2008 she started her PhD research at Plant Research International, Wageningen, The Netherlands in cooperation with the Laboratory of Organic Chemistry at Wageningen University, Wageningen, The Netherlands under supervision of Dr. Jules Beekwilder and Prof. Han Zuilhof. The subject of this research was the oriented immobilization of llama antibodies on tailor-made surfaces for the use in biosensors. The results are described in this thesis. In January 2013 she started as a R&D scientist at Surfix B.V. Wageningen, The Netherlands.

Publications

Anke K. Trilling, Thamara Hesselink, Adèle van Houwelingen, Jan H. G. Cordewener, Maarten A. Jongsma, Sanne Schoffelen, Jan C. M. van Hest, Han Zuilhof and Jules Beekwilder 'Oriented Llama Antibodies Strongly Increase Sensitivity of Biosensors' submitted.

Saurabh K. Srivastava, Vincent J. B. Ruigrok, Natalie J. Thompson, Anke K. Trilling, Albert J.R. Heck, Cees van Rijn, Jules Beekwilder and Maarten A. Jongsma '16 kDa heat shock protein from heat-inactivated *Mycobacterium tuberculosis* is a homodimer - suitability for diagnostic applications with specific llama V_{HH} monoclonals' *PLoS ONE.* accepted.

Anke K. Trilling, Jules Beekwilder and Han Zuilhof 'Antibody Orientation on Biosensor Surfaces: a Minireview' *Analyst.* 2013, 138, 1619-1627.

Anke K. Trilling, Michiel M. Harmsen, Vincent J. B. Ruigrok, Han Zuilhof and Jules Beekwilder 'The Effect of Uniform Capture Molecule Orientation on Biosensor Sensitivity: Dependence on Analyte Properties' *Biosensors & Bioelectronics.* 2013, 40, 219-226.

Anke K. Trilling, Hans de Ronde, Linda Noteboom, Adèle van Houwelingen, Margriet Roelse, Saurabh K. Srivastava, Willem Haasnoot, Maarten A. Jongsma, Arend Kolk, Han Zuilhof and Jules Beekwilder 'A Broad Set of Different Llama Antibodies Specific for a 16 kDa Heat Shock Protein of *Mycobacterium tuberculosis*' *PLoS ONE.* 2011, 6, e26754.

Mabel A. Caipa Campos, Anke K. Trilling, Menglong Yang, Marcel Giesbers, Jules Beekwilder, Jos M. J. Paulusse and Han Zuilhof 'Self-Assembled Functional Organic Monolayers on Oxide-Free Copper' *Langmuir.* 2011, 27, 8126–8133.

Keith L. Wycoff, Archana Belle, Dorothée Deppe, Leah Schaefer, James M. Maclean, Simone Haase, Anke K. Trilling, Shihui Liu, Stephen H. Leppla, Isin N. Geren, Jennifer Pawlik, Johnny W. Peterson 'Recombinant anthrax toxin receptor-Fc fusion proteins produced in plants protect rabbits against inhalational anthrax' *Antimicrobial Agents and Chemotherapy.* 2011, 55, 132-139.

Overview of completed training activities

Discipline-specific activities

Conferences/ Meetings

Annual MicroNano Conference, Ede, 2008 & 2011
Annual Marie Curie Hierarchy Network Meetings, The Netherlands, 2009 - 2012
Annual NWO Conference, Lunteren, 2009 & 2010
Single Domain Antibodies Come of Age, Ghent, 2010
IPOP BIONANO Symposium, Wageningen, 2010
CHAINS (Chemistry As Innovating Science), Maarssen, 2011
2nd International Bio-Sensing Technology Conference, Amsterdam, 2011
Conference: Advances in Biodetection and Biosensors, Hamburg, 2011
Biosensors2012, Cancun, 2012

Courses

Advanced Organic Chemistry, Wageningen University, 2009 & 2010
Introduction to liquid crystals, Radboud University in Nijmegen, 2009
ANAC course ‚Molecular Spectroscopy', Wageningen University, 2009
Phage Display of Proteins & Peptides, Cold Spring Harbour Laboratory, 2009
Advanced spectroscopic methods, Max-Planck-Institut in Göttingen, 2010
Confined geometries, Jozef Stefan Institute in Ljubljana, 2010
Entrepreneurship and patent issues, Philips Research in Eindhoven, 2011
Workshop on assembling of superstructures in soft matter, Jozef Stefan Institute in Ljubljana, 2012

General courses

PhD course Techniques for Writing and Presenting a Scientific Paper, WGS, 2011
VLAG PhD Week, VLAG, 2009
Science and Society Summer School: The Human Animal, EMBL/EMBO, 2011
ExPectationS Career Day, Graduate School Experimental Plant Sciences, 2011
Advanced Course Guide to Scientific Artwork, Wageningen UR Library, 2012
Adobe InDesign, Wageningen UR Library, 2012

Optional activities

Group meetings, PRI & ORC, 2008-2012
Colloquia, PRI & ORC, 2008-2012
Preparation of a PhD research proposal, PRI & ORC, 2008
PhD study trip ORC, China, 2009
Summer School Marie Curie Hierarchy Network, RWTH Aachen, 2010
PhD stude trip ORC, England & Scotland, 2011

Acknowledgements

ACKNOWLEDGEMENTS

"My thesis - that's one small step for the biosensor world, but a giant leap for me!"
with reference to Neil Alden Armstrong.

Many people got involved in my very private ´moon landing` and contributed to this thesis in many ways. I received plenty of help, support and encouragement from colleagues, friends and my family – now is the time to thank them all. For all the people I might have forgotten in the short list that will follow: ..... (please insert full name), I also like to thank you of being part of my way to success.

First of all I like to express my gratitude to my supervisors Jules and Han, for doing an incredible good job in guiding me during the last four years. Jules, ik was jouw eerste AIO, maar hopelijk niet de laatste. Je had altijd tijd voor mij en ik kon altijd bij je binnen lopen - voor advies of om goede (en slechte) resultaten te bespreken. Je efficiënte denkwijze bij het opzetten van experimenten en schrijven van artikelen hebben zeer motiverend gewerkt. Je leidt je groep met veel humor en enthousiasme en ik heb je begleiding als heel prettig ervaren. Han, met jou deel ik de passie voor Californië en nu ook die voor oppervlaktechemie. Ondanks je drukke schema heb je altijd een bijdrage kunnen leveren en je passie voor nieuwe (biologische) onderwerpen werkte aanstekelijk. In de afgelopen jaren heb ik veel geleerd over oppervlaktechemie en jouw visie op dit gebied was een grote inspiratie voor mij. Maarten, jou wil ik bedanken voor je vruchtbare inbreng in mijn project, ik waardeer onze nano groepsbijeenkomsten. Dirk, met jou had ik het eerste contact toen ik op zoek was naar een PhD positie over molecular farming. Helaas had je op dat moment geen juiste PhD positie voor mij, maar ik ben blij dat we elkaar uiteindelijk nog persoonlijk leerden kennen. Kortom, ik wil jullie alle vier hartelijk bedanken voor de kans om dit interessante stuk van onderzoek uit te voeren. Dankzij jullie heb ik mijn onderzoek met succes uit kunnen voeren. Jullie hebben mij veel geleerd en dat komt nu al goed van pas bij mijn huidige baan.

I had the honor to work at two departments – the Organic Chemistry Department (ORC) at Wagenigen University and Plant Research International (PRI). The flexible cooperation between the two departments offered me two enjoyable work environments in which I adored to carry out my scientific project. I haven't been around full-time, but each time I felt welcome in both groups – therefore I like to thank all employees belonging to ORC and PRI. I am especially pleased that I received constant encouragement, support and guidance from all teaching staff and PhDs of the two departments. I like to acknowledge several people of the departments in person:

De group van Jules, maar Adèle, Katja en Nikolay in het bijzonder: dank jullie voor de gezelligheid in het lab en tijdens onze diner avondjes. Adèle, Margriet en Linda, jullie zijn erg goede leraren en hadden altijd tijd voor mij - bedankt voor de

hulp met de lama antilichamen in het begin van mijn project. Thamara en Jan, ik ben blij dat jullie de kennis en expertise over MALDI met mij hebben willen delen. Dankzij jullie heb ik verrassende inzichten verkregen in deze techniek.

Saurabh, I enjoyed to work with you on the llama antibodies. It was a pleasure to discuss science with you and I wish you all the best for your future. Jimmy, Fanny and Desalegn: we started together in Wageningen and I will always remember the good talks we had in our first office before you moved to the new part of the building. Together we shared the ups and downs of a PhD life – thank you for being such nice colleagues.

The PhDs trips with ORC to China and Scotland will always stay in my memory – it was a nice and informative experience. Also the private expeditions with Saurabh, Umesh, Nagendra and Satesh (England) as well as with Jacinthe, Yessie, Willem, Nagesh and Jerome (China) were unforgettable adventures. Jos and Richard, jullie wil ik ook van harte bedanken voor de bijdragen aan mijn oderzoek. Menglong, Ankush and Mabel, you were not only nice roommates but also taught me all about monolayers. Thank you for your patience to teach a biologist the secrets of chemistry and to make me feel home in a fume hood. Mabel, me enseñaste algo más que química. Aprendí muchísimo sobre Ciencia y Sociedad Científica de ti, y con tu experiencia y aportaciones llevaste el trabajo del cobre a buen término. Muchas gracias por ello - fuiste una gran inspiración para mí.

Frans, ook jou wil ik graag bedanken voor de samenwerking, het was altijd prettig om met jou over koper modificatie te praten. Barend en Marcel, hartelijk bedankt voor het delen van jullie kennis over IRRAS, NMR, AFM en XPS. Zonder deze fascinerende technieken kan ik mijn onzichtbare monolagen niet karakteriseren.

I also like to thank my paranymphs Sidhu and Radostina for your friendship and support (not only during my defense).

Elly, Aleida en Jannie, bedankt voor al jullie hulp door de papieren jungle – zonder jullie helpende hand bij alle administratieve klusjes had ik mijn PhD niet kunnen halen. Ik wil Ronald ook graag bedanken – dankzij jou had ik altijd alle chemicaliën die ik nodig had voor mijn experimenten bij de hand. Je was ook altijd een leuke gesprekspartner over allerlei niet-chemische problemen.

I also like to thank my students Marco, Bjorn and Katja. The results you obtained during your internships add to this thesis. Each of you faced different challenges during her/his time in Wageningen, but all of you learned to carry out research. I wish you all the best for your scientific future.

I am very glad that I can look back on four years of fruitful collaborations. Willem en Vincent, dank jullie wel voor de samenwerking die ik in die SPR wereld kon opzetten. Jullie deden altijd je best om mij toegang tot de SPR te geven en bovendien heb ik ontzettend veel van jullie geleerd. Alice, Richard en Hans, met jullie medewerking hebben jullie mijn kennis over tuberculose verrijkt. Ondanks de fysieke

afstand tussen de campus in Wageningen en de KIT in Amsterdam gaven jullie veel input in mijn proefschrift en de passie om tuberculose te verslaan was zeer inspirerend. Michiel, met jouw hulp heb ik mijn onderzoek kunnen uitbreiden naar de mond-en klauwzeer en hier kwam een mooie publicatie uit. Bedankt voor jouw hulp en advies met de lama antilichamen. Sanne en Mark, bedankt voor jullie hulp bij de analyse van mijn lama antilichamen met ESI-ToF en MALDI. Het was elke keer weer super als er een mooi spectrum op het scherm verscheen. Ik wil ook Angelique bedanken de voor nuttige discussies over het gebruik van SPR in combinatie met SPAAC.

I also like to thank the members of the Marie Curie Hierarchy Network. I enjoyed learning about liquid crystals and will always remember the nice time we had during our gatherings. Alex, nunca he conocido a una persona más alegre que tú. A pesar de todos los golpes del destino que te afectaron a ti y a tu familia, tú eres un ´Stehaufmännchen`. Te admiro por tu energía para salir adelante y te deseo todo lo mejor.

I also like to thank Luc, Koen and Sidhu for help with POV-Ray as well as Esther, Anke, Tzema and my mother for proofreading the ´non-English` parts.

Natürlich haben mich auch eine Vielzahl von Menschen fernab der Universität auf meinem Lebensweg unterstützt. Daher möchte ich die Gelegenheit nutzen, auch Ihnen zu danken. Beginnen möchte ich mit den Personen, denen meine Dissertation gewidmet ist, meiner Familie.

Mama und Papa, Ihr habt in jeglicher Hinsicht die Grundsteine für meinen Lebensweg gelegt. Ohne Eure Unterstützung hätte ich nicht so viele Erfahrungen sammeln und mir meinen Traumberuf erfüllen können. Auch meinen drei Geschwistern, ihren Partnern, allen Angeheirateten sowie meiner baldigen Schwiegerfamilie möchte ich für die fröhlichen Stunden in den letzten vier Jahren danken. Auch heute noch steht Ihr mir alle mit Rat und Tat zur Seite, wenn ich Euch brauche. Opa, leider hast du den heutigen Tag nicht mehr miterleben können, aber doch weiß ich, dass Du und Dora immer Vertrauen in meine Arbeit hattet.

Inge, Josef und Heike, auch Euch möchte ich für jegliche Unterstützung im privaten Alltag danken. Ihr habt uns ein neues Zuhause gegeben, auf das ich mich jeden Abend freue - dafür hat sich die lange Fahrt nach Wageningen gelohnt! Jürgen, danke für die unterhaltsamen Stunden im Auto – Du hast das tägliche Pendeln mit Deinen amüsanten Geschichten sehr viel erträglicher gemacht.

Zuletzt danke ich dem Menschen, der mir am nächsten steht. Dennis, mit unendlicher Geduld hast du meine Launen nach fehlgeschlagenen Experimenten ertragen und mich wieder aufgebaut. Du hast mich stets tatkräftig unterstützt und bist in jeder Hinsicht unverzichtbar gewesen. Wir haben uns gegenseitig Kraft gegeben und Höhen und Tiefen gemeistert – jetzt freue ich mich auf unsere gemeinsame Zukunft.

The research described in this thesis was financially supported by the graduate school VLAG, the Wageningen UR strategic research program BioNanotechnology (IPOP/BioNano) and by the EU through the Marie Curie ITN Project Hierarchy (Contract PITN-2007-215851).

Design and Layout: Anke Kristin Trilling, Dennis Schütz and Sidharam Pujari.
Printed by: Wöhrman Print Service, Zutphen, The Netherlands.